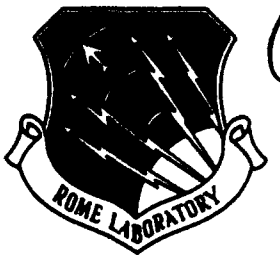

RL-TR-93-210
In-House Report
September 1993

FORMULATION OF TIME-DOMAIN PLANAR NEAR-FIELD MEASUREMENTS WITHOUT PROBE CORRECTION

Thorkild B. Hansen and Arthur D. Yaghjian

APPROVED FOR PUBLIC RELEASE; DISTRIBUTION UNLIMITED.

Rome Laboratory
Air Force Materiel Command
Griffiss Air Force Base, New York

This report has been reviewed by the Rome Laboratory Public Affairs Office (PA) and is releasable to the National Technical Information Service (NTIS). At NTIS it will be releasable to the general public, including foreign nations.

RL-TR-93-210 has been reviewed and is approved for publication.

APPROVED: Robert V. McGahan

ROBERT V. McGAHAN
Chief, Applied Electromagnetics Division
Electromagnetics & Reliability Directorate

FOR THE COMMANDER: John K. Schindler

JOHN K. SCHINDLER
Director of Electromagnetics & Reliability

If your address has changed or if you wish to be removed from the Rome Laboratory mailing list, or if the addressee is no longer employed by your organization, please notify RL (ERCT) Hanscom AFB MA 01731. This will assist us in maintaining a current mailing list.

Do not return copies of this report unless contractual obligations or notices on a specific document require that it be returned.

REPORT DOCUMENTATION PAGE

Form Approved
OMB No. 0704-0188

1. AGENCY USE ONLY *(Leave blank)*	2. REPORT DATE	3. REPORT TYPE AND DATES COVERED
	Sep 1993	In-House Sep 91-Aug 93

4. TITLE AND SUBTITLE

Formulation of Time-Domain Planar Near-Field Measurements Without Probe Correction

5. FUNDING NUMBERS

PE - 61102F
PR - 2304
TA - 2304I4
WU - 2304I403

6. AUTHOR(S)

Thorkild B. Hansen
Arthur D. Yaghjian

7. PERFORMING ORGANIZATION NAME(S) AND ADDRESS(ES)

Rome Laboratory/ERCT
31 Grenier St.
Hanscom AFB, MA 01731-3010

8. PERFORMING ORGANIZATION REPORT NUMBER

RL-TR--93-210

9. SPONSORING/MONITORING AGENCY NAME(S) AND ADDRESS(ES)

10. SPONSORING/MONITORING AGENCY REPORT NUMBER

11. SUPPLEMENTARY NOTES

Thorkild B. Hansen is an NRC Research Associate

12a. DISTRIBUTION/AVAILABILITY STATEMENT

Approved for public release; distribution unlimited.

12b. DISTRIBUTION CODE

13. ABSTRACT *(Maximum 200 words)*

This report addresses the problem of formulating planar near-field antenna measurements in the time domain, so that a single set of time-domain near-field measurements yields the far-field pattern in the time domain or over a wide range of frequencies. The time-domain planar near-field techniques are developed for both acoustic and electromagnetic fields and the space outside the region occupied by the antenna is assumed to be isotropic and homogeneous. Probe correction is ignored, that is, it is assumed that the probe is ideal so that the exact values of the field on the measurement plane are known.

Two fundamentally different approaches are used in deriving time-domain formulas which give the fields in the half space $z > z_o$ in terms of their values on the plane $z = z_o$. In the first approach the time-domain formulas are obtained by inverse Fourier transforming the corresponding frequency-domain formulas. Since this approach requires extensive use of the frequency domain near-field formulas, we start by giving a rigorous derivation and review of the frequency-domain formulation that addresses a number of subtleties that have not been dealt with adequately in the literature. As part of this review, planar near-field formulas for the static electric and magnetic fields are derived for the first time. In the second approach the time-domain near-field formulas are derived directly in the time domain. The equivalence of the resulting time-domain formulas obtained by the two different approaches demonstrates the validity of the formulas and the utility of both approaches.

14. SUBJECT TERMS

Near-field measurements
Planar scanning
Time-domain

15. NUMBER OF PAGES

106

16. PRICE CODE

17. SECURITY CLASSIFICATION OF REPORT	18. SECURITY CLASSIFICATION OF THIS PAGE	19. SECURITY CLASSIFICATION OF ABSTRACT	20. LIMITATION OF ABSTRACT
Unclassified	Unclassified	Unclassified	SAR

Contents

1 Introduction and Summary of Results **1**

2 Frequency-Domain Formulas **6**
2.1 Basic Planar Near-Field Formulas 7
2.1.1 Plane-Wave Spectrum Representations 7
2.1.2 Validation of Plane-Wave Spectrum Representations 10
2.1.3 Singularities of the Spectrum 13
2.1.4 Green's Function Representations 14
2.2 Far-Field Formulas 18
2.2.1 Far Fields Found from Green's Function Representations 18
2.2.2 Frequency Dependence of the Far Fields as ω Approaches Zero 19
2.2.3 Far Fields Found from Plane-Wave Spectrum Representations 20
2.2.4 Spectrum Given in Terms of the Far Field in Spherical Coordinates . 27
2.3 Power Relations for the Electromagnetic Field 28
2.4 Lossy Media 29
2.5 Static Electromagnetic Fields 30
2.5.1 The Lossless Case ($\sigma = 0$, $\sigma_m = 0$) 32
2.5.2 Electric Losses Only ($\sigma \neq 0$, $\sigma_m = 0$) 36
2.5.3 Electric and Magnetic Losses ($\sigma \neq 0$, $\sigma_m \neq 0$) 38

3 Time-Domain Formulas **40**
3.1 Time-Domain Green's Function Formulas 41
3.1.1 Derivation from the Fourier Transform 42
3.1.2 Derivation from Time-Domain Green's Functions 43
3.1.3 Magnetic Field Calculated from Electric-Field Data 45
3.2 Time-Domain Analogs of the Plane-Wave Spectrum Formulas 50
3.2.1 Time-Domain Plane-Wave Spectrum Formulas 51
3.2.2 Formulas Obtained from the Standard Fourier Transform 53
3.2.3 Formulas Obtained from the Analytic Fourier Transform 57
3.3 Near Fields in Terms of Far Fields 59
3.3.1 Electromagnetic Bullets 65
3.3.2 Far Fields Integrated over Time 66

3.3.3 Electromagnetic Missiles 68

4 A Time-Domain Sampling Theorem and Numerical Far-Field Calculations 72
4.1 Frequency-Domain Computation Scheme 73
4.2 Time-Domain Computation Scheme 75
4.3 Number of Near-Field Time Samples Needed for Far-Field Calculation 78
4.4 Comparisons of the Two Computation Schemes 84

References 91

A Differentiability and Analyticity of the Plane-Wave Spectrum and Far-Field Function 95

B Time-Domain Far Fields in Terms of Current Sources 99

List of Figures

2.1 Planar scanning geometry. 7
2.2 Half sphere of radius R_0 in a rectangular coordinate system. 16

3.1 The inversion contour C for the complex Fourier transform. 48
3.2 The semicircle C_a in the complex ω plane. 49
3.3 Square pulse of width 2 and height 1. 50
3.4 The contour Γ in the complex σ_θ plane. 60
3.5 Far-field hemispheres. 63

4.1 Gaussian time function $f(t)$ and its spectrum f_ω. 79
4.2 Realistic time function $f(t)$ and the amplitude of its spectrum $|f_\omega|$. 80
4.3 Open-ended waveguide antenna. 80
4.4 Spectrum of input pulse. 82
4.5 Amplitude of spectrum and time dependence of aperture electric field for open-ended waveguide antenna. 82
4.6 Amplitude of spectrum and time dependence of on-axis value of the far-field pattern for open-ended waveguide antenna. 83
4.7 On-axis values of the far-field pattern for a Gaussian point source calculated with the time-domain computation scheme. (a) exact; (b) $\Delta t = \pi/\omega_{max}$; (c) $\Delta t = \pi/(3\omega_{max})$. 85
4.8 On-axis values of the far-field pattern for a Gaussian point source calculated with the frequency-domain computation scheme. (a) exact; (b) $N_\omega = 16$; (c) $N_\omega = 32$. 87

Acknowledgments

This work was supported by the National Research Council, Washington, DC; by the Danish Technical Research Council, Copenhagen, Denmark; and by the Air Force Office of Scientific Research, Bolling AFB, DC.

Chapter 1

Introduction and Summary of Results

For more than 20 years, near-field techniques have been formulated and applied to the measurement of antenna radiation and target scattering [1], [2]. The theory, computer programs and experimental procedures have been successfully developed for the determination of complex radiation and scattering from measurements taken on planar [3], [4], cylindrical [5], [6], and spherical [7], [8], [9] scanning surfaces in the near field. However, nearly all of the previous work with near-field techniques has been limited to the frequency domain, so that radiation or scattering is determined at one frequency at a time. For antennas and scatterers excited by short pulses, it is therefore appropriate to extend the near-field techniques to the time domain.

This report addresses the problem of formulating planar near-field antenna measurements in the time domain, so that a single set of time-domain near-field measurements yields the entire field and, in particular, the far-field pattern in the time domain or over a wide range of frequencies. The time-domain planar near-field techniques are developed for both acoustic and electromagnetic fields and the space outside the region occupied by the antenna is assumed to be isotropic and homogeneous. Probe correction is ignored, that is, it is assumed that the probe is ideal so that the exact values of the field on the measurement plane are known.

Two fundamentally different approaches are used in deriving time-domain formulas that give the fields in the half space $z > z_0$ in terms of their values on the plane $z = z_0$. In the first approach the time-domain formulas are obtained by inverse Fourier transforming the corresponding frequency-domain formulas. Since this approach requires extensive use of the frequency-domain near-field formulas, we start by giving a rigorous derivation and review of the frequency-domain formulation that addresses a number of subtleties which have not been dealt with adequately in the literature. As part of this review, planar near-field formulas for the static electric and magnetic fields are derived for the first time. In the second approach the time-domain near-field formulas are derived directly in the time domain. The equivalence of the resulting time-domain formulas obtained by the two different approaches demonstrates

the validity of the formulas and the utility of both approaches.

The report is organized as follows. Chapter 1 introduces the subject, outlines the report, and gives a brief summary of the major results.

Chapter 2 gives a rigorous derivation of the frequency-domain planar near-field formulas. These formulas are given in a form that is useful for the subsequent time-domain derivation. The well-known plane-wave spectrum formulas [3] and Green's function formulas [10] are derived for both acoustic and electromagnetic fields. The validity of the plane-wave spectrum formulas is proven rigorously by showing that they produce the correct field for a general source distribution. It is shown that the spectrum in the plane-wave spectrum formulas has one and only one possible nonremovable singularity and its order is determined. A new derivation of the Green's function formula for the electric field is performed, using the dyadic Dirichlet Green's function for a half space and the dyadic version of Green's second identity. Far-field expressions are derived both from the plane-wave spectrum formulas and from the Green's function formulas. The validity of the far-field formulas is also proven rigorously. It is shown that the evanescent modes in the plane-wave spectrum formulas cannot be neglected when the far field is calculated on-axis, that is, in the direction perpendicular to the scan plane, and when the far field is calculated on the scan plane. For all other angles of observation, the far field from the evanescent modes is negligible compared to the far field from the propagating modes. These asymptotic results agree with Sherman, Stammes, and Lalor [11] and with Nieto-Vesperinas [12]. To derive the far-field formulas from the plane-wave spectrum representation, we use the results of Appendix A on the analyticity and differentiability of the plane-wave spectrum. The frequency dependence of the far field is determined as the frequency approaches zero, and it is shown that, in general, this frequency dependence is different for acoustic and electromagnetic fields.

The propagating part of the spectrum is proportional to the far field, and the evanescent part of the spectrum is proportional to the analytical continuation of the far field to complex angles of observation. If this analytic continuation is possible, the complete spectrum can be obtained from the far field and thus the fields everywhere could be calculated from the far field.

The electromagnetic power radiated through a plane parallel to the scan plane is expressed in terms of the spectrum for the electric field. When the medium surrounding the antenna is lossless, only the propagating modes radiate real power and this power is independent of the distance between the radiator and the plane through which the power is radiated.

The frequency-domain formulas discussed so far are derived for a lossless medium surrounding the sources. When losses are present, most of the formulas remain unchanged except for the propagation constant becoming complex. However, a major difference between the lossless and lossy case is that all modes of the spectrum (not just the evanescent modes) are attenuated in the latter case. Also, it is shown that if the proper constitutive relations are used, magnetic monopoles need not be introduced [13] into Maxwell's time-dependent equations to represent a loss in magnetic materials.

Finally, in Chapter 2 we derive formulas that give the static electric and magnetic fields in the half space $z > z_0$ in terms of their values on the plane $z = z_0$. A variety of different losses

are considered and we determine which field components need be specified on the scan plane $z = z_0$ to calculate the static fields in the half space $z > z_0$. The static case is fundamentally different from the general time-harmonic case because of the different coupling between the static electric and magnetic fields. (For example, when no losses are present the static electric and magnetic fields are uncoupled, whereas the time-harmonic electric and magnetic fields are coupled.)

In Chapter 3 we derive four sets of time-domain near-field formulas using the two different approaches mentioned above. The first set of time-domain formulas is obtained by inverse Fourier transforming the frequency-domain Green's function formulas of Chapter 2 to get the corresponding time-domain Green's function formulas. The class of time functions for which the inverse Fourier transform can be applied is discussed along with the determination of the magnetic field. Next a time-domain Green's function is used along with Green's second identity to derive these time-domain Green's function formulas directly in the time domain. The formulas for the electromagnetic fields are derived using a time-domain Dirichlet dyadic Green's function along with the dyadic version of Green's second identity and agree with those derived by Baum [14]. Far fields are also obtained from these Green's function formulas and the far electric field agrees with the result of Hill [15].

Using the inverse Fourier transform along with the frequency-domain formulas giving the plane-wave spectrum in terms of the far field, a formula is derived expressing the time-domain field everywhere at all times in terms of the time-domain far field and its analytic continuation. This general formula requires the values of the far field for complex angles of observation. It is shown that at times after which all sources have been turned off, this formula reduces to the result of Moses, Nagem, and Sandri [16] which gives the time-domain field everywhere in terms of its far field evaluated at only real observation angles. This last formula is valid only after all sources have been turned off, whereas the analytic continuation of the far field (evanescent spectrum) is also needed to calculate the fields while the sources are on.

It is found that the time-domain far field due to bandlimited sources in a finite region of space is an analytic function of the spherical angles θ and ϕ. This means that a far field with zero sidelobes cannot be generated by sources in a finite region of space unless it is identically zero for all angles of observation. This latter result holds even for sources that are not bandlimited, provided the fields outside the source region can be written as a superposition of time-harmonic fields.

Furthermore, it is shown that the time-domain electromagnetic far fields integrated over all time are zero unless the source current remains nonzero as $t \to \infty$ (or equivalently the electromagnetic frequency-domain far fields evaluated at $\omega = 0$ are zero).

Also, it is proven that the time-domain far fields decay as $1/r$ if the first time derivative of the current is a bounded function of time. Consequently, we prove that "electromagnetic missiles" [17] can be excited only if the first time derivative of the current (or the secant slope if the first time derivative does not exist) becomes infinite at some point in time.

Having obtained the Green's function formulas in the time domain, we investigate the possibilities for obtaining time-domain formulas involving the spatial Fourier transform of

a spectrum, similar to the frequency-domain plane-wave spectrum formulas. This leads to the second set of time-domain formulas giving the field in terms of a double spatial Fourier integral and a time dependent plane-wave spectrum. To determine the field in the half space $z > z_0$ in terms of its values on the plane $z = z_0$, the z dependence of the time-dependent spectrum has to be determined. This is done using the "method of descent" [18, ch.6, sec.12] to solve the partial differential equation satisfied by the spectrum. The final time-domain plane-wave formula is then written down, but due to the complicated z dependence of the spectrum, it has not been possible to express the far field directly in terms of the spectrum.

The third set of time-domain near-field formulas is obtained by taking the inverse Fourier transform of the frequency-domain plane-wave spectrum formulas. These time-domain formulas give the fields in the half space $z > z_0$ in terms of the Radon transform of the fields on the plane $z = z_0$, and involve only real fields evaluated at real times. It is shown that the Radon transforms of the electric and magnetic fields on the plane $z = z_0$ satisfy relations similar to those satisfied by the frequency-domain plane-wave spectra. The time-domain far-field formula obtained from the Radon transform formulas is found to be equivalent to the far-field result obtained from the Green's function formulas.

Finally, the fourth set of time-domain formulas are derived in Chapter 3 by using the analytic Fourier transform in conjunction with the frequency-domain plane-wave spectrum formulas. The resulting time-domain planar near-field formulas are three-dimensional vector analogs to two-dimensional scalar formulas in Steinberg, Heyman, and Felsen [19]. These formulas, which also involve the Radon transform, are simpler in form than the formulas of the third set, but they involve analytic fields that cannot be measured directly. This fact makes these formulas less attractive for near-field measurements than the Radon transform formulas derived from the standard Fourier transform and the Green's function formulas.

Chapter 4 presents and compares two different computation schemes to numerically calculate the time-domain far-field pattern from sampled time-domain near-field data. The sampled time-domain near-field data are obtained by measuring the near-field at discrete points on a finite scan plane at discrete times.

The first scheme, called the frequency-domain computation scheme, is based on the frequency-domain formulation in Chapter 2. This frequency-domain scheme consists of the following three steps: (1) use the Fourier transform to calculate the frequency-domain near field from the time-domain near field, (2) calculate the frequency-domain far field from the frequency-domain near field, and (3) use the inverse Fourier transform to calculate the time-domain far field from the frequency-domain far field. This scheme makes use of well-known frequency-domain far-field formulas, sampling theorems, and the fast Fourier transform (FFT).

The second scheme, called the time-domain computation scheme, is based on the time-domain formulation in Chapter 3. This time-domain scheme simply uses the formula that directly gives the time-domain far field in terms of the time-domain near field. A time-domain sampling theorem is derived to determine how small the sample spacing between points on the scan plane has to be to calculate the far field accurately. Furthermore, the number of time samples needed for accurate far-field calculations from the near fields of

different types of radiators is determined.

The two computation schemes are compared and used to calculate the far-field pattern of a simple acoustic point-source antenna from near-field data. It is found that the direct time-domain computation scheme is much simpler to program and use than the frequency-domain computation scheme. However, because the frequency-domain computation scheme uses the FFT it is much faster for large antennas than the time-domain computation scheme when the full far field is calculated for all times.

When only part of the far field is calculated, the difference in computer time for the two computation schemes becomes smaller and the time-domain computation scheme therefore becomes more advantageous because of its simplicity. Furthermore, the duration of the far-field pattern is extended erroneously due to the finite-size scan plane and this longer time-duration has to be taken into account in the frequency-domain calculation scheme. Specifically, the frequency spacing in the frequency-domain computation scheme has to be chosen small enough so that significant time-domain aliasing is avoided in the calculation of the time-domain far-field pattern. The problem of choosing the frequency spacing small enough does not occur for the time-domain computation scheme because no frequency spacing is used.

Furthermore, the time-domain computation scheme can be used to calculate the far-field pattern at early times from near-field measurements taken at early times only. This capability is not possessed by the frequency-domain computation scheme because the near field is required for its entire duration to calculate its Fourier transform. For many antennas fed by short pulses, the time dependence of both the near field and far field consists of an early-time part, which contains most of the power, and a late-time part which is oscillatory and contains little power. The duration of the early-time part may be much smaller than the duration of the entire field. If only the early-time part of the far field is of interest, one can use the time-domain computation scheme to determine this part from near-field measurements taken for early times only; thereby significantly reducing the number of near-field time samples needed for the far-field calculation. If instead, the frequency-domain computation scheme is used, the number of near-field time samples cannot be reduced because time samples taken over the entire duration of the near field are needed to calculate the Fourier transform of the near field.

No matter which scheme is chosen, planar time-domain near-field antenna measurements can eliminate the error in the far-field pattern due to the finite scan plane because this error is separated in time from the correct far-field pattern. This makes it possible to use planar scanning in the time domain to compute the far fields of broadbeam antennas in both the time and frequency domains.

In addition to the four chapters, the report contains two appendices. Appendix A proves differentiability and analyticity with respect to two spectral variables of the frequency-domain plane-wave spectrum and its related far-field functions. In Appendix B, we derive formulas that give the time-domain far field directly in terms of the sources, and determine conditions on the current that assure the validity of the far-field expressions.

Chapter 2

Frequency-Domain Formulas

The planar near-field frequency-domain formulas will be derived in this chapter for both acoustic and electromagnetic fields. Section 2.1 derives the plane-wave spectrum and Green's function representations for both acoustic and electromagnetic fields in a half space in terms their values on a plane. The plane-wave spectrum formulas are proven valid by showing that they produce the correct field of a general source distribution located in a finite region of space. The singularities of the spectrum are also determined explicitly for a finite source distribution. Far-field formulas are derived in Section 2.2, and the contributions to the far field from the evanescent modes are determined. Furthermore, the plane wave spectrum is given in terms of the far field in spherical coordinates. Section 2.3 calculates the power radiated through a plane and Section 2.4 deals with lossy media. The special cases of static electric and magnetic fields in media with different types of losses are analyzed in Section 2.5.

The planar scanning geometry shown in Figure 2.1 will be considered. The arbitrary finite source region is located in the half space $z < z_0$ and the values of the fields are measured on the plane $z = z_0$. Except in Section 2.4 on relations in lossy media, and in Section 2.5 on statics, the part of space not occupied by the sources is lossless free space with permeability μ and permittivity ϵ. In addition to the rectangular coordinates (x, y, z), the usual spherical coordinates (r, θ, ϕ) defined by $x = r\cos\phi\sin\theta$, $y = r\sin\phi\sin\theta$, and $z = r\cos\theta$ will also be used.

The planar near-field formulas will be derived in detail for the case where the measurement plane is located to the right of the source region as in Figure 2.1. The necessary modifications are stated for the case where the sources are located to the left of the measurement plane. Throughout the report, $e^{-i\omega t}$ time dependence is suppressed in all the time-harmonic equations. It is assumed that the frequency ω is positive except, of course, in the static equations of Section 2.5.

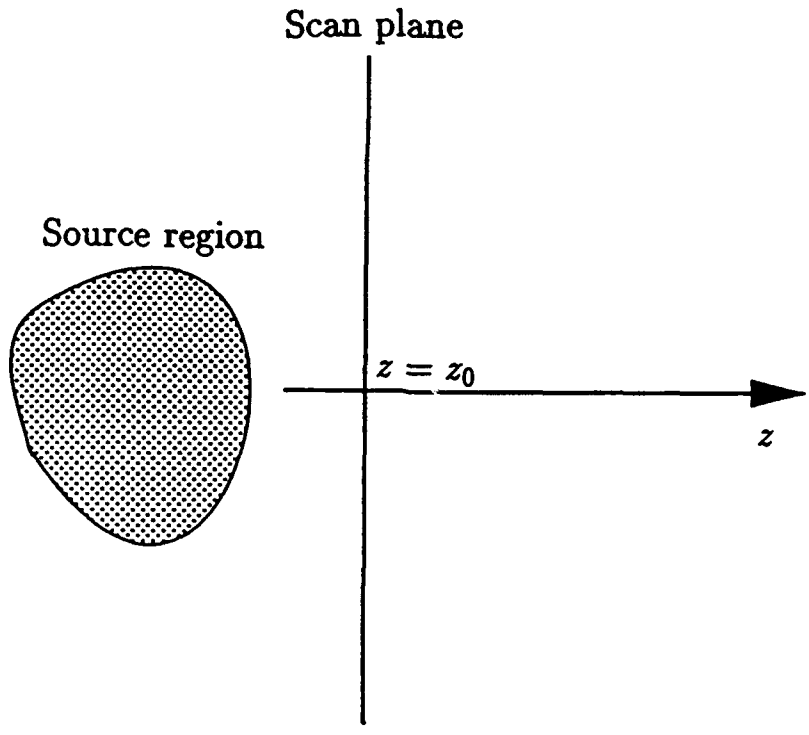

Figure 2.1: Planar scanning geometry.

2.1 Basic Planar Near-Field Formulas

The basic planar near-field formulas are derived in this section for both acoustic and electromagnetic fields. Both plane-wave spectrum and Green's function representations will be derived. Most of the plane-wave spectrum formulas can be found in Kerns [3], [20] and the Green's function formula for the electric field can be found in Jackson [10, sec.9.10]. However, the plane-wave spectrum formulas are proven valid rigorously for the first time and a new derivation of the Green's function formulas is given in this section.

2.1.1 Plane-Wave Spectrum Representations

Let us first derive formulas for a scalar acoustic field Φ satisfying the scalar Helmholtz equation

$$\nabla^2\Phi(\bar{r}) + k^2\Phi(\bar{r}) = 0, \quad z > z_0 \tag{2.1}$$

in the free-space region. (Then Φ can also be any rectangular electric or magnetic-field component.) The finite source region is located in the half space $z < z_0$ as shown in Figure 2.1. The plane-wave spectrum formulas are derived heuristically in this section and then validated rigorously in the next section.

Begin by expressing the field in terms of the spatial Fourier integral

$$\Phi(\bar{r}) = \frac{1}{2\pi}\int_{-\infty}^{+\infty}\int_{-\infty}^{+\infty} b(k_x,k_y,z)e^{i(k_x x+k_y y)}dk_x dk_y, \quad z \geq z_0 \tag{2.2}$$

where b is the Fourier transform of $\Phi(\bar{r})$ given by

$$b(k_x,k_y,z) = \frac{1}{2\pi}\int_{-\infty}^{+\infty}\int_{-\infty}^{+\infty} \Phi(x,y,z)e^{-i(k_x x+k_y y)}dxdy, \quad z \geq z_0. \tag{2.3}$$

Inserting the Fourier integral (2.2) into the Helmholtz equation (2.1), and taking the inverse Fourier transform, one finds that the function b satisfies

$$\left[\frac{\partial^2}{\partial z^2} + \gamma^2\right] b(k_x,k_y,z) = 0, \quad \gamma^2 = k^2 - k_x^2 - k_y^2. \tag{2.4}$$

Consequently for $\gamma \neq 0$ we have

$$b(k_x,k_y,z) = T_1(k_x,k_y)e^{i\gamma z} + T_2(k_x,k_y)e^{-i\gamma z} \tag{2.5}$$

where T_1 and T_2 are independent of z, and γ is defined to be positive for $k_x^2 + k_y^2 < k^2$ and to have a positive imaginary part when $k_x^2 + k_y^2 > k^2$. The field Φ decays as $z \to \infty$ and thus from the Fourier representation (2.2) we see that T_2 must be zero for imaginary γ. For real γ, an asymptotic evaluation (see Section 2.2.3) of (2.2) with b inserted from (2.5) shows that T_2 must be zero if no energy is coming in from $z = +\infty$. Therefore, (2.5) reduces to

$$b(k_x,k_y,z) = T(k_x,k_y)e^{i\gamma z}, \quad z \geq z_0 \tag{2.6}$$

where T is independent of z and is called the plane-wave spectrum of Φ. For $\gamma = 0$ it is found that

$$b(k_x,k_y,z) = b_1(k_x,k_y) + zb_2(k_x,k_y), \quad k_x^2 + k_y^2 = k^2 \tag{2.7}$$

where b_1 and b_2 are independent of z. Since the area in the (k_x,k_y) plane of the region where $k_x^2 + k_y^2 = k^2$ is zero, the contribution to the integral (2.2) from that region is zero and we do not need to include (2.7) in the spectral integral (2.2). (We are assuming the sources are in a finite region of space so that $b(k_x,k_y,z)$ does not contain delta functions in k_x and k_y. Moreover, the solution (2.7) does not satisfy the boundary condition of zero field at $z = +\infty$.)

Inserting b from (2.6) into the Fourier representation (2.2) one finds

$$\Phi(\bar{r}) = \frac{1}{2\pi}\int_{-\infty}^{+\infty}\int_{-\infty}^{+\infty} T(k_x,k_y)e^{i(k_x x+k_y y+\gamma z)}dk_x dk_y, \quad z \geq z_0 \tag{2.8}$$

and that the spectrum is given by

$$T(k_x,k_y) = \frac{e^{-i\gamma z}}{2\pi}\int_{-\infty}^{+\infty}\int_{-\infty}^{+\infty} \Phi(x,y,z)e^{-i(k_x x+k_y y)}dxdy, \quad z \geq z_0. \tag{2.9}$$

If z is set equal to z_0 in (2.9), the formula (2.8) gives the field Φ for $z \geq z_0$ in terms of Φ on the plane $z = z_0$. The formulas (2.8) and (2.9) comprise the plane-wave spectrum representation of Φ. In Section 2.1.2 it is shown that they produce the correct field provided the integral in (2.9) is calculated in a prescribed manner. (If the finite source region is located in the half space $z > z_0$ the field for $z \leq z_0$ is given by (2.8) and (2.9) with γ replaced by $-\gamma$.)

As will be shown in Section 2.1.2, for solutions to the wave equation with sources in a finite region of space, the fields are well-defined by (2.8) at every point in the half space $z \geq z_0$. However, Section 2.1.2 also shows that the spectrum given by (2.9) is well-defined at every (k_x, k_y) except possibly at $k_x = k_y = 0$, and $\gamma = 0$.

Now consider the electric field $\bar{E}$. Since each of its rectangular components satisfies the Helmholtz equation (2.1) in the free-space region, and since they all are of order r^{-1} at infinity, the plane wave spectrum representation of the electric field is immediately found from (2.8) and (2.9) to be

$$\bar{E}(\bar{r}) = \frac{1}{2\pi} \int_{-\infty}^{+\infty} \int_{-\infty}^{+\infty} \bar{T}(k_x, k_y) e^{i(k_x x + k_y y + \gamma z)} dk_x dk_y, \quad z \geq z_0 \tag{2.10}$$

and the spectrum $\bar{T}$ for the electric field is given by

$$\bar{T}(k_x, k_y) = \frac{e^{-i\gamma z}}{2\pi} \int_{-\infty}^{+\infty} \int_{-\infty}^{+\infty} \bar{E}(x, y, z) e^{-i(k_x x + k_y y)} dx dy, \quad z \geq z_0. \tag{2.11}$$

If z is set equal to z_0 in (2.11), the formula (2.10) gives the electric field for $z \geq z_0$ in terms of the electric field on the plane $z = z_0$. Since the electric field has zero divergence it is found that the spectrum for the electric field satisfies

$$\bar{T}(k_x, k_y) \cdot \bar{k} = 0 \tag{2.12}$$

where $\bar{k}$ is defined by

$$\bar{k} = k_x \hat{x} + k_y \hat{y} + \gamma \hat{z}. \tag{2.13}$$

That is, $\bar{T}$ is perpendicular to the propagation direction of the plane wave $e^{i(k_x x + k_y y + \gamma z)} = e^{i\bar{k} \cdot \bar{r}}$. Consequently for $\gamma \neq 0$, T_z can be found from T_x and T_y and thus the electric field in the free-space region $z \geq z_0$ is determined uniquely by specifying E_x and E_y on the measurement plane $z = z_0$.

The z component of the electric field can also be found directly from the x and y components by integrating $\nabla \cdot \bar{E} = 0$ with respect to z, to obtain the formula

$$E_z(\bar{r}) = -\int_{z_0}^{z} \left[\frac{\partial}{\partial x} E_x(x, y, z') + \frac{\partial}{\partial y} E_y(x, y, z') \right] dz' + C(x, y), \quad z \geq z_0 \tag{2.14}$$

where $C(x, y)$ is a function of x and y only. Since the sources of the electromagnetic field are contained in a finite region of space, the amplitude of the electric field is of order r^{-1} at infinity so $E_z \to 0$ as $r \to \infty$. Therefore

$$E_z(\bar{r}) = \int_{z}^{+\infty} \left[\frac{\partial}{\partial x} E_x(x, y, z') + \frac{\partial}{\partial y} E_y(x, y, z') \right] dz', \quad z \geq z_0 \tag{2.15}$$

and thus E_z is determined uniquely from E_x and E_y in the source-free half space $z \geq z_0$.

Using the induction law $\nabla \times \bar{E} = i\omega\mu\bar{H}$, which gives the magnetic field in terms of the electric field, it is found that the magnetic field is given by (2.10) with $\bar{T}$ replaced by

$$\bar{T}_H(k_x, k_y) = \sqrt{\frac{\epsilon}{\mu}}\bar{k} \times \bar{T}(k_x, k_y) \tag{2.16}$$

that is,

$$\bar{H}(\bar{r}) = \frac{1}{2\pi}\int_{-\infty}^{+\infty}\int_{-\infty}^{+\infty} \bar{T}_H(k_x, k_y)e^{i(k_x x + k_y y + \gamma z)}dk_x dk_y, \quad z \geq z_0 \tag{2.17}$$

where $\bar{T}_H$ is the spectrum for the magnetic field also given by

$$\bar{T}_H(k_x, k_y) = \frac{e^{-i\gamma z}}{2\pi}\int_{-\infty}^{+\infty}\int_{-\infty}^{+\infty} \bar{H}(x, y, z)e^{-i(k_x x + k_y y)}dxdy, \quad z \geq z_0 \tag{2.18}$$

and $\hat{k} = k^{-1}\bar{k}$ with $\bar{k}$ given by (2.13). Because the divergence of the magnetic field is zero in the free-space region, the spectrum for the magnetic field also satisfies (2.12) [as is seen directly from (2.16)].

As with the electric field, the tangential components of the magnetic field on the plane $z = z_0$ uniquely determine all the field components in the half space $z > z_0$. Also, H_z can be determined from H_x and H_y in the half space $z \geq z_0$ by the formula (2.15) with $\bar{E}$ replaced by $\bar{H}$. In general, any two of the six components of $\bar{E}$ and $\bar{H}$ on the plane $z = z_0$ determine all fields in the half space $z > z_0$. We do not prove this more general result in this section because the method of proof is identical to that used later in proving the analogous result for the static equations of Section 2.5.3.

In principle, once the spectrum is computed from the measured data on the plane $z = z_0$ (2.10) and (2.17) can be used to compute the electric and magnetic fields on any z plane (not just $z \geq z_0$) up to the source region. In practice, however, the scan plane $z = z_0$ is usually chosen a few wavelengths away from the test antenna to keep multiple reflections between the probe and test antenna at an acceptably low level. This means that most of the evanescent fields have decayed to a value too small to be detected by the measurement system. Thus, most of the evanescent part of the spectrum could not be computed with any accuracy from the measured data in (2.11) or (2.18) on the plane $z = z_0$, and the evanescent fields, which may dominate in the region a few wavelengths from the source, could not be computed from (2.10) or (2.17).

(If the sources are located in the half space $z > z_0$, the electromagnetic field formulas (2.10)-(2.18) are valid for $z \leq z_0$ if γ is replaced by $-\gamma$.)

2.1.2 Validation of Plane-Wave Spectrum Representations

In this section the validity of the plane-wave spectrum formulas is proven. Since the proofs for the acoustic formulas and the electromagnetic formulas are very similar, we shall consider only the acoustic formulas.

Before proving the validity of the acoustic plane-wave spectrum formulas (2.8) and (2.9) we note that the acoustic field is neither absolutely integrable nor square integrable on any plane $z = z_0$. This follows from the fact that $\Phi(x, y, z_0) = O[(x^2 + y^2)^{-1/2}]$ as $(x^2 + y^2)^{1/2} \to \infty$ so that both the integrals $\int_{-\infty}^{+\infty} \int_{-\infty}^{+\infty} |\Phi(x, y, z_0)| dx dy$ and $\int_{-\infty}^{+\infty} \int_{-\infty}^{+\infty} |\Phi(x, y, z_0)|^2 dx dy$ are infinite. Consequently, the theory of the Fourier transform in the Lebesgue spaces L_1 or L_2 [21], [22] cannot be used to prove the validity of (2.8) and (2.9) because the acoustic field belongs neither to L_1 or L_2. (Note that the energy radiated through the plane $z = z_0$ is proportional to the integral of $\Phi \frac{\partial}{\partial z} \Phi^*$ over this plane [20]. This energy is finite even though the integral of $|\Phi|^2$ over the plane $z = z_0$ is infinite.)

To prove (2.8) and (2.9), start with Green's second identity and the radiation condition for the acoustic field to show that the acoustic field can be written as [23, p.62]

$$\Phi(\bar{r}) = \int_S \left[\Phi(\bar{r}') \frac{\partial}{\partial n'} G(\bar{r}, \bar{r}') - G(\bar{r}, \bar{r}') \frac{\partial}{\partial n'} \Phi(\bar{r}') \right] dS'. \tag{2.19}$$

Here S is a finite smooth surface which is located in the free-space part of the half space $z < z_0$ and encloses the finite source region. It is assumed that the fields in free space and their first time derivatives are continuous functions of position. $G(\bar{r}, \bar{r}')$ is the free-space Green's function given by

$$G(\bar{r}, \bar{r}') = \frac{e^{ikR}}{4\pi R}, \quad R = |\bar{r} - \bar{r}'|. \tag{2.20}$$

The formula (2.19) is valid when the observation point $\bar{r}$ is outside S and is the scalar analog to the vector electromagnetic formulas (A.5) and (A.6) of Appendix A.

Next specify that the integral in the expression (2.9) for the spectrum T be calculated in polar coordinates with the angular integration performed first, that is

$$T(k_x, k_y) = \frac{e^{-i\gamma z_0}}{2\pi} \int_0^{+\infty} \rho \int_0^{2\pi} \Phi(\rho \cos\phi, \rho \sin\phi, z_0) e^{-i\rho(k_x \cos\phi + k_y \sin\phi)} d\phi d\rho \tag{2.21}$$

where the polar coordinates (ρ, ϕ) are given by $x = \rho \cos\phi$ and $y = \rho \sin\phi$. Alternatively, this integral could be calculated in rectangular coordinates by first evaluating the double integral over a finite rectangle with a fixed side length ratio and then letting the side lengths of the rectangle approach infinity. These two ways of calculating the spectrum are exactly the two ways used for most practical planar near-field measurements. Section 2.1.3 discusses some practical differences between using circular and rectangular scan planes.

Write the integral (2.21) as the limit

$$T(k_x, k_y) = \frac{e^{-i\gamma z_0}}{2\pi} \lim_{N \to \infty} \int_0^{N} \rho \int_0^{2\pi} \Phi(\rho \cos\phi, \rho \sin\phi, z_0) e^{-i\rho(k_x \cos\phi + k_y \sin\phi)} d\phi d\rho \tag{2.22}$$

where N is an integer, and insert the expression (2.19) for the acoustic field into (2.22). Note that Φ, $\frac{\partial}{\partial n'}\Phi$, G, and $\frac{\partial}{\partial n'}G$ are continuous functions on the bounded closed surface S and on the bounded circular disk with radius N. Then use the theorems of Hobson [24, p.339, p.359] to show that the integral over S can be interchanged with the integrations over ρ and

ϕ and that the normal derivative can be brought outside the ρ and ϕ integrals so that the spectrum is given by

$$T(k_x,k_y)=\frac{e^{-i\gamma z_0}}{2\pi}\lim_{N\to\infty}\int_S\Phi(\bar{r}')\frac{\partial}{\partial n'}\int_0^N\rho\int_0^{2\pi}G(\bar{r},\bar{r}')e^{-i\rho(k_x\cos\phi+k_y\sin\phi)}d\phi d\rho dS'$$
$$-\frac{e^{-i\gamma z_0}}{2\pi}\lim_{N\to\infty}\int_S\int_0^N\rho\int_0^{2\pi}G(\bar{r},\bar{r}')e^{-i\rho(k_x\cos\phi+k_y\sin\phi)}d\phi d\rho\frac{\partial}{\partial n'}\Phi(\bar{r}')dS'. \tag{2.23}$$

We will now use standard theorems on the validity of interchanging limits and integrals to show that the limit in (2.23) can be brought inside the integral over S. To do this define a sequence of functions by

$$f_N(\bar{r}',k_x,k_y)=\int_0^N\rho\int_0^{2\pi}G(\bar{r},\bar{r}')e^{-i\rho(k_x\cos\phi+k_y\sin\phi)}d\phi d\rho \tag{2.24}$$

and introduce new polar coordinates (ρ_1,ϕ_1) so that $x-x'=\rho_1\cos\phi_1$ and $y-y'=\rho_1\sin\phi_1$. With these new polar coordinates as integration variables it is found that

$$\lim_{N\to\infty}f_N(\bar{r}',k_x,k_y)=\frac{e^{-i(k_xx'+k_yy')}}{2\pi}\int_0^{+\infty}\rho_1\frac{e^{ik\sqrt{\rho_1^2+(z_0-z')^2}}}{\sqrt{\rho_1^2+(z_0-z')^2}}\int_0^{\pi}\cos(\rho_1\sqrt{k_x^2+k_y^2}\sin\phi_1)d\phi_1d\rho_1. \tag{2.25}$$

At this point of the derivation we do not know if this limit exists. From the integral expression for the Bessel function of zero order it is found that the integral over ϕ_1 is simply $\pi J_0(\rho_1\sqrt{k_x^2+k_y^2})$. For $(k_x,k_y)\neq(0,0)$ the remaining integral over ρ_1 can then be calculated from the formula in [25, eq.(25), p.9] and we find that

$$\lim_{N\to\infty}f_N(\bar{r}',k_x,k_y)=\frac{i}{2\gamma}e^{-i(k_xx'+k_yy'+\gamma(z'-z_0))}. \tag{2.26}$$

This calculation shows that the limit of the function f_N exists for all $\bar{r}'$ and for all (k_x,k_y) except at $\gamma=0$ and at $(k_x,k_y)=(0,0)$. Furthermore, the limit of f_N is a continuous function of $\bar{r}'$ on the bounded closed surface S so f_N converges uniformly with respect to $\bar{r}'$. From the standard theorem on limits of integrals in Hobson [24, p.293] it now follows that the limit in the second term of (2.23) can be brought inside the integral over S except for $\gamma=0$ and for $(k_x,k_y)=(0,0)$. Similarly, it is found that $\frac{\partial}{\partial n'}f_N$ converges uniformly with respect to $\bar{r}'$ so that the limit in the first term of (2.23) can be brought inside the integral over S [24, p.293] and inside the normal-derivative operator [26, p.282] except for $\gamma=0$ and for $(k_x,k_y)=(0,0)$. For $\gamma\neq0$ and $(k_x,k_y)\neq(0,0)$ the expression (2.23) for the spectrum then becomes

$$T(k_x,k_y)=\frac{i}{4\pi\gamma}\int_S\left[\Phi(\bar{r}')\frac{\partial}{\partial n'}e^{-i(k_xx'+k_yy'+\gamma z')}-e^{-i(k_xx'+k_yy'+\gamma z')}\frac{\partial}{\partial n'}\Phi(\bar{r}')\right]dS'. \tag{2.27}$$

This is the final expression for the spectrum given in terms of the acoustic field on the finite surface S and it is the scalar analog to the vector formula (A.1) in Appendix A with $\bar{F}$ and $\bar{U}$ substituted from (A.2) and (A.7).

Note that although the expression (2.27) is not valid for $(k_x, k_y) = (0,0)$ it remains finite and approaches a bounded value as $(k_x, k_y) \to (0,0)$, which shows that the spectrum has a removable singularity at $(k_x, k_y) = (0,0)$. Furthermore, it is seen that the only other possible singularity of the spectrum is at $\gamma = 0$ and that its order is γ^{-1}, which is integrable with respect to (k_x, k_y).

Insert the expression (2.27) for the spectrum into (2.8) and note that the resulting integrand is absolutely integrable because $\gamma = i|\gamma|$ for $k_x^2 + k_y^2 > k^2$. Therefore we do not have to specify how the integrals over (k_x, k_y) are calculated. We can directly use the theorems in Hobson [24, pp.339, 355] to show that the integral over S can be interchanged with the integral over (k_x, k_y) and that the normal-derivative operator can be brought outside the integral over (k_x, k_y). Thus, the plane-wave spectrum formulas predict that the acoustic field in the half space $z \geq z_0$ is given by

$$\Phi(\bar{r}) = \frac{i}{8\pi^2} \int_S \left[\Phi(\bar{r}') \frac{\partial}{\partial n'} \int_{-\infty}^{+\infty} \int_{-\infty}^{+\infty} \frac{e^{i[k_x(x-x')+k_y(y-y')+\gamma(z-z')]}}{\gamma} dk_x dk_y \right.$$
$$\left. - \int_{-\infty}^{+\infty} \int_{-\infty}^{+\infty} \frac{e^{i[k_x(x-x')+k_y(y-y')+\gamma(z-z')]}}{\gamma} dk_x dk_y \frac{\partial}{\partial n'} \Phi(\bar{r}') \right] dS'. \tag{2.28}$$

Using the identity in Weyl [27] or Lalor [28]

$$\frac{i}{8\pi^2} \int_{-\infty}^{+\infty} \int_{-\infty}^{+\infty} \frac{e^{i[k_x(x-x')+k_y(y-y')+\gamma(z-z')]}}{\gamma} dk_x dk_y = G(\bar{r}, \bar{r}') \tag{2.29}$$

which can be proven by direct calculation, it is seen from the exact formula (2.19) that the result (2.28) predicted by the plane-wave spectrum formulas is correct. We have now shown that the plane-wave spectrum formulas (2.8) and (2.9) are valid provided that the integral for the spectrum is calculated in the way described in this section, which is consistent with the way practical calculations are performed for planar near-field scanning. By starting with $\bar{E}$ from (A.5) inserted into the integrand of (2.11), the validity of the plane-wave spectrum formulas (2.10) and (2.11) for the electromagnetic fields is proven in a manner similar to that used for the acoustic formulas.

2.1.3 Singularities of the Spectrum

This section determines the possible singularities of the spectrum and writes the spectrum in a form that is convenient for the asymptotic analysis of Section 2.2.3. As noted in Section 2.1.2, (2.27) shows that the spectrum $T(k_x, k_y)$ is a continuous bounded function of k_x and k_y except possibly at $\gamma = 0$. Therefore, the spectrum may be written as

$$T(k_x, k_y) = \frac{i}{\gamma} F(k_x, k_y) \tag{2.30}$$

for all (k_x, k_y), where F is a continuous bounded function for all (k_x, k_y). Similarly, in the electromagnetic case, we have

$$\bar{T}(k_x, k_y) = \frac{i}{\gamma} \bar{F}(k_x, k_y). \tag{2.31}$$

Furthermore, in Appendix A it is shown that the function $\bar{F}$ (or F) is infinitely differentiable for all (k_x, k_y) except possibly at $\gamma = 0$. (For F this can also be seen directly from (2.27).) Appendix A shows also that $\bar{F}$ (or F) is an infinitely differentiable function of (γ, k_ϕ), except possibly at $\gamma = k$, when the propagation vector is expressed in polar coordinates.

The γ^{-1} singularity in the spectrum $\bar{T}$ is also exhibited by the formulas in Kerns [3, ch.3, eqs.(2.2-7a), (2.2-7b)] (also see Appendix A) relating spectra to the prescribed currents. Substituting T from (2.30) into (2.64) or $\bar{T}$ from (2.31) into (2.65) shows that $F(k_x, k_y)$ or $\bar{F}(k_x, k_y)$ represents the complex far-field pattern of the source region when $k_x^2 + k_y^2 < k^2$, that is, when γ is real so that the associated plane waves are propagating.

Before leaving this section, note that (2.21) (or its electromagnetic vector analog) is the integral that one evaluates to determine the spectrum (or far field) of a radiator from measured data taken in plane-polar coordinates [29]. For practical measurements the infinite radial limit of integration in (2.21) is replaced by the finite radius of the circular scan plane. Thus, the results of Section 2.1.2 show that the on-axis far field ($k_x = k_y = 0$) evaluated from (2.21) diverges by oscillation no matter how large a radius is chosen for the circular scan plane. (The integral over ϕ_1 in (2.25) is simply equal to π so that the integral over ρ_1 diverges by oscillation.) For the main beam of directive radiators the oscillation is usually negligible. However, for broadbeam radiators the oscillation can severely limit the accuracy of the far-field pattern near the z axis computed from plane-polar, measured near-field data. For a rectangular scan plane, the integral corresponding to (2.21) converges for all $k_x^2 + k_y^2 < k^2$ including the on-axis direction ($k_x = k_y = 0$), as the size of the rectangular scan plane approaches infinity. However, for broadbeam antennas and practical size rectangular scan planes, the computed far fields near the z axis may be in error by several decibels [30]. This limitation in the measurement of broadbeam antennas by planar near-field scanning in the frequency domain was discussed in References [30] and [1]. In Section 4.4 we show that these finite-scan errors can be avoided in the time domain.

(When the sources are located in the half space $z > z_0$ the formulas in this section hold for the fields in the half space $z \leq z_0$ provided that the spectrum is given by (2.9) with γ replaced by $-\gamma$.)

2.1.4 Green's Function Representations

Representations involving the free-space Green's functions for the fields in the half space $z > z_0$ in terms of fields on the plane $z = z_0$ are derived in this section for both acoustic and electromagnetic fields.

First consider the scalar acoustic field Φ satisfying the Helmholtz equation (2.1) in the free-space region. Green's second identity will be used in the following to derive the representation for this field. The free-space Green's function $G(\bar{r}, \bar{r}')$ satisfying $\nabla^2 G(\bar{r}, \bar{r}') + k^2 G(\bar{r}, \bar{r}') = -\delta(\bar{r} - \bar{r}')$ is given by (2.20) and the Dirichlet Green's function for the half space $z \geq z_0$ is given by

$$G_D(\bar{r}, \bar{r}') = G(\bar{r}, \bar{r}') - G(\bar{r}, \bar{r}_i'), \quad \bar{r}_i' = x'\hat{x} + y'\hat{y} + (2z_0 - z')\hat{z}. \tag{2.32}$$

Let the surface $C(R_0)$ be the circular disk: $x^2+y^2 \le R_0^2,\ z=z_0$, and let $S(R_0)$ be the half sphere: $x^2+y^2+(z-z_0)^2=R_0^2,\ z \ge z_0$ as shown in Figure 2.2.

Green's second identity applied to the region bounded by $S(R_0) \cup C(R_0)$ gives

$$-\Phi(\bar{r}') = \int_{S(R_0)\cup C(R_0)} \left[\Phi(\bar{r})\frac{\partial}{\partial n}G_D(\bar{r},\bar{r}') - G_D(\bar{r},\bar{r}')\frac{\partial}{\partial n}\Phi(\bar{r})\right] dS \qquad (2.33)$$

where $\bar{r}'$ is inside the region bounded by $S(R_0) \cup C(R_0)$ and $\hat{n}$ is the normal out of this region. On the disk $C(R_0)$, $\frac{\partial}{\partial n}G_D = -2\frac{\partial}{\partial z}G$ and $G_D = 0$. On the half sphere $S(R_0)$ it is found that the expression in the square brackets in (2.33) can be written in terms of the free-space Green's function as

$$\Phi\frac{\partial}{\partial n}G_D - G_D\frac{\partial}{\partial n}\Phi = \Phi\frac{\partial}{\partial r}G_D - G_D\frac{\partial}{\partial r}\Phi = G\left[\hat{r}\cdot\hat{R}ik\Phi - \frac{\partial}{\partial r}\Phi\right]$$

$$- G_i\left[\hat{r}\cdot\hat{R}_i ik\Phi - \frac{\partial}{\partial r}\Phi\right] - \Phi\left[\frac{1}{R}\hat{r}\cdot\hat{R}G - \frac{1}{R_i}\hat{r}\cdot\hat{R}_i G_i\right] \qquad (2.34)$$

where $G_i = G(\bar{r},\bar{r}_i')$, $\hat{R} = (\bar{r}-\bar{r}')R^{-1}$, $\hat{R}_i = (\bar{r}-\bar{r}_i')R_i^{-1}$, and $R_i = |\bar{r}-\bar{r}_i'|$. Using the asymptotic relations $\hat{r}\cdot\hat{R} = 1+O(r^{-1})$ and $\hat{r}\cdot\hat{R}_i = 1+O(r^{-1})$, the radiation conditions for the acoustic field [23, p.57]: $\Phi = O(r^{-1})$ and $R\left[\frac{\partial}{\partial r}\Phi - ik\Phi\right] \to 0$ at infinity, along with (2.34) shows that the integrand in (2.33) on $S(R_0)$ goes to zero faster than R_0^{-2}. Consequently, the contribution to the integral in (2.33) from $S(R_0)$ vanishes as $R_0 \to +\infty$ and (2.33) reduces to

$$\Phi(\bar{r}) = 2\int_{-\infty}^{+\infty}\int_{-\infty}^{+\infty}\Phi(\bar{r}')\frac{\partial}{\partial z'}G(\bar{r},\bar{r}')dx'dy',\quad z>z_0 \qquad (2.35)$$

where $\bar{r}$ and $\bar{r}'$ have been interchanged and $\bar{r}' = x'\hat{x}+y'\hat{y}+z_0\hat{z}$. Taking the z' derivative of the Green's function, we may write (2.35) as

$$\Phi(\bar{r}) = \frac{z_0-z}{2\pi}\int_{-\infty}^{+\infty}\int_{-\infty}^{+\infty}\Phi(\bar{r}')\left[ik-\frac{1}{R}\right]\frac{e^{ikR}}{R^2}dx'dy',\quad z>z_0 \qquad (2.36)$$

with $R = \sqrt{(x-x')^2+(y-y')^2+(z-z_0)^2}$. The formula (2.36) (or (2.35)) is the Green's function representation for the acoustic field Φ in the half space $z > z_0$ given in terms of Φ on the plane $z = z_0$. These formulas will prove valuable in Chapter 3 for obtaining the corresponding time-domain representations. The Green's function representations can also be derived from the plane-wave representations (2.8) and (2.9) by using the identity

$$2\pi\frac{\partial}{\partial z}\frac{e^{ikR}}{R} = -\int_{-\infty}^{+\infty}\int_{-\infty}^{+\infty}e^{i(k_x(x-x')+k_y(y-y')+\gamma(z-z_0))}dk_x dk_y,\quad z>z_0 \qquad (2.37)$$

which may be proven directly by expanding the free-space Green's function in a plane wave spectrum, or by taking the derivative of (2.29).

(If the sources are located in the half space $z > z_0$, the acoustic field for $z < z_0$ is given by the negative of (2.35) or (2.36).)

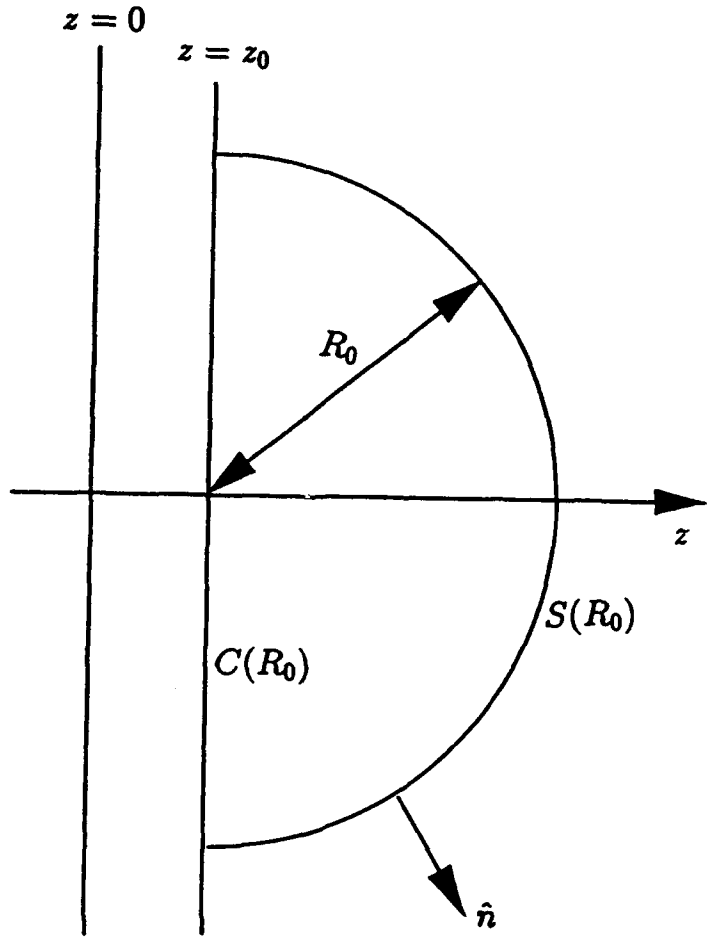

Figure 2.2: Half sphere of radius R_0 in a rectangular coordinate system.

After having dealt with the acoustic fields, consider the electromagnetic fields. Because each of the rectangular components of the electric field $\bar{E}$ satisfies the scalar Helmholtz equation (2.1), the scalar formula (2.36) immediately gives

$$\bar{E}(\bar{r}) = \frac{z_0 - z}{2\pi} \int_{-\infty}^{+\infty} \int_{-\infty}^{+\infty} \bar{E}(\bar{r}') \left[ik - \frac{1}{R} \right] \frac{e^{ikR}}{R^2} dx'dy', \quad z > z_0 \tag{2.38}$$

where it has been assumed that each rectangular component of the electric field satisfies the scalar radiation conditions [23, p.57]. The formula (2.38) gives the field in the half space $z > z_0$ in terms of all three components of the electric field on the plane $z = z_0$.

Next we will derive a formula that gives the electric field in the half space $z > z_0$ in terms of only the tangential components of the electric field on the plane $z = z_0$. To do this, employ the dyadic version of Green's second identity from van Bladel [31, p.509] to the region $V(R_0)$ bounded by $S(R_0) \cup C(R_0)$ shown in Figure 2.2

$$\begin{aligned} &\int_{V(R_0)} \left[\nabla \times \nabla \times \bar{E} \cdot \overline{\overline{G}}_D - \bar{E} \cdot \nabla \times \nabla \times \overline{\overline{G}}_D \right] dV \\ &\qquad = - \int_{S(R_0) \cup C(R_0)} \left[\bar{E} \cdot \hat{n} \times \nabla \times \overline{\overline{G}}_D + \nabla \times \bar{E} \cdot \hat{n} \times \overline{\overline{G}}_D \right] dS \end{aligned} \tag{2.39}$$

where $\overline{\overline{G}}_D$ is the Dirichlet dyadic Green's function for the half space $z \geq z_0$ given by Tai [32, p.68]

$$\overline{\overline{G}}_D(\bar{r},\bar{r}') = \left[\overline{\overline{I}} - \frac{1}{k^2}\nabla\nabla'\right][G(\bar{r},\bar{r}') - G(\bar{r},\bar{r}_i')] + 2\hat{z}\hat{z}G(\bar{r},\bar{r}_i') \tag{2.40}$$

satisfying $\nabla \times \nabla \times \overline{\overline{G}}_D - k^2\overline{\overline{G}}_D = \overline{\overline{I}}\delta(\bar{r}-\bar{r}')$ in the half space $z > z_0$ and the boundary condition $\hat{z} \times \overline{\overline{G}}_D = 0$ on the plane $z = z_0$. Here $\overline{\overline{I}} = \hat{x}\hat{x} + \hat{y}\hat{y} + \hat{z}\hat{z}$ is the identity dyad. When $\bar{r}' \in V(R_0)$, the vector Helmholtz equation for the electric field $\nabla \times \nabla \times \bar{E} - k^2\bar{E} = 0$ and the corresponding equation for $\overline{\overline{G}}_D$ show that the left side of the Green's identity (2.39) is equal to $-\bar{E}(\bar{r}')$. Inserting the Dirichlet boundary condition $\hat{z} \times \overline{\overline{G}}_D = 0$, $z = z_0$, the identity $\nabla \times \overline{\overline{G}}_D = 2\nabla G \times \overline{\overline{I}}$, $z = z_0$, and the vector dyadic formulas from van Bladel [31, pp.507-508, eqs.(15), (18)]

$$\bar{E} \cdot \hat{z} \times (\nabla G \times \overline{\overline{I}}) = -(\hat{z} \times \bar{E}) \cdot (\nabla G \times \overline{\overline{I}}) = -\nabla' G \times (\hat{z} \times \bar{E}) \tag{2.41}$$

into (2.39), one finds

$$-\bar{E}(\bar{r}') = -2\int_{C(R_0)} \nabla' G(\bar{r},\bar{r}_i') \times (\hat{z} \times \bar{E}(\bar{r}))dS - \int_{S(R_0)} \left[\bar{E} \cdot \hat{n} \times \nabla \times \overline{\overline{G}}_D + \nabla \times \bar{E} \cdot \hat{n} \times \overline{\overline{G}}_D\right] dS. \tag{2.42}$$

Using the result of van Bladel [31, p.507, eq.(2)], the integrand in the last integral of (2.42) may be written as $\bar{E} \cdot \hat{n} \times \nabla \times \overline{\overline{G}}_D - \hat{n} \times \nabla \times \bar{E} \cdot \overline{\overline{G}}_D$, which according to the radiation conditions for the dyadic Green's function and the electric field [23, pp.58, 62] goes to zero faster than R_0^{-2} as $R_0 \to \infty$. Thus the contribution from the last integral in (2.42) vanishes as $R_0 \to \infty$ and we have

$$\bar{E}(\bar{r}) = 2\int_{-\infty}^{+\infty}\int_{-\infty}^{+\infty} \nabla G(\bar{r},\bar{r}') \times \left[\hat{z} \times \bar{E}(\bar{r}')\right] dx'dy', \quad z > z_0 \tag{2.43}$$

where $\bar{r}$ and $\bar{r}'$ have been interchanged and $\bar{r}' = x'\hat{x} + y'\hat{y} + z_0\hat{z}$. Upon calculating ∇G this equation becomes

$$\bar{E}(\bar{r}) = \frac{1}{2\pi}\int_{-\infty}^{+\infty}\int_{-\infty}^{+\infty} \frac{e^{ikR}}{R^2}\left[ik - \frac{1}{R}\right]\bar{R} \times \left[\hat{z} \times \bar{E}(\bar{r}')\right] dx'dy', \quad z > z_0 \tag{2.44}$$

with $\bar{R} = (x-x')\hat{x} + (y-y')\hat{y} + (z-z_0)\hat{z}$. Equations (2.43) and (2.44) are the Green's function representations for the electric field in the half space $z > z_0$ given in terms of E_x and E_y on the plane $z = z_0$. These formulas were first derived by Smythe [33] using a double current sheet in the plane $z = z_0$.

Let us finally express the magnetic field $\bar{H}$ in the half space $z > z_0$ in terms of E_x and E_y on the plane $z = z_0$. Since the induction law shows that $\bar{H} = \frac{-i}{\omega\mu}\nabla \times \bar{E}$, the magnetic field can be found by taking the curl of (2.43) to get

$$\bar{H}(\bar{r}) = -\frac{2i}{\omega\mu}\int_{-\infty}^{+\infty}\int_{-\infty}^{+\infty} \left[\left(\overline{\overline{I}}k^2 + \nabla\nabla\right)G(\bar{r},\bar{r}')\right] \cdot \left[\hat{z} \times \bar{E}(\bar{r}')\right] dx'dy', \quad z > z_0. \tag{2.45}$$

With the help of [31, eq.(7.136)], (2.45) can be written in expanded form as

$$\bar{H}(\bar{r}) = \frac{1}{2ik\pi}\sqrt{\frac{\epsilon}{\mu}}\int_{-\infty}^{+\infty}\int_{-\infty}^{+\infty}\left\{(ik)^2\left[\frac{\bar{R}\cdot(\hat{z}\times\bar{E}(\bar{r}'))}{R^2}\bar{R}-\hat{z}\times\bar{E}(\bar{r}')\right]+ik\left[-\frac{3\bar{R}\cdot(\hat{z}\times\bar{E}(\bar{r}'))}{R^3}\bar{R}\right.\right.$$

$$\left.\left.+\frac{1}{R}\hat{z}\times\bar{E}(\bar{r}')\right]+\left[\frac{3\bar{R}\cdot(\hat{z}\times\bar{E}(\bar{r}'))}{R^4}\bar{R}-\frac{1}{R^2}\hat{z}\times\bar{E}(\bar{r}')\right]\right\}\frac{e^{ikR}}{R}dx'dy',\quad z>z_0. \qquad (2.46)$$

This is the Green's function representation of the magnetic field in the half space $z > z_0$ given in terms of the x and y components of the electric field on the plane $z = z_0$.

(When the sources are located in the half space $z > z_0$, the electromagnetic fields in the half space $z < z_0$ are given by the negative of (2.43), (2.44), and (2.46).)

2.2 Far-Field Formulas

The far-field formulas that give the fields as $r \to \infty$ will be derived in this section in terms of the fields on the plane $z = z_0$. We start by deriving the far-field formulas from the Green's function representations and then proceed to derive them from the plane-wave spectrum representations. Both acoustic and electromagnetic fields are considered.

2.2.1 Far Fields Found from Green's Function Representations

Start with the acoustic field Φ given by (2.36). Inserting the far-field approximations $R = r - (x'\cos\phi\sin\theta + y'\sin\phi\sin\theta + z_0\cos\theta) + O(r^{-1})$ and $\frac{z_0-z}{R} = -\cos\theta + O(r^{-1})$ into the Green's function representation (2.36), one finds that the acoustic far field is

$$\Phi(\bar{r}) \sim \frac{-ik\cos\theta}{2\pi}\frac{e^{ikr}}{r}\int_{-\infty}^{+\infty}\int_{-\infty}^{+\infty}\Phi(\bar{r}')e^{-ik\hat{r}\cdot\bar{r}'}dx'dy' + O\left(\frac{1}{r^2}\right),\quad z>z_0 \qquad (2.47)$$

with $\bar{r}' = x'\hat{x} + y'\hat{y} + z_0\hat{z}$, and $\hat{r} = \hat{x}\cos\phi\sin\theta + \hat{y}\sin\phi\sin\theta + \hat{z}\cos\theta$. Note that this may also be written in terms of the spectrum T in (2.9) as

$$\Phi(\bar{r}) \sim -ik\cos\theta\frac{e^{ikr}}{r}T(k\cos\phi\sin\theta, k\sin\phi\sin\theta) + O\left(\frac{1}{r^2}\right),\quad z>z_0. \qquad (2.48)$$

Inserting $\hat{R} = \hat{r} + O(r^{-1})$ along with the asymptotic relations above (2.47) into the Green's function representation (2.44) for the electric field, one finds the following far-field formula for the electric field

$$\bar{E}(\bar{r}) \sim \frac{ik}{2\pi}\frac{e^{ikr}}{r}\hat{r}\times\int_{-\infty}^{+\infty}\int_{-\infty}^{+\infty}\hat{z}\times\bar{E}(\bar{r}')e^{-ik\hat{r}\cdot\bar{r}'}dx'dy' + O\left(\frac{1}{r^2}\right),\quad z>z_0. \qquad (2.49)$$

Inserting the relation $\hat{r}\times(\hat{z}\times\bar{E}) = (\hat{r}\cdot\bar{E})\hat{z} - \cos\theta\bar{E}$, and the definition of the plane-wave spectrum from (2.11) into (2.49) yields

$$\bar{E}(\bar{r}) \sim -ik\cos\theta\frac{e^{ikr}}{r}\bar{T}(k\cos\phi\sin\theta, k\sin\phi\sin\theta) + O\left(\frac{1}{r^2}\right),\quad z>z_0 \qquad (2.50)$$

where we have made use of (2.12), that is, $\hat{r} \cdot \bar{T}(x,y) = 0$.

The far magnetic field is similarly written as

$$\bar{H}(\bar{r}) \sim \sqrt{\frac{\epsilon}{\mu}}\hat{r} \times \bar{E}(\bar{r}) \sim -\sqrt{\frac{\epsilon}{\mu}} ik \cos\theta \frac{e^{ikr}}{r} \hat{r} \times \bar{T}(k\cos\phi\sin\theta, k\sin\phi\sin\theta) + O\left(\frac{1}{r^2}\right), \quad z > z_0 \tag{2.51}$$

or alternatively

$$\bar{H}(\bar{r}) \sim \sqrt{\frac{\epsilon}{\mu}} \frac{ik}{2\pi} \frac{e^{ikr}}{r} \hat{r} \times \left[\hat{r} \times \int_{-\infty}^{+\infty}\int_{-\infty}^{+\infty} \hat{z} \times \bar{E}(\bar{r}') e^{-ik\hat{r}\cdot\bar{r}'} dx'dy'\right] + O\left(\frac{1}{r^2}\right), \quad z > z_0. \tag{2.52}$$

It should be noted that the derivation of the formulas (2.47), (2.49), and (2.52) required that the limit as $r \to \infty$ be interchanged with the infinite (x', y') integration. We cannot use standard theorems of calculus to justify this interchange because Φ and $\bar{E}$ are not absolutely integrable on the infinite (x', y') plane. However, these far-field formulas can be proven valid by first expressing $\Phi(\bar{r}')$ and $\bar{E}(\bar{r}')$ in the integrals of (2.47), (2.49), and (2.52) in terms of their volume sources, (2.53) and (2.54)-(2.56), or equivalent surface sources, (2.19) and (A.5); and then proceeding as in Section 2.1.2.

(When the sources are located in the half space $z > z_0$, the far fields in the half space $z < z_0$ are given by the negative of (2.47), (2.48), (2.49), and (2.51).)

2.2.2 Frequency Dependence of the Far Fields as ω Approaches Zero

The integral over all time of a time-dependent function equals the function's frequency spectrum evaluated at ω equal to zero. Thus, it is of interest for both frequency-domain and time-domain representations to determine the behavior of the far fields as ω approaches zero.

As ω approaches zero, (2.48), (2.50), and (2.51) show that the far fields behave as ω times the frequency dependence of their plane-wave spectra. However, because we do not know the frequency dependence of the plane-wave spectra, let us express the acoustic and electromagnetic far fields in terms of their sources, $Q(\bar{r})$ and $\bar{J}(\bar{r})$, respectively,

$$\Phi(\bar{r}) \sim \frac{e^{ikr}}{4\pi r} \int_V Q(\bar{r}') e^{-ik\hat{r}\cdot\bar{r}'} dV' + O\left(\frac{1}{r^2}\right) \tag{2.53}$$

$$\bar{A}(\bar{r}) \sim \frac{\mu e^{ikr}}{4\pi r} \int_V \bar{J}(\bar{r}') e^{-ik\hat{r}\cdot\bar{r}'} dV' + O\left(\frac{1}{r^2}\right) \tag{2.54}$$

where $\bar{H}$ and $\bar{E}$ are given in terms of the vector potential $\bar{A}$ as

$$\bar{H} = \frac{1}{\mu}\nabla \times \bar{A}, \quad \bar{E} = -\frac{1}{i\omega\mu\epsilon}\nabla \times \left(\nabla \times \bar{A}\right) \tag{2.55}$$

or as $r \to \infty$

$$\bar{H}(\bar{r}) \sim i\omega\sqrt{\frac{\epsilon}{\mu}}\hat{r} \times \bar{A}(\bar{r}) + O\left(\frac{1}{r^2}\right), \quad \bar{E}(\bar{r}) \sim -i\omega\hat{r} \times \left(\hat{r} \times \bar{A}(\bar{r})\right) + O\left(\frac{1}{r^2}\right). \tag{2.56}$$

(The interchange of the volume integral with the limit as $r \to \infty$ required to derive (2.53)-(2.54), and with the curl to obtain (2.56) is allowed as shown in Hobson [24, pp.324, 355] under the assumption that the source functions Q and $\bar{J}$ are absolutely integrable over the volume V.)

Assuming the acoustic sources are in a volume V of finite extent, (2.53) shows that the frequency dependence of the far field as $\omega \to 0$ is the same as that of the spatially integrated source function Q. However, (2.56) and (2.54) show that the frequency dependence of electromagnetic far fields as $\omega \to 0$ is ω times the frequency dependence of the integrated current over the volume of finite extent. This means that the far electric and magnetic fields in the time domain will depend on the time derivative of the spatial integrated current. A further implication, proven in Section 3.3.2, is that the far electric and magnetic fields integrated over all time will be zero for currents that turn on and off in a finite time period. Only if the current stays on forever, so that the fields, for example, eventually become static, can the far electric and magnetic fields integrated over all time have nonzero values.

2.2.3 Far Fields Found from Plane-Wave Spectrum Representations

Asymptotic evaluations of the spectral integrals in the plane-wave spectrum representations of the acoustic and electromagnetic fields are performed in this section. Most of the acoustic far-field results have been derived previously in Sherman, Stammes, and Lalor [11] and in Nieto-Vesperinas [12]. Start with the acoustic field Φ and write its plane-wave spectrum representation (2.8) as

$$\Phi(\bar{r}) = \frac{1}{2\pi}\int_{-\infty}^{+\infty}\int_{-\infty}^{+\infty} T(k_x, k_y)e^{ir\psi(\hat{r},k_x,k_y)}dk_x dk_y, \quad z \geq z_0 \tag{2.57}$$

where T is the spectrum (2.9) and the phase ψ is

$$\psi(\hat{r}, k_x, k_y) = k_x \cos\phi \sin\theta + k_y \sin\phi \sin\theta + \gamma\cos\theta \tag{2.58}$$

with θ and ϕ being the spherical angles at the observation point. Equation (2.57) will now be evaluated asymptotically for $r \to \infty$. According to Bleistein and Handelsman [34, p.341], the critical points for this integral are (1) stationary points of the phase ψ, and (2) points where the spectrum T or the phase ψ is not infinitely differentiable.

Far fields for $0 < \theta < \pi/2$

Start by considering the stationary points of the phase where $\frac{\partial}{\partial k_x}\psi = \frac{\partial}{\partial k_y}\psi = 0$. With ψ given by (2.58), the following equations are satisfied at the stationary points

$$x - \frac{zk_x}{\gamma} = 0, \quad y - \frac{zk_y}{\gamma} = 0 \tag{2.59}$$

which imply that

$$k_x^2 = k^2\frac{x^2}{r^2}, \quad k_y^2 = k^2\frac{y^2}{r^2}. \tag{2.60}$$

Now, as $z \to \infty$, (2.59) shows that k_x and k_y must have the same signs as x and y, respectively, so that the stationary point is found from (2.60) to be

$$k_x = k\cos\phi\sin\theta, \quad k_y = k\sin\phi\sin\theta. \tag{2.61}$$

To determine the asymptotic contribution from the stationary point (2.61) we have to evaluate $\frac{\partial^2}{\partial k_x^2}\psi$, $\frac{\partial^2}{\partial k_y^2}\psi$, and $\frac{\partial^2}{\partial k_x k_y}\psi$ which at the stationary point are found to be

$$\frac{\partial^2}{\partial k_x^2}\psi = -\frac{1}{k}\left[1 + \frac{\cos^2\phi\sin^2\theta}{\cos^2\theta}\right], \quad \frac{\partial^2}{\partial k_y^2}\psi = -\frac{1}{k}\left[1 + \frac{\sin^2\phi\sin^2\theta}{\cos^2\theta}\right],$$

$$\frac{\partial^2}{\partial k_x k_y}\psi = -\frac{\cos\phi\sin\phi\sin^2\theta}{k\cos^2\theta}. \tag{2.62}$$

Consequently, at the stationary point (2.61)

$$\sqrt{\left|\frac{\partial^2}{\partial k_x^2}\psi\frac{\partial^2}{\partial k_y^2}\psi - \left(\frac{\partial^2}{\partial k_x \partial k_y}\psi\right)^2\right|} = \frac{1}{k^2\cos^2\theta} \tag{2.63}$$

and [34, p.347] then shows that the asymptotic contribution from the stationary point (2.61) to the spectral integral (2.57) is

$$\Phi(\bar{r}) \sim -ik\cos\theta\frac{e^{ikr}}{r}T(k\cos\phi\sin\theta, k\sin\phi\sin\theta) + O\left(\frac{1}{r^2}\right), \quad z > z_0. \tag{2.64}$$

This well-known result is identical to the far field (2.48) found from the Green's function representation.

Similarly, one finds that the far electric field is

$$\bar{E}(\bar{r}) \sim -ik\cos\theta\frac{e^{ikr}}{r}\bar{T}(k\cos\phi\sin\theta, k\sin\phi\sin\theta) + O\left(\frac{1}{r^2}\right), \quad z > z_0 \tag{2.65}$$

where $\bar{T}$ is the spectrum for the electric field given in (2.11). The far magnetic field is

$$\bar{H}(\bar{r}) \sim -\sqrt{\frac{\epsilon}{\mu}}ik\cos\theta\frac{e^{ikr}}{r}\hat{r}\times\bar{T}(k\cos\phi\sin\theta, k\sin\phi\sin\theta) + O\left(\frac{1}{r^2}\right), \quad z > z_0 \tag{2.66}$$

where the relation (2.16) between the spectra for the electric and magnetic fields has been used. The asymptotic results (2.65) and (2.66) are identical to (2.50) and (2.51) obtained from the Green's function representation.

We have calculated the asymptotic contribution from the stationary points of the phase ψ and will now proceed to calculate the asymptotic contributions from points where the

spectrum and/or phase ψ are not infinitely differentiable. To perform such a calculation, the singularities of the spectrum T must be known. In Section 2.1.3 and in Appendix A it is shown that the spectrum may be written as

$$T(k_x, k_y) = \frac{i}{\gamma} F(k_x, k_y) \tag{2.67}$$

where the far-field function F is a bounded infinitely differentiable function of (k_x, k_y) for all (k_x, k_y) except possibly at $\gamma = 0$. In addition, Appendix A shows that when the propagation vector is written in polar coordinates, as in the following paragraph, F is infinitely differentiable with respect to γ and k_ϕ, except possibly at $\gamma = k$. Thus, the spectrum has a possible singularity of order γ^{-1} at $\gamma = 0$. Furthermore, the only point at which the phase ψ is not infinitely differentiable with respect to (k_x, k_y) is at $\gamma = 0$, so the only asymptotic contribution (apart from the stationary point contribution) comes from the point $\gamma = 0$. This asymptotic contribution will be calculated by adding the contributions from $\gamma = 0$ to the integrals over the regions $k_x^2 + k_y^2 < k^2$ (the propagating part of the spectrum) and $k_x^2 + k_y^2 > k^2$ (the evanescent part of the spectrum).

Start with the propagating part of the spectrum. The contribution Φ^p from $\gamma = 0$ to the integral over the propagating part of the spectrum can be written

$$\Phi^p(\bar{r}) = \frac{i}{2\pi} \int_0^{2\pi} \int^0 F(k_\rho \cos k_\phi, k_\rho \sin k_\phi) e^{ir\left[\frac{x}{r} k_\rho \cos k_\phi + \frac{y}{r} k_\rho \sin k_\phi + \frac{z}{r}\gamma\right]} d\gamma dk_\phi, \quad z > z_0 \tag{2.68}$$

where we have introduced the polar integration variables ($k_x = k_\rho \cos k_\phi$ and $k_y = k_\rho \sin k_\phi$) and used the relation $k_\rho dk_\rho = -\gamma d\gamma$. The integral denoted by $\int^0$ in (2.68) refers to the upper end-point contribution from the γ integration, and F is the far-field function defined in (2.67). Standard integration by parts [34, p.78] applied to the γ integration of (2.68) gives

$$\Phi^p(\bar{r}) \sim -\frac{1}{2\pi r \cos\theta} \int_0^{2\pi} F(k \cos k_\phi, k \sin k_\phi) e^{ikr\left[\frac{x}{r}\cos k_\phi + \frac{y}{r}\sin k_\phi\right]} dk_\phi + O\left(\frac{1}{r^2}\right), \quad z > z_0. \tag{2.69}$$

The asymptotic value of the integral (2.69) is found by the method of stationary phase. The stationary points k_{ϕ_0} satisfy the equation $\tan k_{\phi_0} = \frac{y}{x} = \tan\phi$ which has the solutions $k_{\phi_0} = \phi$ and $k_{\phi_0} = \phi + \pi$. The second derivative of the phase of the integrand in (2.69) at these two stationary points is equal to $-k \sin\theta$ and $k \sin\theta$, respectively. Consequently the stationary phase formula [34, p.220, eq.(6.1.5)] shows that [12, p.63]

$$\Phi^p(\bar{r}) \sim \frac{e^{i\pi/4}}{\sqrt{2\pi k}} \frac{1}{\cos\theta \sqrt{\sin\theta}} \frac{i}{r\sqrt{r}} \Big[F(k\cos\phi, k\sin\phi) e^{ikr\sin\theta}$$

$$+ iF(-k\cos\phi, -k\sin\phi) e^{-ikr\sin\theta} \Big] + O\left(\frac{1}{r^2}\right), \quad z > z_0. \tag{2.70}$$

It is seen that this contribution is of order $r^{-3/2}$ and is thus negligible compared to the stationary-phase contribution (2.64) which is of order r^{-1}.

Having calculated the asymptotic contribution from $\gamma = 0$ to the integral over the propagating modes, we will now calculate the corresponding contribution Φ^e from the evanescent modes. It is found that the first term in the asymptotic expansion of the contribution from the upper limit of the integral $\int_0^k$ equals the negative of the first term in the asymptotic expansion of the contribution from the lower limit of the integral $\int_k^{+\infty}$, so (2.70) shows that

$$\Phi^e(\bar{r}) \sim -\frac{e^{i\pi/4}}{\sqrt{2\pi k}} \frac{1}{\cos\theta\sqrt{\sin\theta}} \frac{i}{r\sqrt{r}} \left[F(k\cos\phi, k\sin\phi)e^{ikr\sin\theta}\right.$$

$$\left. + iF(-k\cos\phi, -k\sin\phi)e^{-ikr\sin\theta}\right] + O\left(\frac{1}{r^2}\right), \quad z > z_0. \quad (2.71)$$

The total asymptotic contribution to the acoustic field Φ (2.57) from the singularity at $\gamma = 0$ is the sum of Φ^p and Φ^e given in (2.70) and (2.71). From these equations it is seen that this total asymptotic contribution is of order r^{-2} or smaller, so that it is negligible compared to the stationary-phase contribution (2.64).

The corresponding formulas for the electric field are given by

$$\bar{E}^p(\bar{r}) \sim \frac{e^{i\pi/4}}{\sqrt{2\pi k}} \frac{1}{\cos\theta\sqrt{\sin\theta}} \frac{i}{r\sqrt{r}} \left[\bar{F}(k\cos\phi, k\sin\phi)e^{ikr\sin\theta}\right.$$

$$\left. + i\bar{F}(-k\cos\phi, -k\sin\phi)e^{-ikr\sin\theta}\right] + O\left(\frac{1}{r^2}\right), \quad z > z_0 \quad (2.72)$$

and

$$\bar{E}^e(\bar{r}) \sim -\frac{e^{i\pi/4}}{\sqrt{2\pi k}} \frac{1}{\cos\theta\sqrt{\sin\theta}} \frac{i}{r\sqrt{r}} \left[\bar{F}(k\cos\phi, k\sin\phi)e^{ikr\sin\theta}\right.$$

$$\left. + i\bar{F}(-k\cos\phi, -k\sin\phi)e^{-ikr\sin\theta}\right] + O\left(\frac{1}{r^2}\right), \quad z > z_0. \quad (2.73)$$

where $\bar{F} = -i\gamma\bar{T}$, with $\bar{T}$ equal to the electric field spectrum (2.11). The formulas for the magnetic field are given by (2.72) and (2.73) with $\bar{F}(k_x, k_y)$ replaced by $\sqrt{\frac{\varepsilon}{\mu}}\hat{k} \times \bar{F}(k_x, k_y)$ (see (2.16)). By direct calculation one finds that $\hat{z} \cdot \bar{E}^e \times \bar{H}^{e*} = 0$ for all observation points so the evanescent modes do not radiate any electromagnetic power into the half space $z > z_0$. The same statement holds for the contribution of $\hat{z} \cdot \bar{E}^p \times \bar{H}^{p*}$ to the electromagnetic power. Thus all the radiated electromagnetic power comes from the stationary-phase contribution given in (2.65) and (2.66).

Far fields for $\theta = 0$

The above far-field results were derived for $0 < \theta < \pi/2$. Here we consider the special case of the far fields along the z axis, that is, $\theta = 0$. From (2.64) it is immediately seen that the contribution from the stationary point in the region $k_x^2 + k_y^2 < k^2$ is given by

$$\Phi(z\hat{z}) \sim -ik\frac{e^{ikz}}{z}T(0,0) + O\left(\frac{1}{z^2}\right), \quad z > z_0. \quad (2.74)$$

Similarly, (2.69) shows that the contribution from $\gamma = 0$ to the integral over the propagating part of the spectrum is

$$\Phi^p(z\hat{z}) \sim -\frac{1}{2\pi z}\int_0^{2\pi} F(k\cos k_\phi, k\sin k_\phi)dk_\phi + O\left(\frac{1}{z^2}\right), \quad z > z_0 \tag{2.75}$$

and that the corresponding contribution from the evanescent part of the spectrum is

$$\Phi^e(z\hat{z}) \sim \frac{1}{2\pi z}\int_0^{2\pi} F(k\cos k_\phi, k\sin k_\phi)dk_\phi + O\left(\frac{1}{z^2}\right), \quad z > z_0. \tag{2.76}$$

Thus it is seen that along the z axis both the propagating and evanescent modes give an asymptotic contribution from $\gamma = 0$ of order z^{-1}, the same far-field dependence as the contribution (2.74) from the stationary point. However, the dominant terms in (2.75) and (2.76) cancel upon addition to leave a dependence of $O(z^{-2})$.

For the electric field one finds that the contribution from the stationary point in the region $k_x^2 + k_y^2 < k^2$ is given from (2.65) as

$$\bar{E}(z\hat{z}) \sim -ik\frac{e^{ikz}}{z}\bar{T}(0,0) + O\left(\frac{1}{z^2}\right), \quad z > z_0. \tag{2.77}$$

The contribution from $\gamma = 0$ to the integral over the propagating part of the spectrum is

$$\bar{E}^p(z\hat{z}) \sim -\frac{1}{2\pi z}\int_0^{2\pi} \bar{F}(k\cos k_\phi, k\sin k_\phi)dk_\phi + O\left(\frac{1}{z^2}\right), \quad z > z_0 \tag{2.78}$$

and the corresponding contribution from the evanescent part of the spectrum is

$$\bar{E}^e(z\hat{z}) \sim \frac{1}{2\pi z}\int_0^{2\pi} \bar{F}(k\cos k_\phi, k\sin k_\phi)dk_\phi + O\left(\frac{1}{z^2}\right), \quad z > z_0. \tag{2.79}$$

The formulas for the magnetic field are given by (2.77), (2.78), and (2.79) with $\bar{F}(k_x, k_y)$ replaced by $\sqrt{\frac{\epsilon}{\mu}}\hat{k}\times\bar{F}(k_x, k_y)$ (see (2.16)). In this case one finds that in general $\hat{z}\cdot\bar{E}^e\times\bar{H}^{e*} \neq 0$. However, since the contribution to the far field from the evanescent modes is of order r^{-1} only on the z axis ($\theta = 0$), and is of higher order for $\theta > 0$, no power is radiated by the evanescent modes. Similarly, no power is radiated by the contribution of $\hat{z}\cdot\bar{E}^p\times\bar{H}^{p*}$ at $\theta = 0$.

Far fields for $\theta = \pi/2$

Finally, let us consider the far fields in the scan plane $z = z_0$. For simplicity, assume that $z_0 = 0$ and that $\bar{r} = x\hat{x}$ with $x > 0$. The plane-wave spectrum representation (2.57) then reduces to

$$\begin{aligned}\Phi(x\hat{x}) &= \frac{1}{2\pi}\int_{-\infty}^{+\infty}\int_{-\infty}^{+\infty} T(k_x, k_y)e^{ixk_x}dk_x dk_y \\ &= \frac{i}{2\pi}\int_0^{+\infty}\int_0^{2\pi} F(k_\rho\cos k_\phi, k_\rho\sin k_\phi)e^{ixk_\rho\cos k_\phi}dk_\phi\frac{k_\rho}{\gamma}dk_\rho\end{aligned} \tag{2.80}$$

where again $k_x = k_\rho \cos k_\phi$, $k_y = k_\rho \sin k_\phi$, and the far-field function F is defined in (2.67). Denoting the k_ϕ integral in (2.80) by $G(k_\rho, x)$ and noting that the phase of the integrand of this function has a stationary point at $k_\phi = 0$ and at $k_\phi = \pi$, the method of stationary phase shows that

$$G(k_\phi, x) \sim ie^{ixk_\rho} F(k_\rho, 0)\sqrt{\frac{2\pi}{xk_\rho}} e^{-i\pi/4} + ie^{-ixk_\rho} F(-k_\rho, 0)\sqrt{\frac{2\pi}{xk_\rho}} e^{i\pi/4} + O\left(\frac{1}{x}\right). \tag{2.81}$$

Inserting this asymptotic expression for $G(k_\phi, x)$ into (2.80) one finds that

$$\Phi(x\hat{x}) \sim \frac{ie^{-i\pi/4}}{\sqrt{2\pi x}} \int_0^{+\infty} \left[F(k_\rho, 0)e^{ixk_\rho} + iF(-k_\rho, 0)e^{-ixk_\rho}\right] \sqrt{k_\rho} \frac{dk_\rho}{\gamma} \left[1 + O(x^{-1/2})\right]. \tag{2.82}$$

The only critical point for this integral is at $\gamma = 0$, that is, at $k_\rho = k$. The asymptotic contribution to the integral from this point is found as the sum of the asymptotic end point contributions at $k_\rho = k$ to the integrals over propagating ($k_\rho < k$) and evanescent ($k_\rho > k$) modes. Because of the singularity of the integrand at these end points, the standard method of integration by parts cannot be used. However, one can change the integration variable in (2.82) from k_ρ to γ and use the method of stationary phase for a stationary point at an end point [34, p.222] to prove that

$$\int_0^k F(k_\rho, 0)e^{ixk_\rho} \sqrt{k_\rho} \frac{dk_\rho}{\gamma} \sim F(k, 0)\sqrt{\frac{\pi}{2x}} e^{-i\pi/4} e^{ikx} + O\left(\frac{1}{x}\right) \tag{2.83}$$

and that

$$\int_k^{+\infty} F(k_\rho, 0)e^{ixk_\rho} \sqrt{k_\rho} \frac{dk_\rho}{\gamma} \sim F(k, 0)\sqrt{\frac{\pi}{2x}} e^{-i\pi/4} e^{ikx} + O\left(\frac{1}{x}\right) \tag{2.84}$$

which is seen to equal (2.83). Equation (2.83) shows that

$$\begin{aligned} i\int_0^k F(-k_\rho, 0)e^{-ixk_\rho} \sqrt{k_\rho} \frac{dk_\rho}{\gamma} &= \left(-i\int_0^k F^*(-k_\rho, 0)e^{ixk_\rho} \sqrt{k_\rho} \frac{dk_\rho}{\gamma}\right)^* \\ &\sim iF(-k, 0)\sqrt{\frac{\pi}{2x}} e^{i\pi/4} e^{-ikx} + O\left(\frac{1}{x}\right) \end{aligned} \tag{2.85}$$

where $\gamma^* = \gamma$, $k_\rho < k$ has been used (the * indicates complex conjugation), and (2.84) shows that

$$\begin{aligned} i\int_k^{+\infty} F(-k_\rho, 0)e^{-ixk_\rho} \sqrt{k_\rho} \frac{dk_\rho}{\gamma} &= \left(i\int_k^{+\infty} F^*(-k_\rho, 0)e^{ixk_\rho} \sqrt{k_\rho} \frac{dk_\rho}{\gamma}\right)^* \\ &\sim -iF(-k, 0)\sqrt{\frac{\pi}{2x}} e^{i\pi/4} e^{-ikx} + O\left(\frac{1}{x}\right) \end{aligned} \tag{2.86}$$

where $\gamma^* = -\gamma$, $k_\rho > k$ has been employed. Inserting (2.83) and (2.85) into (2.82) it is found that the far-field contribution from the propagating modes is

$$\Phi^p(x\hat{x}) \sim \frac{1}{2x}\left[F(k, 0)e^{ikx} - F(-k, 0)e^{-ikx}\right] + O(x^{-3/2}) \tag{2.87}$$

or for an arbitrary direction $\bar{r} = x\hat{x} + y\hat{y}$ in the scan plane

$$\Phi^p(\bar{r}) \sim \frac{1}{2r}\left[F(k\cos\phi, k\sin\phi)e^{ikr} - F(-k\cos\phi, k\sin\phi)e^{-ikr}\right] + O(r^{-3/2}). \tag{2.88}$$

Inserting(2.84) and (2.86) into (2.82) one finds that the far-field contribution from the evanescent modes, generalized to an arbitrary point in the scan plane, is

$$\Phi^e(\bar{r}) \sim \frac{1}{2r}\left[F(k\cos\phi, k\sin\phi)e^{ikr} + F(-k\cos\phi, k\sin\phi)e^{-ikr}\right] + O(r^{-3/2}). \tag{2.89}$$

Consequently, both propagating and evanescent modes contribute to the far field with a term of order r^{-1} and they both contribute with incoming as well as outgoing waves. Adding the contributions from the propagating and evanescent modes one finds that the total far field is an outgoing wave given by

$$\Phi(\bar{r}) \sim F(k\cos\phi, k\sin\phi)\frac{e^{ikr}}{r} + O(r^{-3/2}) \tag{2.90}$$

whose first term agrees with the result obtained by letting $\theta \to \pi/2$ in the stationary-point formula (2.64). A more detailed analysis would show that the $O(r^{-3/2})$ terms in (2.88) and (2.89) cancel to leave an $O(r^{-2})$ instead of $O(r^{-3/2})$ in (2.90) and (2.93) below. This expression shows that the incoming waves in the expressions (2.87) and (2.89) cancel and thus incoming waves result from dividing the spectrum into propagating and evanescent parts. Consequently, when the sources are in a finite region of space and radiate in a direction for which $\theta = \pi/2$, the evanescent part of the spectrum cannot be zero. Furthermore, by neglecting the contribution from this part of the spectrum one obtains the erroneous result that waves are coming in from infinity.

For the electric field one finds that the contribution to the far field in the scan plane from the propagating part of the spectrum is

$$\bar{E}^p(\bar{r}) \sim \frac{1}{2r}\left[\bar{F}(k\cos\phi, k\sin\phi)e^{ikr} - \bar{F}(-k\cos\phi, -k\sin\phi)e^{-ikr}\right] + O(r^{-3/2}) \tag{2.91}$$

and that the contribution from the evanescent part of the spectrum is

$$\bar{E}^e(\bar{r}) \sim \frac{1}{2r}\left[\bar{F}(k\cos\phi, k\sin\phi)e^{ikr} + \bar{F}(-k\cos\phi, -k\sin\phi)e^{-ikr}\right] + O(r^{-3/2}). \tag{2.92}$$

The total far electric field is then

$$\bar{E}(\bar{r}) \sim \bar{F}(k\cos\phi, k\sin\phi)\frac{e^{ikr}}{r} + O(r^{-3/2}) \tag{2.93}$$

whose first term agrees with the result (2.65) with $\theta \to \pi/2$. The formulas for the magnetic field are given by (2.91), (2.92), and (2.93) with $\bar{F}(k_x, k_y)$ replaced by $\sqrt{\frac{\epsilon}{\mu}}\hat{k} \times \bar{F}(k_x, k_y)$ (see (2.16)).

To determine if the evanescent modes radiate any real power in the scan plane, consider

$$\begin{aligned}\mathrm{Re}(\hat{r}\cdot\bar{E}^e\times\bar{H}^{e*}) &= \frac{1}{r^2}\sqrt{\frac{\epsilon}{\mu}}\mathrm{Re}\Big(\Big[|\bar{F}(k\cos\phi,k\sin\phi)|^2-|\bar{F}(-k\cos\phi,-k\sin\phi)|^2\\ &- \bar{F}(k\cos\phi,k\sin\phi)\cdot\bar{F}^*(-k\cos\phi,-k\sin\phi)e^{2ikr}\\ &+ \bar{F}(-k\cos\phi,-k\sin\phi)\cdot\bar{F}^*(k\cos\phi,k\sin\phi)e^{-2ikr}\Big]\Big)\\ &= \frac{1}{r^2}\sqrt{\frac{\epsilon}{\mu}}\left[|\bar{F}(k\cos\phi,k\sin\phi)|^2-|\bar{F}(-k\cos\phi,-k\sin\phi)|^2\right] \qquad (2.94)\end{aligned}$$

where $\hat{r}\cdot\bar{F}(k\cos\phi,k\sin\phi)=0$ and $\hat{r}\cdot\bar{F}(-k\cos\phi,-k\sin\phi)=0$ have been used. Although this real part of the evanescent Poynting's vector in (2.94) decays as r^{-2}, it is valid only for $\theta=\pi/2$. For $0<\theta<\pi/2$ we have shown above that the real part of the evanescent Poynting's vector decays faster than r^{-2}. Thus, an integration over θ of the real part of the evanescent Poynting's vector shows that evanescent modes do not radiate power in the scan plane.

In summary, the evanescent spectrum can contribute to the far fields at $\theta=0$ and $\theta=\pi/2$, but do not contribute to the radiated power. This latter result, of course, can be proven directly from the plane-wave spectrum representation of the $\bar{E}$ and $\bar{H}$ fields; see Section 2.3.

The result that the evanescent spectrum contributes to the far field at $\theta=0$ and at $\theta=\pi/2$ has important practical consequences. When computing fields for radiators from the plane-wave spectrum formulas (2.8) or (2.10) [35], usually only the propagating part of the spectrum (the radiated field) has been determined from measurements. Thus, the computed fields will contain errors near the $\theta=0$ and $\theta=\pi/2$ directions caused by the neglect of the evanescent spectrum regardless of how large the distance is from the radiator.

(If the sources are located in the half space $z>z_0$, the asymptotic contributions for the fields in the half space $z\le z_0$ are given by the negative of the expressions derived in this section.)

2.2.4 Spectrum Given in Terms of the Far Field in Spherical Coordinates

To derive a formula that gives the spectrum in terms of the far field in spherical coordinates (r,θ,ϕ), write the far field as

$$\Phi(\bar{r})\sim\frac{e^{ikr}}{r}\mathcal{F}(\theta,\phi),\quad r\to\infty \qquad (2.95)$$

where $\mathcal{F}$ is the complex far-field pattern in terms of the spherical coordinates (θ,ϕ). From the expression (2.48) we see that the far-field pattern $\mathcal{F}$ can be expressed in terms of the plane-wave spectrum

$$\mathcal{F}(\theta,\phi)=-ik\cos\theta T(k\cos\phi\sin\theta,k\sin\phi\sin\theta). \qquad (2.96)$$

To find the spectrum in terms of the far-field pattern we need to express θ and ϕ in terms of $k_x = k\cos\phi\sin\theta$ and $k_y = k\sin\phi\sin\theta$. For $k_x^2 + k_y^2 < k^2$ and $z > z_0$ it is found that $\theta = \arccos\frac{\gamma}{k}$ and $\phi = \arctan\frac{k_x}{k_y}$, so that the spectrum is given by

$$T(k_x, k_y) = \frac{i}{\gamma}F(k_x, k_y) = \frac{i}{\gamma}\mathcal{F}(\arccos\frac{\gamma}{k}, \arctan\frac{k_x}{k_y}), \quad k_x^2 + k_y^2 < k^2 \tag{2.97}$$

where the first equation in (2.97) is taken from (2.30). For $k_x^2 + k_y^2 > k^2$, the far-field pattern $\mathcal{F}$ does not immediately give us the spectrum since its values for complex observation angles is required ($\arccos\frac{\gamma}{k}$ is complex when γ is complex). However, for sources in a finite region, it can be shown [12, sec.4.3] that the function $\mathcal{F}(\theta, \phi)$ is part of an entire (analytic) function defined for complex observation angles. Thus, in principle, it is possible to analytically continue the far-field pattern $\mathcal{F}$ to complex values of θ, and still use the expression (2.97) to calculate the spectrum. (Appendix A reduces the conditions required for the proof in Nieto-Vesperinas [12, sec.4.3] from continuous source functions to fields that are continuous outside the source region.) Appendix A generalizes the theorem in Nieto-Vesperinas [12, sec.4.3] to electromagnetic fields that are continuous outside the source region, a condition that is satisfied by fields that obey Maxwell's differential curl and divergence equations outside the source region.

Writing the far electric field as

$$\bar{E}(\bar{r}) \sim \frac{e^{ikr}}{r}\bar{\mathcal{F}}(\theta, \phi), \quad r \to \infty \tag{2.98}$$

where $\bar{\mathcal{F}}$ is the electric far-field pattern, one finds similarly, that the spectrum (2.11) for the electric field is given by

$$\bar{T}(k_x, k_y) = \frac{i}{\gamma}\bar{F}(k_x, k_y) = \frac{i}{\gamma}\bar{\mathcal{F}}(\arccos\frac{\gamma}{k}, \arctan\frac{k_x}{k_y}), \quad k_x^2 + k_y^2 < k^2. \tag{2.99}$$

Thus, in principle, one can analytically continue the electric far-field pattern $\bar{\mathcal{F}}$ to complex values of θ, and (2.99) can be used to calculate the spectrum everywhere. In practice, numerical errors usually prevent the analytic continuation of a measured far-field pattern. When a closed-form expression for $\mathcal{F}(\theta, \phi)$ is known for real (θ, ϕ), one way to obtain the analytic continuation to complex values of θ is to expand the far field in a series of spherical harmonics [36, eqs.(3.9), (4.10)], [9, eq.(6)]. With such an analytic continuation, the near fields can be computed from the far electric field through formulas (2.10) and (2.17).

(If the sources are located in the half space $z > z_0$, the relations in this section still hold for the fields in the half space $z \leq z_0$ provided that γ is replaced with $-\gamma$.)

2.3 Power Relations for the Electromagnetic Field

The electromagnetic power radiated through the plane $z = z_1 > z_0$ will be given in terms of the electromagnetic spectrum $\bar{T}$ in (2.11). Poynting's and Parseval's theorems show that

the complex power $P(z_1)$ radiated through the plane $z = z_1$ is given by

$$\begin{aligned} P(z_1) &= \frac{1}{2}\hat{z} \cdot \int_{-\infty}^{+\infty} \int_{-\infty}^{+\infty} \bar{E} \times \bar{H}^*(x', y', z_1) dx' dy' \\ &= \frac{1}{2}\hat{z} \cdot \int_{-\infty}^{+\infty} \int_{-\infty}^{+\infty} \bar{T} \times \bar{T}_H^*(k_x, k_y) e^{iz_1(\gamma - \gamma^*)} dk_x dk_y, \quad z_1 \geq z_0 \end{aligned} \tag{2.100}$$

where $\bar{T}$ is the spectrum for the electric field given in (2.11) and $\bar{T}_H$ is the spectrum for the magnetic field given in (2.16) and (2.18). The superscript $*$ denotes complex conjugation. Now, from (2.16),

$$\begin{aligned} \bar{T} \times \bar{T}_H^*(k_x, k_y) &= \frac{1}{\omega\mu} \bar{T} \times \left[\bar{k}^* \times \bar{T}^*(k_x, k_y) \right] \\ &= \frac{1}{\omega\mu} |\bar{T}|^2 \bar{k}^* - \frac{1}{\omega\mu} T^* \bar{T} \cdot \bar{k}^*. \end{aligned} \tag{2.101}$$

Using (2.12) to show that $\bar{T} \cdot \bar{k}^* = (\gamma^* - \gamma) T_z$ we find that

$$\hat{z} \cdot \bar{T} \times \bar{T}_H^*(k_x, k_y) = \frac{1}{\omega\mu} |\bar{T}|^2 \gamma^* - \frac{1}{\omega\mu} (\gamma^* - \gamma) |T_z|^2 \tag{2.102}$$

and (2.100) then gives

$$P(z_1) = \frac{1}{2\omega\mu} \left[\int\int_{k_\rho < k} |\bar{T}|^2 \gamma dk_x dk_y + i \int\int_{k_\rho > k} |\gamma| \left[2|T_z|^2 - |\bar{T}|^2 \right] e^{-2z_1|\gamma|} dk_x dk_y \right] \tag{2.103}$$

where the fact that γ is real for $k_\rho = \sqrt{k_x^2 + k_y^2} < k$, has been used. The first and second integrals in (2.103) are the real and imaginary power, respectively, radiated through the plane $z = z_1$. It is seen that the real power (the first term of (2.103)) is carried solely by the propagating part of the spectrum and is independent of z_1. The imaginary power (the second term of (2.103)) involves only the evanescent part of the spectrum and decays as $z_1 \to +\infty$. No real power is radiated by the evanescent part of the spectrum as we showed previously in Section 2.2.3.

(When the sources are located in the half space $z > z_0$, the power radiated (to the left) through the plane $z = z_1 < z_0$ is given by (2.103) with z_1 replaced by $-z_1$.)

2.4 Lossy Media

In this section we assume that the space surrounding the sources is lossy. The losses are accounted for by the complex permittivity $\epsilon = \epsilon' + i\epsilon''$ and the complex permeability $\mu = \mu' + i\mu''$ where ϵ', ϵ'', μ', and μ'' are real. (For example, $\epsilon'' = \frac{\sigma}{\omega}$ for a medium with conductivity σ.) The propagation constant in the lossy medium can be expressed as

$$k = \omega\sqrt{\mu\epsilon} = \beta + i\alpha \tag{2.104}$$

where both the attenuation constant α and the phase constant β are positive ($\beta = k$ and $\alpha = 0$ for a lossless medium).

All the plane-wave spectrum formulas in Section 2.1.1 are valid with k replaced by $\beta + i\alpha$ when losses are present. This means that γ is complex for all (k_x, k_y) so that every plane-wave mode is attenuated. Thus, the spectrum does not divide into propagating and evanescent parts. Also, the Green's function representations in Section 2.1.4 hold with k replaced by $\beta + i\alpha$. The far-field expressions in Section 2.2.1 found from the Green's function representations hold with k replaced by $\beta + i\alpha$, and we see that the fields are exponentially attenuated as $r \to +\infty$.

The asymptotic far-field analysis in Section 2.2.3 of the plane-wave spectrum representations is no longer valid because there is no stationary point and the entire spectrum is decaying. To obtain the far field from the plane-wave spectrum representation one would have to use the method of steepest descent. However, the result (2.48) from the Green's function representation still holds and thus we have the far field in terms of the spectrum with argument $(k\cos\phi\sin\theta, k\sin\phi\sin\theta)$, where k is complex.

The spectrum has no singularities when losses are present because the electric field in the plane $z = z_0$ decays exponentially at infinity so that the integral of $|\bar{E}|$ over the plane $z = z_0$ converges. Equation (2.97), which gives the spectrum in terms of the far field, still applies. However, now γ is complex for all real (k_x, k_y) and thus to get any part of the spectrum one has to know the far-field pattern $\mathcal{F}$ for complex angles of observation.

The power $P(z_1)$ radiated through the plane $z = z_1 > z_0$ in the lossy medium is found by inserting the value of $\hat{z} \cdot \bar{T} \times \bar{T}_H^*$ given in (2.102) into the general power relation (2.100). One finds

$$P(z_1) = \frac{1}{2\omega\mu}\left[\int_{-\infty}^{+\infty}\int_{-\infty}^{+\infty} |\bar{T}|^2 \gamma_r e^{-2z_1\gamma_r} dk_x dk_y + i\int_{-\infty}^{+\infty}\int_{-\infty}^{+\infty} \gamma_i \left[2|T_z|^2 - |\bar{T}|^2\right] e^{-2z_1\gamma_r} dk_x dk_y\right] \tag{2.105}$$

where both integrals are real and γ_r and γ_i are the real and imaginary parts of γ, respectively. Since the definition of γ ensures that $\gamma_i > 0$ it is seen that both the real and imaginary power decay as $z_1 \to +\infty$.

(When the sources are located in the half space $z > z_0$, the power radiated (to the left) through the plane $z = z_1 < z_0$ is given by (2.105) with z_1 replaced by $-z_1$.)

2.5 Static Electromagnetic Fields

This section derives formulas that give the static electric and static magnetic fields in the half space $z > z_0$ in terms of static electric or magnetic fields on the plane $z = z_0$. The cases where the half space $z > z_0$ is (a) lossless, (b) has only electric losses, (c) has only magnetic losses, and (d) has both electric and magnetic losses, are analyzed. We start by obtaining the static Maxwell equations from the time-harmonic ones and discuss the class of losses treated by the following analysis.

In a lossy medium with zero charge the time-harmonic Maxwell equations can be written

as

$$\nabla \times \bar{H} = -i\omega\epsilon\bar{E}, \quad \nabla \times \bar{E} = i\omega\mu\bar{H}, \quad \nabla \cdot \bar{H} = 0, \quad \nabla \cdot \bar{E} = 0 \tag{2.106}$$

where

$$\epsilon(\omega) = \epsilon'(\omega) + i\epsilon''(\omega), \quad \mu(\omega) = \mu'(\omega) + i\mu''(\omega) \tag{2.107}$$

with ϵ', ϵ'', μ', and μ'' real. From an entropy argument [37, p.274] (for passive media) it follows that for $\omega > 0$, $\epsilon'' \geq 0$ and $\mu'' \geq 0$.

Because the time-domain fields calculated from the integral over ω of the time-harmonic fields are real, the real and imaginary parts of $\epsilon(\omega)$ and $\mu(\omega)$ are always even and odd functions of ω, respectively. That is

$$\epsilon'(-\omega) = \epsilon'(\omega), \quad \mu'(-\omega) = \mu'(\omega) \tag{2.108}$$

$$\epsilon''(-\omega) = -\epsilon''(\omega), \quad \mu''(-\omega) = -\mu''(\omega) \tag{2.109}$$

regardless of the frequency dependence of these functions. This implies that no material can have a constant loss in permittivity or permeability for all values of frequency ($-\infty < \omega < \infty$). [1] In particular, the constitutive relations

$$\bar{D}(\bar{r}, t) = \epsilon_0\bar{E}(\bar{r}, t), \quad \bar{B}(\bar{r}, t) = \mu_0\bar{H}(\bar{r}, t) \tag{2.110}$$

for time-domain fields, where ϵ_0 and μ_0 are constants, imply that there are no losses in the material. When losses are present these simple constitutive relations must be replaced by the more complicated convolutions

$$\bar{D}(\bar{r}, t) = \int_{-\infty}^{+\infty} \epsilon_\omega(\bar{r})\bar{E}_\omega(\bar{r})e^{-i\omega t}d\omega = \frac{1}{2\pi}\int_{-\infty}^{+\infty} \epsilon(\bar{r}, t - t')\bar{E}(\bar{r}, t')dt' \tag{2.111}$$

$$\bar{B}(\bar{r}, t) = \int_{-\infty}^{+\infty} \mu_\omega(\bar{r})\bar{H}_\omega(\bar{r})e^{-i\omega t}d\omega = \frac{1}{2\pi}\int_{-\infty}^{+\infty} \mu(\bar{r}, t - t')\bar{H}(\bar{r}, t')dt' \tag{2.112}$$

where the frequency dependent parameters in (2.111) and (2.112) are denoted by the subscript ω. For example, if $\epsilon_\omega(\bar{r}) = \epsilon_0 + i\sigma/\omega$ or $\mu_\omega(\bar{r}) = \mu_0 + i\sigma_m/\omega$, both of which satisfy the dispersion relations [37, p.281], then (2.111) and (2.112) reduce to

$$\bar{D}(\bar{r}, t) = \epsilon_0\bar{E}(\bar{r}, t) + \sigma\int_{-\infty}^{t} \bar{E}(\bar{r}, t')dt' \tag{2.113}$$

$$\bar{B}(\bar{r}, t) = \mu_0\bar{H}(\bar{r}, t) + \sigma_m\int_{-\infty}^{t} \bar{H}(\bar{r}, t')dt'. \tag{2.114}$$

Contrary to the statements in [13], if the proper constitutive relations are used, magnetic monopoles need not be introduced into Maxwell's time-dependent equations to represent loss in magnetic materials.

[1] In the words of E.J. Post [38, p.162], "The imaginary elements, therefore, if different from zero, should be functions of frequency under all circumstances. One can express this in another way by saying that the imaginary elements are associated with effects which are essentially dispersive."

For many lossy materials it is found that [37, p.281]

$$\epsilon(\omega) \sim \epsilon'(0) + i\frac{\sigma}{\omega}, \ \omega \to 0 \tag{2.115}$$

where σ is the static electric conductivity and $\epsilon'(0)$ is the finite static permittivity. Similarly one can postulate a permeability that behaves like

$$\mu(\omega) \sim \mu'(0) + i\frac{\sigma_m}{\omega}, \ \omega \to 0 \tag{2.116}$$

where σ_m is the static magnetic conductivity and $\mu'(0)$ is the finite static permeability. From the facts that $\epsilon'' \geq 0$ and $\mu'' \geq 0$ for $\omega > 0$ it follows that $\sigma \geq 0$ and $\sigma_m \geq 0$. (Also, $\sigma \geq 0$ can be proven directly from a static entropy argument [37, p.87] for passive materials.) Although a constant σ_m (independent of frequency) can be postulated for lossy magnetic materials, no physical material has been found that maintains a constant σ_m as ω approaches zero [37, p.283]. However, for the sake of completeness we will also consider cases with σ_m constant as ω approaches zero.

For materials with permittivity and permeability obeying (2.115) and (2.116) the time-harmonic Maxwell equations (2.106) show that the static Maxwell equations are given by

$$\nabla \times \bar{H} = \sigma \bar{E}, \ \nabla \times \bar{E} = -\sigma_m \bar{H}, \ \nabla \cdot \bar{H} = 0, \ \nabla \cdot \bar{E} = 0 \tag{2.117}$$

where both the electric conductivity σ and the magnetic conductivity σ_m are non-negative constants.

2.5.1 The Lossless Case ($\sigma = 0$, $\sigma_m = 0$)

The static Maxwell equations (2.117) show that for a lossless medium ($\sigma = 0$, $\sigma_m = 0$) the electric and magnetic fields are uncoupled and satisfy the same differential equations. In this section we will therefore consider only the electric field satisfying $\nabla \times \bar{E} = 0$, $\nabla \cdot \bar{E} = 0$, which imply $\nabla^2 \bar{E} = 0$. For finite source regions Stratton [39, p.168] shows that $|\bar{E}| = O(r^{-2})$ as $r \to \infty$ and the standard Fourier theorem allows $\bar{E}(\bar{r})$ to be expanded as

$$\bar{E}(\bar{r}) = \frac{1}{2\pi} \int_{-\infty}^{+\infty} \int_{-\infty}^{+\infty} \bar{b}(k_x, k_y, z) e^{i(k_x x + k_y y)} dk_x dk_y, \ z \geq z_0 \tag{2.118}$$

where $\bar{b}$ is the Fourier transform of $\bar{E}(\bar{r})$. Because $\nabla^2 \bar{E} = 0$, the function $\bar{b}$ satisfies

$$\left[\frac{\partial^2}{\partial z^2} - k_x^2 - k_y^2\right] \bar{b}(k_x, k_y, z) = 0. \tag{2.119}$$

By using the fact that $\bar{b} \to 0$ as $z \to \infty$, one finds the solution to (2.119) is

$$\bar{b}(k_x, k_y, z) = \bar{T}(k_x, k_y) e^{-z\sqrt{k_x^2 + k_y^2}}. \tag{2.120}$$

Insertion of (2.120) into (2.118) shows that the static electric field can be expressed by the plane-wave spectrum representation

$$\bar{E}(\bar{r}) = \frac{1}{2\pi}\int_{-\infty}^{+\infty}\int_{-\infty}^{+\infty}\bar{T}(k_x,k_y)e^{i(k_x x+k_y y+i\sqrt{k_x^2+k_y^2}z)}dk_x dk_y, \quad z \geq z_0. \tag{2.121}$$

Taking the inverse Fourier transform of (2.121) yields the plane-wave spectrum of the electric field

$$\bar{T}(k_x,k_y) = \frac{e^{z\sqrt{k_x^2+k_y^2}}}{2\pi}\int_{-\infty}^{+\infty}\int_{-\infty}^{+\infty}\bar{E}(x',y',z)e^{-i(k_x x'+k_y y')}dx'dy', \quad z \geq z_0. \tag{2.122}$$

Because $|\bar{E}| = O(r^{-2})$ at infinity, (2.122) shows that the spectrum $\bar{T}$ has no singularities. Bringing the derivatives inside the integral in (2.121) one finds that $\nabla \cdot \bar{E} = 0$ implies that

$$\bar{T}(k_x,k_y)\cdot\bar{k} = 0 \tag{2.123}$$

where $\bar{k} = k_x\hat{x} + k_y\hat{y} + i\sqrt{k_x^2+k_y^2}\hat{z}$. Similarly, $\nabla \times \bar{E} = 0$ implies

$$\bar{T}(k_x,k_y)\times\bar{k} = 0. \tag{2.124}$$

Crossing $\bar{k}$ into (2.124) shows that (2.123) is implied by (2.124) because $\bar{k}\cdot\bar{k} = 0$. Equation (2.124) with $\bar{k}\cdot\bar{k} = 0$ implies that the spectrum can be written as

$$\bar{T}(k_x,k_y) = L(k_x,k_y)\bar{k} \tag{2.125}$$

where L is a scalar function. (This means that $\bar{T}\cdot\bar{T} = 0$ (since $\bar{k}\cdot\bar{k} = 0$), which does not imply that $\bar{T} = 0$, because $\bar{T}$ is a complex vector. In other words, the dot operation is not a scalar product.) Thus the spectrum is parallel to the propagation direction $\bar{k}$ of the "plane wave" $e^{i(k_x x+k_y y+i\sqrt{k_x^2+k_y^2}z)}$ (even though it is also perpendicular to $\bar{k}$ in the sense of (2.123)), and consequently only one of the spectrum's three rectangular components is necessary to specify it completely. This means from (2.121) and (2.122) that the electric field in the half space $z > z_0$ is completely determined from one component of the electric field (for example E_x) on the plane $z = z_0$.

The static analysis in this section has been based so far on the static plane-wave spectrum representations for the fields. The static Green's function representation can be obtained from the limit of (2.44) as k approaches zero; namely

$$\bar{E}(\bar{r}) = -\frac{1}{2\pi}\int_{-\infty}^{+\infty}\int_{-\infty}^{+\infty}\frac{1}{R^3}\bar{R}\times\left[\hat{z}\times\bar{E}(\bar{r}')\right]dx'dy', \quad z > z_0 \tag{2.126}$$

where $\bar{R} = (x-x')\hat{x}+(y-y')\hat{y}+(z-z_0)\hat{z}$. Equation (2.126) gives the electric field for $z > z_0$ in terms of the x and y components of the electric field on the plane $z = z_0$. Combining (2.126) with the Stratton-Chu formula [39, p.467] for $\omega = 0$ shows that the electric field is also given by the integral

$$\bar{E}(\bar{r}) = \frac{1}{2\pi}\int_{-\infty}^{+\infty}\int_{-\infty}^{+\infty}\frac{\bar{R}}{R^3}E_z(\bar{r}')dx'dy', \quad z > z_0 \tag{2.127}$$

involving only the z component of the electric field on the plane $z = z_0$.

We can also find a Green's function representation for the static electric field in the half space $z > z_0$ in terms of either the x or y components of the electric field on the plane $z = z_0$. An easy way to do this is to insert (2.125) into (2.121) and (2.122) to get

$$\bar{E}(\bar{r}) = \frac{1}{2\pi}\int_{-\infty}^{+\infty}\int_{-\infty}^{+\infty}\bar{k}L(k_x,k_y)e^{i\bar{k}\cdot\bar{r}}dk_xdk_y = \frac{1}{2\pi i}\nabla\int_{-\infty}^{+\infty}\int_{-\infty}^{+\infty}L(k_x,k_y)e^{i\bar{k}\cdot\bar{r}}dk_xdk_y \quad (2.128)$$

$$\bar{k}L(k_x,k_y) = \frac{e^{z_0\sqrt{k_x^2+k_y^2}}}{2\pi}\int_{-\infty}^{+\infty}\int_{-\infty}^{+\infty}\bar{E}(x',y',z_0)e^{-i(k_xx'+k_yy')}dx'dy'. \quad (2.129)$$

Substitute the x, y, and z components of (2.129), respectively, into the right side of (2.128), and use the relationships

$$\frac{1}{|\bar{r}-\bar{r}'|} = -\frac{1}{2\pi i}\int_{-\infty}^{+\infty}\int_{-\infty}^{+\infty}\frac{e^{i\bar{k}\cdot(\bar{r}-\bar{r}')}}{i\sqrt{k_x^2+k_y^2}}dk_xdk_y, \quad z > z' \quad (2.130)$$

$$\frac{\partial}{\partial z}\int_{-\infty}^{x}\frac{dx'}{|\bar{r}-\bar{r}'|} = -\frac{1}{2\pi i}\int_{-\infty}^{+\infty}\int_{-\infty}^{+\infty}\frac{e^{i\bar{k}\cdot(\bar{r}-\bar{r}')}}{k_x}dk_xdk_y, \quad z > z' \quad (2.131)$$

$$\frac{\partial}{\partial z}\int_{-\infty}^{y}\frac{dy'}{|\bar{r}-\bar{r}'|} = -\frac{1}{2\pi i}\int_{-\infty}^{+\infty}\int_{-\infty}^{+\infty}\frac{e^{i\bar{k}\cdot(\bar{r}-\bar{r}')}}{k_y}dk_xdk_y, \quad z > z' \quad (2.132)$$

to obtain

$$\bar{E}(\bar{r}) = -\frac{1}{2\pi}\nabla\int_{-\infty}^{+\infty}\int_{-\infty}^{+\infty}\frac{E_z(\bar{r}')}{R}dx'dy' = -\frac{1}{2\pi}\nabla\frac{\partial}{\partial z}\int_{-\infty}^{x}dx\int_{-\infty}^{+\infty}\int_{-\infty}^{+\infty}\frac{E_x(\bar{r}')}{R}dx'dy'$$

$$= -\frac{1}{2\pi}\nabla\frac{\partial}{\partial z}\int_{-\infty}^{y}dy\int_{-\infty}^{+\infty}\int_{-\infty}^{+\infty}\frac{E_y(\bar{r}')}{R}dx'dy', \quad z > z_0 \quad (2.133)$$

which are expressions for the static electric field in the half space $z > z_0$ in terms of one rectangular component on the plane $z = z_0$. The first integral expression in (2.133) is, of course, identical to (2.127). These formulas could also have been derived using the scalar potential for the electric field and the scalar static Dirichlet and Neumann Green's functions.

The magnetic field, which is uncoupled from the electric field, can be found from the same expressions with $\bar{E}$ replaced by $\bar{H}$. (When the sources are located in the half space $z > z_0$ the formulas (2.122)-(2.125) hold for the fields in the half space $z \leq z_0$ provided that $\sqrt{k_x^2+k_y^2}$ is replaced by $-\sqrt{k_x^2+k_y^2}$. The Green's function formulas (2.126), (2.127), and (2.133) hold also for $z < z_0$ provided they are multiplied by -1.)

By working directly with the static equations instead of the spectra, we will now give an alternative proof that by specifying one component of the static electric field and one component of the static magnetic field on the plane $z = z_0$ one can determine all static field components in the half space $z > z_0$. To do this, we start by showing that the equations for the electric field $\nabla \times \bar{E} = 0$ and $\nabla \cdot \bar{E} = 0$ together with one component of $\bar{E}$ on the measurement plane $z = z_0$, are sufficient to determine $\bar{E}$ in the half space $z > z_0$. The curl

equation shows that $\bar{E}$ may be expressed as the gradient of a scalar field, and thus $\bar{E}$ is uniquely determined except for an additive gradient field. Therefore consider the field

$$\bar{E}_1 = \bar{E} + \nabla\Psi \tag{2.134}$$

where $\bar{E}$ is the correct electric field and Ψ is a scalar function satisfying Laplace's equation $\nabla^2\Psi = 0$. Our proof is now reduced to showing that if one rectangular component of $\bar{E}_1$ on the plane $z = z_0$ equals that of $\bar{E}$, then $\nabla\Psi = 0$ for $z > z_0$. From Morse and Feshbach [40, p.1265] it follows that a scalar field Ψ satisfying Laplace's equation can be written in terms of spherical harmonics as

$$\Psi(\bar{r}) = \sum_{n=-\infty}^{n=+\infty} A_n(\theta,\phi)r^n \tag{2.135}$$

outside the source region. Since the source region is finite it is found that $A_n = 0$ for $n > 0$ and since $A_0 = C$ is a constant, it is found that $\Psi = C + O(r^{-1})$ at infinity. The constant C may be chosen to be zero and consequently $\Psi = O(r^{-1})$ at infinity.

Assume now that we know $E_x = E_{1x}$ on the plane $z = z_0$. Then $\frac{\partial}{\partial x}\Psi = 0$ on that plane. Because $\Psi \to 0$ at infinity, this means that $\Psi \equiv 0$ on the plane $z = z_0$. Using the facts that Ψ satisfies the Laplace' equation and is of order r^{-1} at infinity, the divergence theorem now shows that

$$\int_{z\geq z_0} |\nabla\Psi|^2 dV = \int_{z\geq z_0} \nabla\cdot(\Psi\nabla\Psi)dV = -\int_{-\infty}^{+\infty}\int_{-\infty}^{+\infty} \Psi\frac{\partial}{\partial z}\Psi|_{z=z_0}dxdy = 0 \tag{2.136}$$

since there is no contribution from the semicircle at infinity. Consequently Ψ is identically zero in the half space $z > z_0$. Thus $\bar{E} = \bar{E}_1$ and it has been shown that by specifying the x component of the electric field on the plane $z = z_0$, all electric field components can be calculated in the half space $z > z_0$. Similarly, by specifying the y component of the electric field on the plane $z = z_0$, all electric field components can be calculated in the half space $z > z_0$.

Assume now that we know $E_z = E_{1z}$ on the plane $z = z_0$. Then one finds that Ψ satisfies the Neumann boundary condition on the plane $z = z_0$, and (2.136) again shows that Ψ is identically zero in the half space $z > z_0$. Thus, specifying any component of the electric field on the plane $z = z_0$ determines all electric field components in the half space $z > z_0$. Of course, the same is true for the magnetic field. Thus, the specification of one rectangular component of both the static electric and magnetic fields on the plane $z = z_0$ determines all static field components for $z > z_0$.

In the time-harmonic case ($\omega \neq 0$), non-zero far fields always have e^{ikr}/r radial dependence (except at isolated nulls in the far-field pattern). Thus, the convenient far-field formula (2.49) could be derived from (2.44) by inserting the asymptotic form of the Green's function. The same procedure applied to the static Green's function representations (2.126), (2.127), and (2.133) fails, in general, to produce the correct static far field. There are two reasons for this failure. First, the radial dependence of the static far field differs depending on the lowest multipole present in the source distribution (r^{-n-2} for the n^{th} multipole, $n = 0, 1, 2, ...$). Secondly, the limit as $r \to \infty$ of the integral in (2.126), (2.127), and (2.133) does not, in general,

equal the integral of the limit. For example, if one replaces $\bar{R}/R^3$ by $\bar{r}/r^3$ in the integral of (2.126) one gets the ridiculous result that the far electric field is always perpendicular to the far-field direction $\bar{r}$. (For a point charge Q to the left of $z = z_0$ the integral in (2.126) can be evaluated to show that as $r \to \infty$, $\bar{E}(\bar{r})$ correctly approaches $Q\hat{r}/(4\pi\epsilon_0 r^2)$. If however, the limit as $r \to \infty$ is mistakenly taken under the integral first, so that $\bar{R}/R^3$ becomes $\bar{r}/r^3$, the integral evaluates to zero.) Thus in general, there is no single simple expression for static far fields analogous to (2.49) for the time-harmonic fields.

2.5.2 Electric Losses Only ($\sigma \neq 0$, $\sigma_m = 0$)

From the static Maxwell equations (2.117) it is seen that the electric field in this case satisfies the same differential equations ($\nabla \times \bar{E} = 0$, $\nabla \cdot \bar{E} = 0$, and $\nabla^2 \bar{E} = 0$) as in the lossless case. Consequently from Section 2.5.1, the electric field is given by the plane wave spectrum representation (2.121) and its spectrum $\bar{T}$ satisfies (2.122), (2.123), (2.124), and (2.125). The magnetic field satisfies $\nabla \cdot \bar{H} = 0$, $\nabla^2 \bar{H} = 0$ (but not $\nabla \times \bar{H} = 0$) and the analysis of Section 2.5.1 shows that

$$\bar{H}(\bar{r}) = \frac{1}{2\pi} \int_{-\infty}^{+\infty} \int_{-\infty}^{+\infty} \bar{T}_H(k_x, k_y) e^{i(k_x x + k_y y + i\sqrt{k_x^2 + k_y^2} z)} dk_x dk_y, \quad z \geq z_0 \tag{2.137}$$

where the spectrum $\bar{T}_H$ for the magnetic field is

$$\bar{T}_H(k_x, k_y) = \frac{e^{z\sqrt{k_x^2 + k_y^2}}}{2\pi} \int_{-\infty}^{+\infty} \int_{-\infty}^{+\infty} \bar{H}(x', y', z) e^{-i(k_x x' + k_y y')} dx' dy', \quad z \geq z_0. \tag{2.138}$$

One finds that $\nabla \cdot \bar{H} = 0$ implies that

$$\bar{T}_H(k_x, k_y) \cdot \bar{k} = 0 \tag{2.139}$$

and that $\nabla \times \bar{H} = \sigma \bar{E}$ shows

$$i\bar{k} \times \bar{T}_H(k_x, k_y) = \sigma \bar{T}(k_x, k_y) \tag{2.140}$$

where $\bar{T}$ is the spectrum for the electric field. As in the lossless case, $\bar{k} = k_x \hat{x} + k_y \hat{y} + i\sqrt{k_x^2 + k_y^2}\hat{z}$. Taking the vector cross product of $\bar{k}$ with (2.140) shows that (2.124) and (2.140) imply (2.139).

Let us now discuss which field components must be specified on the plane $z = z_0$ to determine all field components in the half space $z > z_0$. As in the lossless case, one component of the electric field on the plane $z = z_0$ is sufficient for calculating all electric field components in the half space $z > z_0$. Because of (2.139) (which is a consequence of $\nabla \cdot \bar{H} = 0$) it is seen that two components of the magnetic field on the plane $z = z_0$ completely determine all components of the magnetic field in the half space $z > z_0$. One component of the magnetic field is not sufficient because $\nabla \times \bar{H} \neq 0$. Furthermore it is seen from (2.140) that $\bar{T}$ can be determined from $\bar{T}_H$ so two components of the magnetic field on the plane $z = z_0$ are sufficient for calculating all electric and magnetic fields in the half space $z > z_0$.

Since a vector parallel to $\bar{k}$ may be added to $\bar{T}_H$ in (2.140) without changing $\bar{T}$, it is seen that the electric field does not determine the magnetic field. Thus, it is necessary to specify at least one component of the magnetic field on the plane $z = z_0$ to find the fields for $z > z_0$. To find out if one component of both electric and magnetic field on the plane $z = z_0$ is sufficient to calculate the fields for $z > z_0$, use (2.125) and write (2.140) in matrix form as

$$i\sigma L(k_x, k_y) \begin{pmatrix} k_x \\ k_y \\ i\sqrt{k_x^2 + k_y^2} \end{pmatrix} = \begin{pmatrix} 0 & i\sqrt{k_x^2 + k_y^2} & -k_y \\ -i\sqrt{k_x^2 + k_y^2} & 0 & k_x \\ k_y & -k_x & 0 \end{pmatrix} \begin{pmatrix} T_{Hx} \\ T_{Hy} \\ T_{Hz} \end{pmatrix}. \qquad (2.141)$$

Assur now that any one of the components of the electric field is known on $z = z_0$ (which means that all components of the electric field can be calculated) and that H_x is known on $z = z_0$ (which means that T_{Hx} is known). Then (2.141) can be solved uniquely for T_{Hy} and T_{Hz}. Consequently, any component of the electric field and H_x on $z = z_0$ completely determine all fields for $z > z_0$. Similarly one finds that all electric and magnetic field components can be calculated in the half space $z > z_0$ if a single component of both the magnetic field and the electric field on the plane $z = z_0$ is specified.

After having determined the plane-wave spectrum formulas, we now turn to the Green's function representations. Clearly the electric field is given by the Green's function formulas (2.126), (2.127), and (2.133). The magnetic field is also given by the formula (2.126) (but not (2.127) because $\nabla \times \bar{H} \neq 0$) with $\bar{E}$ replaced by $\bar{H}$. This shows again, that by specifying H_x and H_y on the plane $z = z_0$ one can determine all fields for $z > z_0$ because the electric field can be determined from $\bar{E} = \frac{1}{\sigma}\nabla \times \bar{H}$.

Using the static equations instead of the spectra, we will now give an alternative proof that one rectangular component of both the electric and magnetic field on the plane $z = z_0$ determines all field components in the half space $z > z_0$. To do this assume first that one component of the electric field, and the x component of the magnetic field, are known on the plane $z = z_0$ (then the electric field is known for $z \geq z_0$). The equations for the magnetic field $\nabla \times \bar{H} = \sigma\bar{E}$ (where $\bar{E}$ is known) and $\nabla \cdot \bar{H} = 0$ determine the magnetic field except for an additive gradient field. The scalar Ψ in this gradient field satisfies Laplace's equation and the boundary condition $\frac{\partial}{\partial x}\Psi = 0$ on the plane $z = z_0$. Proceeding as in Section 2.5.1 shows that $\Psi \equiv 0$ and thus all field components are uniquely determined in the half space $z > z_0$. Similarly, one finds that this is true when the y or z component of the magnetic field is specified on the plane $z = z_0$. Thus we have an alternative proof that all fields in the half space $z > z_0$ can be calculated if one component of both electric and magnetic fields are known on the plane $z = z_0$.

(When the sources are located in the half space $z > z_0$ the formulas in this section hold for the fields in the half space $z \leq z_0$ provided that $\sqrt{k_x^2 + k_y^2}$ is replaced by $-\sqrt{k_x^2 + k_y^2}$.)

For the case with only magnetic losses ($\sigma = 0, \sigma_m \neq 0$) the analysis of this section applies with $\bar{E}$ and $\bar{H}$ interchanged and σ replaced by σ_m.

2.5.3 Electric and Magnetic Losses ($\sigma \neq 0$, $\sigma_m \neq 0$)

The static Maxwell equations (2.117) show that the electric field satisfies

$$\nabla^2 \bar{E} - \sigma_m \sigma \bar{E} = 0, \quad \nabla \cdot \bar{E} = 0 \tag{2.142}$$

and the magnetic field satisfies the same equations with $\bar{E}$ replaced by $\bar{H}$. The identity $\nabla^2 = \nabla(\nabla\cdot) - \nabla \times \nabla\times$ easily shows that (2.142) along with $\nabla \times \bar{E} = -\sigma_m \bar{H}$ is equivalent to the static Maxwell equations (2.117). Although (2.142) has the same form as the time-harmonic Helmholtz equation, there is a major difference; namely $-\sigma_m \sigma$ is less than zero while $k^2 = (\omega/c)^2$ is greater than zero. Thus the solutions have a very different character. (In particular, the plane-wave spectra of $\bar{E}$ and $\bar{H}$ have only attenuating modes.) Performing a derivation similar to the one in Section 2.1.1, we find that

$$\bar{E}(\bar{r}) = \frac{1}{2\pi} \int_{-\infty}^{+\infty} \int_{-\infty}^{+\infty} \bar{T}(k_x, k_y) e^{i(k_x x + k_y y + i\sqrt{\sigma_m \sigma + k_x^2 + k_y^2} z)} dk_x dk_y, \quad z \geq z_0 \tag{2.143}$$

with the spectrum $\bar{T}$ for the electric field given by

$$\bar{T}(k_x, k_y) = \frac{e^{z\sqrt{\sigma_m \sigma + k_x^2 + k_y^2}}}{2\pi} \int_{-\infty}^{+\infty} \int_{-\infty}^{+\infty} \bar{E}(x, y, z) e^{-i(k_x x + k_y y)} dx dy, \quad z \geq z_0. \tag{2.144}$$

The condition $\nabla \cdot \bar{E} = 0$ implies that

$$\bar{T}(k_x, k_y) \cdot \bar{k} = 0 \tag{2.145}$$

where $\bar{k} = k_x \hat{x} + k_y \hat{y} + i\sqrt{\sigma_m \sigma + k_x^2 + k_y^2}\hat{z}$. The spectrum $\bar{T}_H$ for the magnetic field is given by (2.144) with $\bar{E}$ replaced by $\bar{H}$, and the magnetic field is given by (2.143) with $\bar{T}$ replaced by $\bar{T}_H$. Of course $\bar{T}_H$ also satisfies (2.145). The static Maxwell equation $\nabla \times \bar{E} = -\sigma_m \bar{H}$ shows that

$$i\bar{k} \times \bar{T}(k_x, k_y) = -\sigma_m \bar{T}_H(k_x, k_y) \tag{2.146}$$

and $\nabla \times \bar{H} = \sigma \bar{E}$ shows that

$$i\bar{k} \times \bar{T}_H(k_x, k_y) = \sigma \bar{T}(k_x, k_y). \tag{2.147}$$

Note that (2.147) can be obtained from $i\bar{k}\times$(2.146) along with the relation $\bar{k} \cdot \bar{k} = -\sigma_m \sigma$ and (2.145). Similarly (2.146) can be obtained from (2.147). Because $\bar{T}$ and $\bar{T}_H$ are both perpendicular to $\bar{k}$, only two components of $\bar{E}$ or two components of $\bar{H}$ are needed on the plane $z = z_0$ to calculate all fields in the half space $z > z_0$.

Let us now see if it is sufficient to specify one component of the electric field and one component of the magnetic field on the plane $z = z_0$. Assume first that we know H_x and E_x on the plane $z = z_0$. Then T_x and T_{Hx} can be calculated from (2.144) and its equivalent equation for $\bar{T}_H$, respectively. Taking the dot product of $\hat{x}$ and (2.146) we get

$$(\sqrt{\sigma_m \sigma + k_x^2 + k_y^2}\hat{y} + ik_y \hat{z}) \cdot \bar{T} = -\sigma_m T_{Hx}. \tag{2.148}$$

Along with (2.145), (2.148) gives two equations that determine $\bar{T}$ completely and (2.146) then determines $\bar{T}_H$. Thus, all fields are determined in the region $z > z_0$ by specifying H_x and E_x on the plane $z = z_0$. Assume now that H_y and E_x are known on the plane $z = z_0$. Then T_x and T_{Hy} can be calculated, and taking the dot product of $\hat{x}$ and (2.147) we get

$$(\sqrt{\sigma_m \sigma + k_x^2 + k_y^2}\hat{y} + ik_y\hat{z}) \cdot \bar{T}_H = -\sigma T_x \tag{2.149}$$

which determines T_{Hz}. Equation (2.145) with $\bar{T}$ replaced by $\bar{T}_H$ now gives us T_{Hx} and thus $\bar{T}_H$ is completely determined. Equation (2.147) then gives $\bar{T}$ and all fields are determined in the half space $z > z_0$. Repeating this analysis for any combination of rectangular components of the electric and magnetic fields one finds that a single component of both the electric and magnetic field on the plane $z = z_0$ is sufficient for calculating all fields in the half space $z > z_0$.

Let us now consider the Green's function representations. The expressions for the permeability and permittivity in (2.115) and (2.116), and the equation for the static electric field (2.142) show that the time harmonic results from Section 2.1.4 can be used after replacing the propagation constant k with

$$\lim_{\omega \to 0_+} \omega\sqrt{\epsilon(\omega)\mu(\omega)} = i\sqrt{\sigma_m \sigma}. \tag{2.150}$$

The time harmonic equation (2.44) now shows that the electric field is given by

$$\bar{E}(\bar{r}) = \frac{-1}{2\pi} \int_{-\infty}^{+\infty} \int_{-\infty}^{+\infty} \frac{e^{-\sqrt{\sigma_m \sigma} R}}{R^2} \left[\sqrt{\sigma_m \sigma} + \frac{1}{R}\right] \bar{R} \times \left[\hat{z} \times \bar{E}(\bar{r}')\right] dx'dy', \quad z > z_0 \tag{2.151}$$

with $\bar{R} = (x - x')\hat{x} + (y - y')\hat{y} + (z - z_0)\hat{z}$ and $\bar{r}' = x'\hat{x} + y'\hat{y} + z_0\hat{z}$. From (2.46) it is found that the static magnetic field is

$$\begin{aligned} \bar{H}(\bar{r}) = \frac{-1}{2\sigma_m \pi} \int_{-\infty}^{+\infty} \int_{-\infty}^{+\infty} \Bigg\{ & \sigma_m \sigma \left[\frac{\bar{R} \cdot (\hat{z} \times \bar{E}(\bar{r}'))}{R^2} \bar{R} - \hat{z} \times \bar{E}(\bar{r}')\right] \\ & - \sqrt{\sigma_m \sigma} \left[-\frac{3\bar{R} \cdot (\hat{z} \times \bar{E}(\bar{r}'))}{R^3} \bar{R} + \frac{1}{R} \hat{z} \times \bar{E}(\bar{r}')\right] \\ & + \left[\frac{3\bar{R} \cdot (\hat{z} \times \bar{E}(\bar{r}'))}{R^4} \bar{R} - \frac{1}{R^2} \hat{z} \times \bar{E}(\bar{r}')\right] \Bigg\} \frac{e^{-\sqrt{\sigma_m \sigma} R}}{R} dx'dy', \quad z > z_0. \end{aligned} \tag{2.152}$$

(When the sources are located in the half space $z > z_0$ the spectral formulas in this section hold for the fields in the half space $z \leq z_0$ provided that $\sqrt{k_x^2 + k_y^2}$ is replaced by $-\sqrt{k_x^2 + k_y^2}$. The Green's function formulas (2.151)-(2.152) hold also for $z < z_0$ provided they are multiplied by -1.)

Chapter 3

Time-Domain Formulas

In this chapter, we derive the time-domain planar near-field formulas for both acoustic and electromagnetic fields. As in the previous chapter, the planar scanning geometry is shown in Figure 2.1 with the finite source region located in the half space $z < z_0$. The fields are specified on the plane $z = z_0$ and we are interested in calculating the fields in the half space $z > z_0$. All fields are assumed to be zero for $t < 0$ and to have arbitrary time dependence for $t \geq 0$.

The electric and magnetic fields in the source-free half space satisfy the time dependent Maxwell equations

$$\nabla \times \bar{H} = \sigma \bar{E} + \epsilon \frac{\partial}{\partial t} \bar{E}, \quad \nabla \times \bar{E} = -\sigma_m \bar{H} - \mu \frac{\partial}{\partial t} \bar{H}, \quad \nabla \cdot \bar{H} = 0, \quad \nabla \cdot \bar{E} = 0 \tag{3.1}$$

where ϵ, μ, σ, and σ_m are the space and time independent permittivity, permeability, electric conductivity, and magnetic conductivity, respectively, all discussed in Section 2.5. (In particular, it was shown in Section 2.5 that, in principle, a constant σ_m can be obtained from the proper constitutive relations for lossy magnetic material without postulating magnetic monopoles.) For a lossless medium both σ and σ_m are zero.

Maxwell's equations (3.1) show that

$$\frac{\partial}{\partial t} \bar{H} + \frac{\sigma_m}{\mu} \bar{H} = -\frac{1}{\mu} \nabla \times \bar{E} \tag{3.2}$$

which, under the assumption that all fields are zero for $t < 0$, gives the expression

$$\bar{H}(\bar{r}, t) = -\frac{e^{-t\sigma_m/\mu}}{\mu} \int_0^t e^{t'\sigma_m/\mu} \nabla \times \bar{E}(\bar{r}, t') dt' \tag{3.3}$$

for the magnetic field. Also, recall from (2.15) that E_x and E_y in the half space $z \geq z_0$ determines E_z in that half space. Consequently, all components of both the magnetic and electric fields can be calculated from (3.3) and (2.15) if E_x and E_y are known for $z \geq z_0$. Moreover, the derivations of Section 3.1 will prove that causal E_x and E_y for $z \geq z_0$ are uniquely determined from their values on the infinite plane $z = z_0$. Thus, the complete

causal electromagnetic fields obeying Maxwell's equations are uniquely determined in the $z \geq z_0$ half space from the transverse electric field on the plane $z = z_0$.

Maxwell's equations (3.1) in the half space $z \geq z_0$ show that $\bar{E}_{xy} = E_x\hat{x} + E_y\hat{y}$ satisfies

$$\nabla^2 \bar{E}_{xy}(\bar{r},t) - \frac{1}{c^2}\frac{\partial^2}{\partial t^2}\bar{E}_{xy}(\bar{r},t) - (\sigma_m\epsilon + \sigma\mu)\frac{\partial}{\partial t}\bar{E}_{xy}(\bar{r},t) - \sigma_m\sigma\bar{E}_{xy}(\bar{r},t) = 0 \tag{3.4}$$

where $c = (\epsilon\mu)^{-1/2}$ is the speed of light. Because $\bar{E}_{xy}$ satisfies (3.4), (2.15) shows that E_z satisfies (3.4), and thus

$$\nabla^2 \bar{E}(\bar{r},t) - \frac{1}{c^2}\frac{\partial^2}{\partial t^2}\bar{E}(\bar{r},t) - (\sigma_m\epsilon + \sigma\mu)\frac{\partial}{\partial t}\bar{E}(\bar{r},t) - \sigma_m\sigma\bar{E}(\bar{r},t) = 0 \tag{3.5}$$

which, of course, also follows directly from Maxwell's equations (3.1). Since $\nabla^2\bar{E} = -\nabla \times \nabla \times \bar{E}$, the curl of $\bar{E}$ from (3.2) (an equation implied by (3.3)) can be inserted into the first term of (3.5) to give

$$\left(\sigma_m + \mu\frac{\partial}{\partial t}\right)\left(\nabla \times \bar{H} - \sigma\bar{E} - \epsilon\frac{\partial}{\partial t}\bar{E}\right) = 0 \tag{3.6}$$

a differential equation with the zero-initial-value solution

$$\nabla \times \bar{H} - \sigma\bar{E} - \epsilon\frac{\partial}{\partial t}\bar{E} = 0. \tag{3.7}$$

Therefore, we have shown that (3.4) along with $\nabla \cdot \bar{E} = 0$ and (3.3) imply that $\bar{E}$ and $\bar{H}$ satisfy Maxwell's equations (3.1). In other words, it is sufficient to work with the time-domain wave equation (3.4), satisfied by E_x and E_y, to determine fields for $z \geq z_0$. A similar statement holds, of course, for the magnetic field.

3.1 Time-Domain Green's Function Formulas

This section derives time-domain formulas that are analogs to the frequency-domain Green's function formulas of Section 2.1.4. These time-domain formulas are obtained in Section 3.1.1 by Fourier transforming the frequency-domain Green's function formulas, and are rederived in Section 3.1.2 by working directly in the time domain with time-domain Green's functions. In Section 3.1.3 a formula is derived that gives the time-domain magnetic field in the half space $z > z_0$ in terms of the time-domain electric field on the plane $z = z_0$, and the class of time functions for which the Fourier transform can be used to calculate the time-domain fields is discussed. The space surrounding the sources is assumed in the following sections to be lossless, that is, $\sigma = 0$ and $\sigma_m = 0$, because for lossy space the expressions for the time-domain fields in the half space $z \geq z_0$ do not reduce, in general, to simple integrals of the time-domain fields on the plane $z = z_0$.

3.1.1 Derivation from the Fourier Transform

Start by considering the acoustic field Φ satisfying the wave equation

$$\nabla^2\Phi(\bar{r},t) - \frac{1}{c^2}\frac{\partial^2}{\partial t^2}\Phi(\bar{r},t) = 0, \quad z > z_0. \tag{3.8}$$

(In the acoustic field equations, c is the speed of sound.) Clearly $\Phi(\bar{r},t)$ can be found from its Fourier transform $\Phi_\omega(\bar{r})$ given in (2.36) using the Fourier inversion formula

$$\Phi(\bar{r},t) = \int_{-\infty}^{+\infty} \Phi_\omega(\bar{r})e^{-i\omega t}d\omega. \tag{3.9}$$

(In this chapter frequency-domain fields are labeled with subscript ω.) Writing the propagation constant as $k = \omega/c$, the frequency-domain formula (2.36) becomes

$$\Phi_\omega(\bar{r}) = \frac{z_0 - z}{2\pi}\int_{-\infty}^{+\infty}\int_{-\infty}^{+\infty}\Phi_\omega(\bar{r}')\left[\frac{i\omega}{c} - \frac{1}{R}\right]\frac{e^{i\omega R/c}}{R^2}dx'dy', \quad z > z_0 \tag{3.10}$$

with $\bar{r}' = x'\hat{x} + y'\hat{y} + z_0\hat{z}$ and $R = \sqrt{(x-x')^2 + (y-y')^2 + (z-z_0)^2}$. Inserting Φ_ω from (3.10) into (3.9) and interchanging the orders of integration, (3.9) becomes

$$\Phi(\bar{r},t) = \frac{z - z_0}{2\pi c}\int_{-\infty}^{+\infty}\int_{-\infty}^{+\infty}\frac{1}{R^2}\left[\frac{\partial\Phi}{\partial t}(\bar{r}',t - R/c) + \frac{c}{R}\Phi(\bar{r}',t-R/c)\right]dx'dy', \quad z > z_0 \tag{3.11}$$

where the derivative rule

$$\frac{\partial\Phi}{\partial t}(\bar{r},t) = \int_{-\infty}^{+\infty} -i\omega\Phi_\omega(\bar{r})e^{-i\omega t}d\omega \tag{3.12}$$

has been used. Equation (3.11) gives the time-domain field in the region $z > z_0$ in terms of the field on the plane $z = z_0$. Because we assume that all fields are zero for $t < 0$ and that the sources are in a finite region of space, the $\bar{r}'$ integration in (3.11) is over a finite region. Therefore, the expansion $R = r - \hat{r}\cdot\bar{r}' + O(r^{-1})$ as $r \to \infty$ can be inserted into (3.11) to obtain the time-domain far-field expression

$$\Phi(\bar{r},t) \sim \frac{\cos\theta}{2\pi cr}\int_{-\infty}^{+\infty}\int_{-\infty}^{+\infty}\frac{\partial\Phi}{\partial t}(\bar{r}',t - r/c + \bar{r}'\cdot\hat{r}/c)dx'dy' + O\left(\frac{1}{r^2}\right), \quad z > z_0 \tag{3.13}$$

where $\hat{r} = \hat{x}\cos\phi\sin\theta + \hat{y}\sin\theta\sin\phi + \hat{z}\cos\theta$. This result could also have been obtained by Fourier transforming the frequency-domain far field (2.47). Note that the far field is of order r^{-1} if the first time derivative of the field on the measurement plane $z = z_0$ is a finite function of time (see Section 3.3.3 and Appendix B).

Similarly, by Fourier transforming the electromagnetic frequency domain formula (2.44), one finds that the time-domain electric field is given by

$$\bar{E}(\bar{r},t) = \frac{-1}{2\pi}\int_{-\infty}^{+\infty}\int_{-\infty}^{+\infty}\frac{\bar{R}}{R^2}\times\left[\frac{1}{c}\hat{z}\times\frac{\partial}{\partial t}\bar{E}(\bar{r}',t - R/c) + \frac{1}{R}\hat{z}\times\bar{E}(\bar{r}',t-R/c)\right]dx'dy', \quad z > z_0 \tag{3.14}$$

and that the time-domain far electric field is

$$\bar{E}(\bar{r},t) \sim \frac{-1}{2\pi cr}\hat{r} \times \int_{-\infty}^{+\infty}\int_{-\infty}^{+\infty} \hat{z} \times \frac{\partial}{\partial t}\bar{E}(\bar{r}', t - r/c + \bar{r}' \cdot \hat{r}/c)dx'dy' + O\left(\frac{1}{r^2}\right), \quad z > z_0 \quad (3.15)$$

which shows that the far electric field is of order r^{-1} if the first time derivative of the x and y components of the electric field on the plane $z = z_0$ are finite functions of time (see Section 3.3.3 and Appendix B). This far-field result was derived previously by Hill [15] by taking the inverse Fourier transform of (2.49). Although it has been assumed that all fields are zero for $t < 0$, the formula (3.14) is also valid for static electric fields, as can be seen from (2.126). The corresponding formulas for the magnetic field will be derived in Section 3.1.3.

In this section it has been assumed that the time dependence of the field is such that its time Fourier transform exists. For time signals with infinite energy, such as the unit step function, the standard Fourier transform cannot be used because the Fourier integral does not exist and the analysis in this section does not apply. However, one can repair this deficiency in the derivation of (3.14) and (3.15) in a number of ways: One way is to use distribution theory. Another way is to give the time signal with infinite energy an exponential decay and then let the decay go to zero after having derived the near-field formulas. Still another way is to use the complex Fourier transform, described in Dettman [41, pp.365-369], which is obtained by letting the real contour from the standard Fourier integration become complex. The use of the complex Fourier transform is illustrated in Section 3.1.3 where the magnetic field is calculated.

(When the sources are located in the half space $z > z_0$, the fields in the half space $z < z_0$ are given by the negative of the time-domain formulas derived in this section.)

3.1.2 Derivation from Time-Domain Green's Functions

This section derives the time-domain near-field transformation formulas (3.11) and (3.14) for the acoustic and electric field using a time-domain Green's function approach. The idea of this approach comes from Stratton [39, sec.8.1], who deals only with scalar fields, and is based on Green's second identity.

First consider the acoustic field Φ satisfying the wave equation (3.8) in the free-space region. Green's second identity will be used in the following to derive the representation for this field. The time-domain free-space Green's function $G(\bar{r}, \bar{r}', t, t')$ is

$$G(\bar{r}, \bar{r}', t, t') = \frac{\delta(t - t' + R/c)}{4\pi R}, \quad R = |\bar{r} - \bar{r}'| \quad (3.16)$$

and the Dirichlet Green's function for the half space $z \geq z_0$ equals

$$G_D(\bar{r}, \bar{r}', t, t') = G(\bar{r}, \bar{r}', t, t') - G(\bar{r}, \bar{r}_i', t, t'), \quad \bar{r}_i' = x'\hat{x} + y'\hat{y} + (2z_0 - z')\hat{z}. \quad (3.17)$$

The Dirichlet Green's function satisfies the wave equation

$$\nabla^2 G_D(\bar{r}, \bar{r}', t, t') - \frac{1}{c^2}\frac{\partial^2}{\partial t^2} G_D(\bar{r}, \bar{r}', t, t') = -\delta(\bar{r} - \bar{r}')\delta(t - t'), \quad z > z_0 \quad (3.18)$$

and the Dirichlet boundary condition $G_D = 0$ when $z = z_0$ or $z' = z_0$. Employing Green's second identity in the region bounded by the circular disk $C(R_0)$ and the half sphere $S(R_0)$ in Figure 2.2, the identity

$$\Phi\nabla^2 G_D - G_D\nabla^2\Phi = \frac{1}{c^2}\frac{\partial}{\partial t}\left[\Phi\frac{\partial}{\partial t}G_D - G_D\frac{\partial}{\partial t}\Phi\right] - \Phi\delta(\bar{r}-\bar{r}')\delta(t-t') \tag{3.19}$$

and the Dirichlet boundary condition for G_D, one finds that

$$-\Phi\delta(t-t') = -\frac{1}{c^2}\frac{\partial}{\partial t}\int_{V(R_0)}\left[\Phi\frac{\partial}{\partial t}G_D - G_D\frac{\partial}{\partial t}\Phi\right]dV$$
$$-\int_{C(R_0)}\Phi\frac{\partial}{\partial z}G_D dx dy, \quad \bar{r}' \in V(R_0) \tag{3.20}$$

where $V(R_0)$ is the region bounded by $S(R_0)\cup C(R_0)$. It has been assumed that $\Phi(\bar{r},t) \equiv 0$ for $t < 0$ and that $R_0 \gg ct$ so that speed-of-light causality insures there is no contribution to the integral over the half sphere $S(R_0)$. Integrating (3.20) with respect to t from $-\infty$ to $+\infty$ yields

$$\Phi(\bar{r}',t') = \int_{C(R_0)}\int_{-\infty}^{+\infty}\Phi\frac{\partial}{\partial z}G_D\,dt\,dx\,dy, \quad \bar{r}' \in V(R_0) \tag{3.21}$$

where $\lim_{t\to\pm\infty} G_D = 0$ has been used to show that the first integral in (3.20) does not contribute. Letting $R_0 \to +\infty$, using

$$\frac{\partial}{\partial z}G_D|_{z=z_0} = \frac{z_0 - z'}{2\pi c R^2}\left[\delta'(t-t'+R/c) - \frac{c}{R}\delta(t-t'+R/c)\right] \tag{3.22}$$

and integrating by parts to show that $\int_{-\infty}^{+\infty}\delta'(t-t_0)\Phi(\bar{r},t)dt = -\frac{\partial}{\partial t}\Phi(\bar{r},t_0)$, (3.21) becomes

$$\Phi(\bar{r},t) = \frac{z-z_0}{2\pi c}\int_{-\infty}^{+\infty}\int_{-\infty}^{+\infty}\frac{1}{R^2}\left[\frac{\partial\Phi}{\partial t}(\bar{r}',t-R/c) + \frac{c}{R}\Phi(\bar{r}',t-R/c)\right]dx'dy', \quad z > z_0 \tag{3.23}$$

where $\bar{r}'$ and t' have been interchanged with $\bar{r}$ and t. The near-field formula (3.23), obtained directly in the time domain, is seen to agree with the near-field formula (3.11), obtained by Fourier transforming the frequency-domain formula (2.36).

To derive the corresponding near-field formula for the electric field, it is convenient to use the time-domain Dirichlet dyadic Green's function $\overline{\overline{G}}_D(\bar{r},\bar{r}',t,t')$ for the half space $z \geq z_0$. This function can be found by Fourier transforming the corresponding frequency-domain dyadic Green's function (2.40). The expression for $\overline{\overline{G}}_D(\bar{r},\bar{r}',t,t')$ is found to be

$$\overline{\overline{G}}_D(\bar{r},\bar{r}',t,t') = \overline{\overline{I}}G_D(\bar{r},\bar{r}',t,t') + c^2\int_{-\infty}^{t-t'}\int_{-\infty}^{u}\nabla\nabla' G_D(\bar{r},\bar{r}',u',0)du'du + 2\hat{z}\hat{z}G(\bar{r},\bar{r}_i',t,t') \tag{3.24}$$

where $G_D(\bar{r},\bar{r}',t,t')$ is the Dirichlet Green's function (3.17) and $G(\bar{r},\bar{r}',t,t')$ is the free-space Green's function (3.16). The dyadic Green's function (3.24) satisfies the dyadic wave equation

$$\nabla\times\nabla\times\overline{\overline{G}}_D + \frac{1}{c^2}\frac{\partial^2}{\partial t^2}\overline{\overline{G}}_D = \overline{\overline{I}}\delta(\bar{r}-\bar{r}')\delta(t-t'), \quad z > z_0 \tag{3.25}$$

and the Dirichlet boundary condition $\hat{z} \times \overline{\overline{G}}_D = 0$ on the plane $z = z_0$. The dyadic version of Green's second identity (2.39) will now be used to derive a time-domain near-field formula for the electric field. Applying this identity to the region bounded by the circular disk $C(R_0)$ and the half sphere $S(R_0)$ in Figure 2.2, and using the identity

$$\nabla \times \nabla \times \bar{E} \cdot \overline{\overline{G}}_D - \bar{E} \cdot \nabla \times \nabla \times \overline{\overline{G}}_D = -\frac{1}{c^2} \frac{\partial}{\partial t} \left[\left(\frac{\partial}{\partial t} \bar{E} \right) \cdot \overline{\overline{G}}_D - \bar{E} \cdot \frac{\partial}{\partial t} \overline{\overline{G}}_D \right] - \bar{E} \delta(\bar{r} - \bar{r}') \delta(t - t') \tag{3.26}$$

and the Dirichlet boundary condition for $\overline{\overline{G}}_D$, one gets

$$-\bar{E} \delta(t - t') = \frac{1}{c^2} \frac{\partial}{\partial t} \int_{V(R_0)} \left[\left(\frac{\partial}{\partial t} \bar{E} \right) \cdot \overline{\overline{G}}_D - \bar{E} \cdot \frac{\partial}{\partial t} \overline{\overline{G}}_D \right] dV$$

$$- \int_{C(R_0)} \bar{E} \cdot \left[-\hat{z} \times \nabla \times \overline{\overline{G}}_D \right] dS, \quad \bar{r}' \in V(R_0) \tag{3.27}$$

where R_0 is assumed to be sufficiently large so that the causal field is zero on $S(R_0)$. The identity $\nabla \times \overline{\overline{G}}_D = 2 \nabla G \times \overline{\overline{I}}$ for $z = z_0$, along with (2.41) show that $\bar{E} \cdot \left[-\hat{z} \times \nabla \times \overline{\overline{G}}_D \right] = 2 \nabla' G \times (\hat{z} \times \bar{E})$ where G is the time domain free-space Green's function (3.16). Inserting this into (3.27), integrating (3.27) with respect to t from $-\infty$ to $+\infty$, and letting $R_0 \to \infty$ one finds that

$$\bar{E}(\bar{r}', t') = 2 \int_{-\infty}^{+\infty} \int_{-\infty}^{+\infty} \int_{-\infty}^{+\infty} \nabla' G(\bar{r}, \bar{r}', t, t') \times \left[\hat{z} \times \bar{E}(\bar{r}', t) \right] dt \, dx \, dy, \quad z > z_0 \tag{3.28}$$

where the fact that $\lim_{t \to \pm\infty} \overline{\overline{G}}_D = 0$ has been used to show that there is no contribution from the first integral in (3.27). Now from (3.16)

$$\nabla' G(\bar{r}, \bar{r}', t, t') = \bar{R}' \frac{1}{4\pi c R^2} \left[\delta'(t - t' + R/c) - \frac{c}{R} \delta(t - t' + R/c) \right] \tag{3.29}$$

where $\bar{R}' = (x' - x)\hat{x} + (y' - y)\hat{y} + (z' - z_0)\hat{z}$. Inserting this result into (3.28) and interchanging $\bar{r}$ with $\bar{r}'$ and t with t', (3.28) becomes

$$\bar{E}(\bar{r}, t) = \frac{-1}{2\pi} \int_{-\infty}^{+\infty} \int_{-\infty}^{+\infty} \frac{\bar{R}}{R^2} \times \left[\frac{1}{c} \hat{z} \times \frac{\partial}{\partial t} \bar{E}(\bar{r}', t - R/c) + \frac{1}{R} \hat{z} \times \bar{E}(\bar{r}', t - R/c) \right] dx' dy', \; z > z_0 \tag{3.30}$$

which is seen to agree with the near-field formula (3.14), obtained by Fourier transforming the frequency-domain formula (2.44).

3.1.3 Magnetic Field Calculated from Electric-Field Data

In this section the time-domain magnetic field in the half space $z > z_0$ is calculated from the time-domain electric field on the plane $z = z_0$. This time-domain result is first derived by taking the inverse Fourier transform of the corresponding frequency-domain result. Then we

explain how it could also have been obtained by working directly in the time domain with a time-domain Green's function.

It is seen from (2.46) that there are terms of order ω^{-1} in the frequency-domain formula for the magnetic field. To avoid this possible singularity at $\omega = 0$, we first multiply (2.46) by $-i\omega$ and then take the inverse Fourier transform to get an expression for the time derivative of the magnetic field. (When we multiply (2.46) by $-i\omega$, we recover the time-harmonic form of Maxwell's equation, $-i\omega\bar{H}_\omega = -\nabla \times \bar{E}_\omega$, which holds for all ω including $\omega = 0$.) Finally, we integrate this expression for the time derivative of the magnetic field with respect to time, recall that all fields are zero for $t < 0$, and thereby obtain the following time-domain near-field formula for the magnetic field

$$\begin{aligned}\bar{H}(\bar{r},t) = \frac{1}{2\pi}\sqrt{\frac{\epsilon}{\mu}}\int_{-\infty}^{+\infty}\int_{-\infty}^{+\infty}\Bigg\{&-\frac{1}{cR^3}\bar{R}\cdot\left[\hat{z}\times\frac{\partial}{\partial t}\bar{E}(\bar{r}',t-R/c)\right]\bar{R}+\frac{1}{cR}\hat{z}\times\frac{\partial}{\partial t}\bar{E}(\bar{r}',t-R/c)\\ &-\frac{3}{R^4}\bar{R}\cdot\left[\hat{z}\times\bar{E}(\bar{r}',t-R/c)\right]\bar{R}+\frac{1}{R^2}\hat{z}\times\bar{E}(\bar{r}',t-R/c)\\ &-\frac{3c}{R^5}\bar{R}\cdot\left[\int_0^{t-R/c}\hat{z}\times\bar{E}(\bar{r}',t')dt'\right]\bar{R}+\frac{c}{R^3}\int_0^{t-R/c}\hat{z}\times\bar{E}(\bar{r}',t')dt'\Bigg\}dx'dy',\quad z>z_0\end{aligned} \tag{3.31}$$

where $\bar{R} = \bar{r} - \bar{r}'$ and $\bar{r}' = x'\hat{x} + y'\hat{y} + z_0\hat{z}$. This is the time-domain formula, which gives the magnetic field in the region $z > z_0$ in terms of the x and y components of the electric field on the plane $z = z_0$. Both this formula for the magnetic field and formula (3.14) for the electric field were derived previously by Baum [14], [42] by taking the inverse Fourier transform of the Smythe formulas [33].

The formula (3.31) could have been derived directly in the time-domain in the following way: Use Maxwell's equations and the initial conditions $\bar{E}(\bar{r},t) = 0$, $\bar{H}(\bar{r},t) = 0$ for $t < 0$ to prove (3.3) for $\sigma_m = 0$, that is, $\bar{H}(\bar{r},t) = -\frac{1}{\mu}\int_0^t \nabla \times \bar{E}(\bar{r},t')dt'$. Insert the time-domain formula (3.30) for the electric field into this expression for the magnetic field, and (3.31) is recovered. Alternatively, equation (3.31) can be derived in a manner similar to the derivation of the electric field formula (3.30), using the Neumann dyadic Green's function for the half space $z > z_0$. This shows that (3.31) is valid for all electromagnetic fields for which both $\bar{E}$ and $\bar{H}$ are identically zero for $t < 0$; even for fields with a time dependence like the unit step function that cannot be represented by a standard Fourier integral. However, (3.31) cannot represent a purely magnetostatic field, that is, a non-zero magnetic field that remains constant for all time ($-\infty < t < \infty$), unlike (3.30), which remains valid for electrostatic fields. If such a magnetostatic field is present, one has to add its value to the formula (3.31) to get the correct total magnetic field.

The discussion of static fields brings up a subtlety in (3.30) and (3.31) that may be easily overlooked. Suppose all sources and fields are zero for $t < 0$ so that (3.30) and (3.31) apply. At $t = 0$, close a switch that charges a conductor and produces current to flow through a resistor. After a time t_0 assume all charge and current have practically reached a constant value, so that for $r \ll c(t - t_0)$ there remain only static electric and magnetic fields. These remnant static electric and magnetic fields, which build up from zero fields at $t = 0$, are

entirely determined from the formulas (3.30) and (3.31), respectively. This is unremarkable for (3.30) which, as mentioned before, remains valid for electrostatic fields ($-\infty < t < \infty$). However, it seems quite remarkable that (3.31) can represent a remnant static magnetic field for $t > 0$ even though it cannot represent a purely magnetostatic field for all time ($-\infty < t < \infty$). Of course, the explanation lies in the fact that the remnant static magnetic field is generated by time varying sources with electric and magnetic fields intimately related through Maxwell's equations, whereas a purely magnetostatic field ($-\infty < t < \infty$) exists independently of an electric field turned on at $t = 0$.

The time-domain far magnetic field in the half space $z > z_0$ is found from (3.31) to be

$$\bar{H}(\bar{r},t) \sim -\frac{1}{2\pi cr}\sqrt{\frac{\epsilon}{\mu}}\hat{r} \times \left[\hat{r} \times \int_{-\infty}^{+\infty}\int_{-\infty}^{+\infty} \hat{z} \times \frac{\partial}{\partial t}\bar{E}(\bar{r}', t - r/c + \bar{r}' \cdot \hat{r}/c)dx'dy'\right] + O\left(\frac{1}{r^2}\right) \tag{3.32}$$

which shows that the far magnetic field is of order r^{-1} if the first time derivatives of the x and y components of the electric field are finite functions of time on the plane $z = z_0$. It also shows that the far magnetic field equals $\sqrt{\frac{\epsilon}{\mu}}\hat{r} \times \bar{E}$ where $\bar{E}$ is the far electric field in (3.15).

So far we have not been concerned with the restrictions on the time functions we impose by assuming they can be represented by standard Fourier-transform integrals. The standard theorems for the Fourier transform hold for time functions that are either absolutely integrable or square integrable [21], [22] and are therefore not valid for time functions like the unit step. Furthermore, even though a time function $f(t)$ can be represented by a standard Fourier integral, it is not guaranteed that we can calculate the time integral of $f(t)$ directly from its Fourier transform, that is calculate the integral $\int_{-\infty}^{+\infty}(-i\omega)^{-1}f_\omega e^{-i\omega t}d\omega$ in which the integrand possibly has a singularity at $\omega = 0$. Such an integral with a ω^{-1} singularity has to be computed if one has to determine the time-domain magnetic field directly from the frequency-domain electric field on the scan plane [see (2.46)]. We thus see that the standard Fourier transform is insufficient for analyzing certain types of problems which can occur in planar near-field measurements.

One way of dealing with this problem is to use the complex Fourier transform explained in Dettman [41, pp.365-369] instead of the standard Fourier transform. Let us illustrate the use of the complex Fourier transform by calculating the time integral of $f(t)$ directly from its spectrum f_ω for the case where $f(t)$ is the unit step function, that is $f(t) = 0$, $t < 0$ and $f(t) = 1$, $t \geq 0$. The complex Fourier transform is given by Dettman [41, p.365]

$$f_\omega = \frac{1}{2\pi}\int_{-\infty}^{+\infty} f(t)e^{i\omega t}dt = -\frac{1}{2\pi i\omega}, \quad \mathrm{Im}(\omega) > 0 \tag{3.33}$$

and the inversion formula is

$$f(t) = \int_C f_\omega e^{-i\omega t}d\omega \tag{3.34}$$

where C is the complex contour above the real axis shown in Figure 3.1. (Note that Dettman uses $e^{i\omega t}$ time dependence and thus has $\mathrm{Im}(\omega) < 0$.)

The inverse Fourier transform of $\frac{1}{-i\omega}f_\omega$ will now be calculated. When $t < 0$ the function $\frac{1}{2\pi\omega^2}e^{-i\omega t}$ is exponentially decaying on the semicircle $\omega = Re^{i\theta}$, $0 < \theta < \pi$ as $R \to \infty$, and

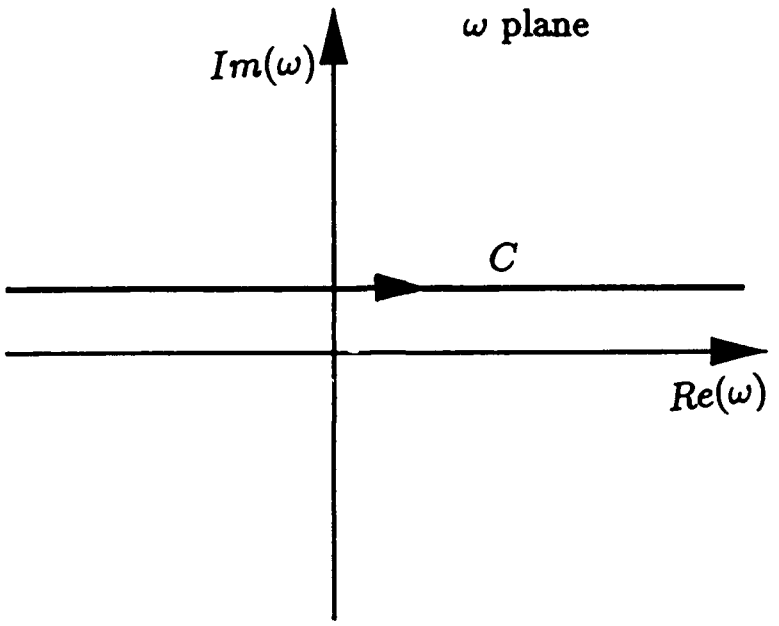

Figure 3.1: The inversion contour C for the complex Fourier transform.

because it has no singularities above the contour C, it follows that the inversion integral (3.34) is zero.

When $t > 0$ the function $\frac{1}{2\pi\omega^2}e^{-i\omega t}$ is exponentially decaying on the semicircle $\omega = Re^{i\theta}$, $\pi < \theta < 2\pi$ as $R \to \infty$, and the inversion integral (3.34) equals $-2\pi i$ times the sum of all residues in the half plane below the contour C. The only singularity is the pole of order 2 at $\omega = 0$ and its residue is $\frac{it}{2\pi}$ so the inversion integral (3.34) equals t. Thus

$$-\frac{1}{2\pi}\int_C \frac{e^{-i\omega t}}{\omega^2}d\omega = \begin{cases} 0, & t < 0 \\ t, & t \geq 0 \end{cases} \tag{3.35}$$

which is seen to equal $\int_{-\infty}^{t} f(t')dt'$. Thus, we have demonstrated how one can use the rigorous complex Fourier transform to directly evaluate the time-domain magnetic field from the frequency-domain electric field even when the time dependence of the electric field is a unit step function.

If the time function $f(t)$ is absolutely integrable, that is $\int_{-\infty}^{+\infty} |f(t)|dt < \infty$, and satisfies $f(t) = O(|t|^{-1-\alpha})$, $0 < \alpha < 1$ as $t \to \pm\infty$, one may derive a formula that gives the time integral of $f(t)$ in terms of f_ω evaluated at only *real* ω. To do this write f_ω as

$$f_\omega = f_0 + \int_{-R}^{R} f(t)\left[e^{i\omega t} - 1\right]dt + \int_{|t|>R} f(t)\left[e^{i\omega t} - 1\right]dt \tag{3.36}$$

where $f_0 = f_\omega|_{\omega=0}$ and R is a positive constant. The assumed asymptotic behavior of f shows that there exists a positive constant C_0 such that

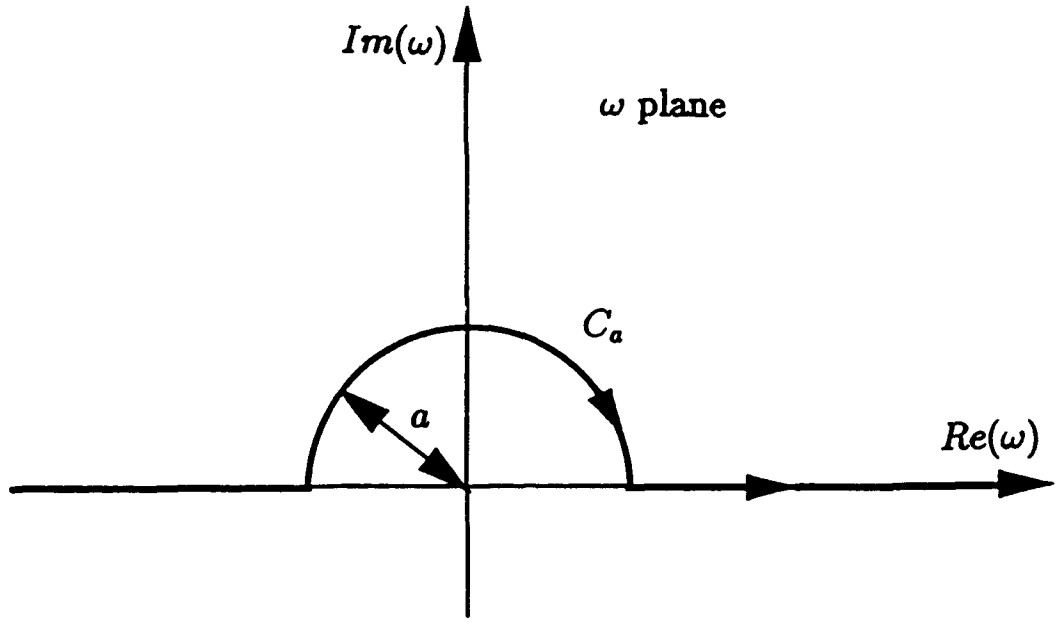

Figure 3.2: The semicircle C_a in the complex ω plane.

$$\left|\int_R^{+\infty} f(t)\left[e^{i\omega t}-1\right]dt\right| \le \int_R^{+\infty} |f(t)|\left|e^{i\omega t}-1\right|dt \le C_0\int_R^{+\infty} t^{-1-\alpha}\left|e^{i\omega t}-1\right|dt$$

$$= C_0\omega^\alpha\int_{\omega R}^{+\infty} u^{-1-\alpha}\left|e^{iu}-1\right|du \le C_0\omega^\alpha\int_0^{+\infty} u^{-1-\alpha}\left|e^{iu}-1\right|du \qquad (3.37)$$

where we have used the transformation $u=\omega t$ and the fact that $u^{-1-\alpha}|e^{iu}-1| = O(u^{-\alpha})$ as $u\to 0$ to show that the last integral converges. A similar result holds for the integral $\int_{-\infty}^{-R} f(t)\left[e^{i\omega t}-1\right]dt$ and since the integral $\int_{-R}^{R} f(t)\left[e^{i\omega t}-1\right]dt = O(\omega)$ it follows from (3.36) that $f_\omega = f_0 + O(\omega^\alpha)$ as $\omega\to 0$.

After having determined the behavior of f_ω at $\omega=0$, write the complex Fourier inversion formula (3.34) for the function $\frac{1}{-i\omega}f_\omega$ as

$$\int_{-\infty}^{t} f(t')dt' = \int_C \frac{f_\omega e^{-it\omega}}{-i\omega}d\omega = \fint_{-\infty}^{+\infty}\frac{f_\omega e^{-it\omega}}{-i\omega}d\omega + \lim_{a\to 0}\int_{C_a}\frac{f_\omega e^{-it\omega}}{-i\omega}d\omega \qquad (3.38)$$

where the bar indicates a Cauchy principal value integration and C_a is the semicircle of radius a shown in Figure 3.2. Using the facts that on the contour C_a we have $\omega = ae^{i\theta}$, $0<\theta<\pi$, $f_\omega = f_0 + O(a^\alpha)$, and $e^{-i\omega t} = 1+O(a)$, one finds that the last integral in (3.38) simply equals πf_0 and the final inversion formula (3.38) becomes

$$\int_{-\infty}^{t} f(t')dt' = \fint_{-\infty}^{+\infty}\frac{f_\omega e^{-it\omega}}{-i\omega}d\omega + \pi f_0 \qquad (3.39)$$

which involves only a real integral. The right side of (3.39) gives one a practical formula for evaluating the inverse Fourier transform of the problematic integrals in (2.46) that involve $1/k$.

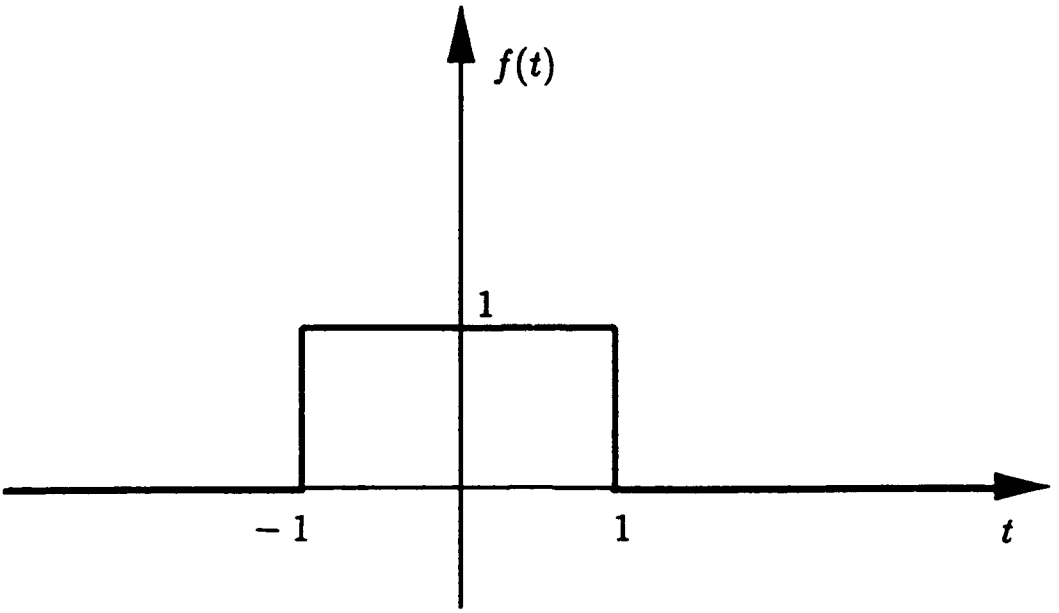

Figure 3.3: Square pulse of width 2 and height 1.

Let us illustrate the use of this formula with the example where $f(t)$ is the square pulse of width 2 and height 1, shown in Figure 3.3. In this case $f_\omega = \frac{\sin\omega}{\pi\omega}$ and $f_0 = \frac{1}{\pi}$. Furthermore,

$$\int_{-\infty}^{+\infty} \frac{f_\omega e^{-it\omega}}{-i\omega} d\omega = \frac{1}{\pi}\int_0^{+\infty} \frac{\sin\omega \sin\omega t}{\omega^2} d\omega = \begin{cases} -1, & t \le -1 \\ t, & -1 < t \le 1 \\ 1, & t > 1 \end{cases} \tag{3.40}$$

so that (3.39) becomes

$$\int_{-\infty}^{t} f(t')dt' = \begin{cases} 0, & t \le -1 \\ t+1, & -1 < t \le 1 \\ 2, & t > 1 \end{cases} \tag{3.41}$$

which is seen to be correct. We have now illustrated how the complex Fourier transform can be used to compute time-domain fields that cannot be computed from the standard Fourier transform.

3.2 Time-Domain Analogs of the Plane-Wave Spectrum Formulas

The formulas derived in Section 3.1 for the time-domain field in the half space $z > z_0$ are the time-domain analogs to the frequency-domain Green's function formulas of Section 2.1.4. In the present section, time-domain analogs to the frequency-domain plane-wave spectrum

formulas of Section 2.1.1 are derived. (In Section 3.3 we will derive formulas for time-domain near fields in terms of far fields that are analogous to the frequency-domain formulas of Sections 2.2.4 and 2.1.1.) First, in Section 3.2.1 we proceed as in Section 2.1.1 and write the time-domain field in terms of a double spatial Fourier integral over a time-dependent spectrum. This approach leads to a formula for which it has not been possible to explicitly calculate the far field, and thus it does not seem attractive for measurement purposes.

A more fruitful approach is taken in Section 3.2.2 where the frequency-domain plane-wave spectrum formulas are Fourier transformed. This approach leads to time-domain near-field formulas which give the field in the half-space $z > z_0$ in terms of the Radon transform of the field on the plane $z = z_0$. Only real measurable time-domain fields evaluated at real times occur in these formulas.

Finally, in Section 3.2.3 the analytic Fourier transform [19] is used in conjunction with the frequency-domain plane-wave spectrum formulas to obtain time-domain near-field formulas that also involve the Radon transform. These formulas are simpler than those of Section 3.2.2 but they involve complex times and analytic fields which means that they are less attractive for measurement purposes.

3.2.1 Time-Domain Plane-Wave Spectrum Formulas

Proceed as in Section 2.1.1 and write the acoustic field $\Phi(\bar{r}, t)$ in terms of plane waves

$$\Phi(\bar{r}, t) = \frac{1}{2\pi} \int_{-\infty}^{+\infty} \int_{-\infty}^{+\infty} b(k_x, k_y, z, t) e^{i(k_x x + k_y y)} dk_x dk_y, \quad z \geq z_0 \tag{3.42}$$

where b is the time-domain spectrum given by

$$b(k_x, k_y, z, t) = \frac{1}{2\pi} \int_{-\infty}^{+\infty} \int_{-\infty}^{+\infty} \Phi(x, y, z, t) e^{-i(k_x x + k_y y)} dx dy, \quad z \geq z_0. \tag{3.43}$$

Inserting the Fourier integral (3.42) into the time-domain wave equation (3.8) one finds that the spectrum b satisfies

$$\left[\frac{1}{c^2} \frac{\partial^2}{\partial t^2} + k_x^2 + k_y^2 \right] b(k_x, k_y, z, t) = \frac{\partial^2}{\partial z^2} b(k_x, k_y, z, t). \tag{3.44}$$

Our objective here, as in Section 2.1.1, is to determine the z dependence of the spectrum so that it can be expressed in terms of the field on the plane $z = z_0$. Therefore assume that the spectrum b is known on the plane $z = z_0$. The solution to the boundary value problem in which b satisfies the partial differential equation (3.44) and is given on the plane $z = z_0$ can be found from the method of descent described in Courant and Hilbert [18, Ch.6, sec.12]. To solve it uniquely one must specify both b and its normal derivative on the plane $z = z_0$ [18, Ch.6, sec.12]. To construct the spectrum b, two solutions to two related boundary value problems will now be written down.

According to Courant and Hilbert [18, pp.692-694] the solution $u(z,t)$ to the boundary value problem

$$\left[\frac{1}{c^2}\frac{\partial^2}{\partial t^2}+k_x^2+k_y^2\right]u(z,t)=\frac{\partial^2}{\partial z^2}u(z,t),\quad u(0,t)=0,\quad \frac{\partial}{\partial z}u(0,t)\neq 0 \tag{3.45}$$

is given by ([18, p.694] with $n=1$)

$$u(z,t)=\frac{1}{2}\int_{-z}^{z}\frac{\partial}{\partial z}u(0,t+z'/c)J_0(i\sqrt{k_x^2+k_y^2}\sqrt{z^2-z'^2})dz' \tag{3.46}$$

and the solution $v(z,t)$ to the problem

$$\left[\frac{1}{c^2}\frac{\partial^2}{\partial t^2}+k_x^2+k_y^2\right]v(z,t)=\frac{\partial^2}{\partial z^2}v(z,t),\quad v(0,t)\neq 0,\quad \frac{\partial}{\partial z}v(0,t)=0 \tag{3.47}$$

is, according to ([18, p.682] and (3.46)) given by

$$v(z,t)=\frac{1}{2}\frac{\partial}{\partial z}\int_{-z}^{z}v(0,t+z'/c)J_0(i\sqrt{k_x^2+k_y^2}\sqrt{z^2-z'^2})dz' \tag{3.48}$$

where J_0 is the Bessel function of the first kind and order zero. Replacing z with $z-z_0$ and using $J_0(ix)=I_0(x)$, where I_0 is the modified Bessel function of the first kind and order zero, one finds that the spectrum b is given by

$$b(k_x,k_y,z,t)=\frac{1}{2}\int_{-(z-z_0)}^{z-z_0}\frac{\partial}{\partial z}b(k_x,k_y,z_0,t+z'/c)I_0(\sqrt{k_x^2+k_y^2}\sqrt{(z-z_0)^2-z'^2})dz'$$

$$+\frac{1}{2}\frac{\partial}{\partial z}\int_{-(z-z_0)}^{z-z_0}b(k_x,k_y,z_0,t+z'/c)I_0(\sqrt{k_x^2+k_y^2}\sqrt{(z-z_0)^2-z'^2})dz',\quad z>z_0 \tag{3.49}$$

where $\frac{\partial}{\partial z}b(k_x,k_y,z_0,t+z'/c)$ is defined to be $\frac{\partial}{\partial z}b(k_x,k_y,z,t)$ evaluated at $(k_x,k_y,z,t)=(k_x,k_y,z_0,t+z'/c)$. The expression (3.49) determines the time-domain spectrum b for $z>z_0$ in terms of its values on the plane $z=z_0$. Note that the time-domain spectrum (3.49) has a very complicated z dependence, whereas the frequency-domain spectrum (2.9) has the simple z dependence $e^{i\gamma z}$. To use the time-domain plane wave spectrum formulas derived in this section one has to know both the acoustic field and its normal derivative on the plane $z=z_0$. To use the frequency-domain plane-wave spectrum formulas from Section 2.1.1, one needs only the acoustic field on the plane $z=z_0$.

The complicated z dependence of the spectrum b has made it impossible to express the far fields in terms of the spectrum, which makes the formulas in this section unattractive for far-field calculations.

3.2.2 Formulas Obtained from the Standard Fourier Transform

This section derives representations for both acoustic and electromagnetic fields in the region $z > 0$ involving the Radon transform of the fields on the plane $z = 0$. Without loss of generality it is assumed that $z_0 = 0$ because it substantially simplifies the analysis of this section. The starting point of the derivation is the frequency-domain plane-wave spectrum formulas of Section 2.1.1 with the spectrum T_ω in (2.9) rewritten as

$$T_\omega(\omega\xi, \omega\eta) = \frac{1}{2\pi} \int_{-\infty}^{+\infty} \int_{-\infty}^{+\infty} \Phi_\omega(x', y', 0) e^{-i\omega(\xi x' + \eta y')} dx' dy', \quad z \geq 0. \tag{3.50}$$

Because the time-domain field Φ is real it is found that $\Phi_\omega = \Phi^*_{-\omega}$ where $*$ indicates complex conjugation. From (3.50) it is then seen that $T_\omega(\omega\xi, \omega\eta)$ also satisfies this relationship, that is, $T_\omega(\omega\xi, \omega\eta) = T^*_{-\omega}(-\omega\xi, -\omega\eta)$.

The inverse Fourier transform of $T_\omega(\omega\xi, \omega\eta)$ is denoted by $T(\xi, \eta, t)$ and is given by

$$\begin{aligned} T(\xi, \eta, t) &= \frac{1}{2\pi} \int_{-\infty}^{+\infty} \int_{-\infty}^{+\infty} \int_{-\infty}^{+\infty} \Phi_\omega(x', y', 0) e^{-i\omega(t + \xi x' + \eta y')} d\omega dx' dy' \\ &= \frac{1}{2\pi} \int_{-\infty}^{+\infty} \int_{-\infty}^{+\infty} \Phi(x', y', 0, t + \xi x' + \eta y') dx' dy' \end{aligned} \tag{3.51}$$

which is seen to equal the Radon transform of the time-domain field Φ on the plane $z = 0$.

Writing the frequency-domain plane-wave spectrum formula (2.8) in terms of the function $T_\omega(\omega\xi, \omega\eta)$ and introducing $(k_x, k_y) = (\omega\xi, \omega\eta)$ one finds for $\omega > 0$ that

$$\Phi_\omega(\bar{r}) = \frac{1}{2\pi} \int_{-\infty}^{+\infty} \int_{-\infty}^{+\infty} \omega^2 T_\omega(\omega\xi, \omega\eta) e^{i\omega(\xi x + \eta y)} e^{i\gamma(\omega) z} d\xi d\eta, \quad z \geq 0. \tag{3.52}$$

For $\omega > 0$ the definition of γ shows that we can write $\gamma(\omega) = \omega\zeta$ where ζ is a new spectral variable given by

$$\zeta = \begin{cases} |\sqrt{c^{-2} - \xi^2 - \eta^2}|, & \xi^2 + \eta^2 < c^{-2} \\ i|\sqrt{\xi^2 + \eta^2 - c^{-2}}|, & \xi^2 + \eta^2 > c^{-2} \end{cases} . \tag{3.53}$$

The relationships $\Phi_\omega = \Phi^*_{-\omega}$ and $T_\omega(\omega\xi, \omega\eta) = T^*_{-\omega}(-\omega\xi, -\omega\eta)$ show that for $\omega < 0$ the expression for Φ_ω is given by (3.52) with $\gamma(\omega) = \omega\zeta^*$. This means that $\gamma(\omega) = -\gamma^*(-\omega)$ for all real ω and that the following expression for Φ_ω is valid for all real ω

$$\begin{aligned} \Phi_\omega(\bar{r}) &= \frac{1}{2\pi} \int\int_{\xi^2+\eta^2<c^{-2}} \omega^2 T_\omega(\omega\xi, \omega\eta) e^{i\omega(\xi x + \eta y + \zeta z)} d\xi d\eta \\ &+ \frac{1}{2\pi} \int\int_{\xi^2+\eta^2>c^{-2}} \omega^2 T_\omega(\omega\xi, \omega\eta) e^{i\omega(\xi x + \eta y)} e^{-|\omega||\zeta| z} d\xi d\eta, \quad z \geq 0. \end{aligned} \tag{3.54}$$

Taking the inverse Fourier transform of (3.54) and using the convolution rule

$$\int_{-\infty}^{+\infty} f_\omega g_\omega e^{-i\omega t} d\omega = \frac{1}{2\pi} \int_{-\infty}^{+\infty} f(t - t') g(t') dt' \tag{3.55}$$

in the last integral, one finds that the time-domain field in the half space $z > 0$ is given by

$$\Phi(\bar{r},t) = -\frac{1}{2\pi}\int\int_{\xi^2+\eta^2<c^{-2}} \frac{\partial^2}{\partial t^2} T(\xi,\eta,t-\xi x-\eta y-\zeta z)d\xi d\eta$$

$$-\frac{1}{2\pi^2}\int\int_{\xi^2+\eta^2>c^{-2}}\int_{-\infty}^{+\infty} \frac{\partial^2}{\partial t^2} T(\xi,\eta,t-t'-\xi x-\eta y)\frac{|\zeta|z}{|\zeta|^2z^2+t'^2}dt'd\xi d\eta, \quad z>0 \quad (3.56)$$

where the identity

$$\int_{-\infty}^{+\infty} e^{-k\omega\|\zeta\|z}e^{-i\omega t}d\omega = \frac{2|\zeta|z}{|\zeta|^2z^2+t^2}, \quad z>0 \quad (3.57)$$

has been used.

Note that (3.56) gives the field in the half space $z > 0$ in terms of the Radon transform of the field on the plane $z = 0$. Note also that the second time derivative of the Radon transform, and therefore also the second time derivative of the field on the plane $z = 0$, is required to calculate the field for $z > 0$. The formula (3.56) is a time-domain analog to the frequency-domain plane-wave spectrum formula (2.8).

Finally let us express the time-domain far field in terms of the Radon transform of the field on the plane $z = 0$. Writing the frequency-domain far field (2.48) in terms of T_ω defined in (3.50) one finds

$$\Phi_\omega(\bar{r}) \sim -\frac{i\omega\cos\theta}{c}\frac{e^{i\omega r/c}}{r}T_\omega(k\cos\phi\sin\theta, k\sin\phi\sin\theta) + O\left(\frac{1}{r^2}\right), \quad z>0. \quad (3.58)$$

Taking the inverse Fourier transform of (3.58) gives us the time-domain far-field result

$$\Phi(\bar{r},t) \sim \frac{\cos\theta}{cr}\frac{\partial}{\partial t}T(c^{-1}\cos\phi\sin\theta, c^{-1}\sin\phi\sin\theta, t-r/c) + O\left(\frac{1}{r^2}\right), \quad z>0 \quad (3.59)$$

which, upon inserting the definition of T from (3.51), is seen to equal the far field (3.13) found from a Green's function representation.

The formulas derived in this section hold for each of the rectangular components of the electric and magnetic fields and one finds from

$$\bar{T}_\omega(\omega\xi,\omega\eta) = \frac{1}{2\pi}\int_{-\infty}^{+\infty}\int_{-\infty}^{+\infty}\bar{E}_\omega(x',y',0)e^{-i\omega(\xi x'+\eta y')}dx'dy', \quad z\geq 0 \quad (3.60)$$

that

$$\bar{T}(\xi,\eta,t) = \frac{1}{2\pi}\int_{-\infty}^{+\infty}\int_{-\infty}^{+\infty}\bar{E}(x',y',0,t+\xi x'+\eta y')dx'dy' \quad (3.61)$$

which is the Radon transform of the electric field on the plane $z = 0$.

From (3.56) the time-domain electric field is given by the Radon transform representation

$$\bar{E}(\bar{r},t) = -\frac{1}{2\pi}\int\int_{\xi^2+\eta^2<c^{-2}} \frac{\partial^2}{\partial t^2}\bar{T}(\xi,\eta,t-\xi x-\eta y-\zeta z)d\xi d\eta$$

$$-\frac{1}{2\pi^2}\int\int_{\xi^2+\eta^2>c^{-2}}\int_{-\infty}^{+\infty}\frac{\partial^2}{\partial t^2}\bar{T}(\xi,\eta,t-t'-\xi x-\eta y)\frac{z|\zeta|}{|\zeta|^2z^2+t'^2}dt'd\xi d\eta,\quad z>0. \tag{3.62}$$

The formula (2.12), showing that the spectrum $\bar{T}_\omega$ is perpendicular to the complex propagation direction $k_x\hat{x}+k_y\hat{y}+\gamma\hat{z}$, gives

$$\bar{T}_\omega(\omega\xi,\omega\eta)\cdot(\xi\hat{x}+\eta\hat{y}+\zeta\hat{z})=0,\quad \omega>0 \tag{3.63}$$

and the same result with ζ replaced by ζ^* for $\omega<0$. Noting that ζ is real for $\xi^2+\eta^2<c^{-2}$, (3.63) shows that the Radon transform of the electric field on the plane $z=0$ satisfies

$$\bar{T}(\xi,\eta,t)\cdot(\xi\hat{x}+\eta\hat{y}+\zeta\hat{z})=0,\quad \xi^2+\eta^2<c^{-2} \tag{3.64}$$

that is, for $\xi^2+\eta^2<c^{-2}$ the Radon transform of the electric field on the plane $z=0$ is perpendicular to the direction $\xi\hat{x}+\eta\hat{y}+\zeta\hat{z}$ and thus is completely determined from two components of the electric field on the plane $z=0$. For $\xi^2+\eta^2>c^{-2}$ it is found that for all real ω

$$\bar{T}_\omega(\omega\xi,\omega\eta)\cdot(\xi\hat{x}+\eta\hat{y}+\frac{\omega}{|\omega|}\zeta\hat{z})=0,\quad \xi^2+\eta^2>c^{-2} \tag{3.65}$$

which by use of the relationships

$$\int_{-\infty}^{+\infty}\frac{\omega}{|\omega|}f_\omega e^{-i\omega t}d\omega = 2i\mathrm{Im}\int_0^{+\infty}f_\omega e^{-i\omega t}d\omega = -i\mathcal{H}f(t) \tag{3.66}$$

($f_\omega = f^*_{-\omega}$ for any real time signal $f(t)$) leads to

$$\bar{T}(\xi,\eta,t)\cdot(\xi\hat{x}+\eta\hat{y})+|\zeta|\mathcal{H}\bar{T}(\xi,\eta,t)\cdot\hat{z}=0,\quad \xi^2+\eta^2>c^{-2} \tag{3.67}$$

where $\mathcal{H}$ denotes the Hilbert transform defined below in (3.76). The last part of (3.66) follows from the facts that $f(t)=2\mathrm{Re}\int_0^{+\infty}f_\omega e^{-i\omega t}d\omega$, $\int_0^{+\infty}f_\omega e^{-i\omega t}d\omega$ is analytic for $\mathrm{Im}(t)<0$, and that the real and imaginary parts of an analytic function are related on the real axis through the Hilbert transform [40, pp.370-372].

(The minus sign on the right side of (3.66) occurs because we are dealing with analyticity in the lower half of the complex t plane rather than in the upper half as in Morse and Feshbach [40]. Sufficient conditions for the existence of the Hilbert transform of $f(t)$ is that $f(t)$ be Hölder continuous and that $f(t)$ approaches the definite value $f(\infty)$ as $t\to\pm\infty$ such that $|f(t)-f(\infty)|\le C/|t|^\alpha$, where C and α are positive constants [43, sec.43]. This latter condition plays the role of the Hölder condition at $t=\pm\infty$, and of course, $f(\infty)=0$ for the functions of time we are considering that are zero for $t<0$. The Hilbert-transform relationships in (3.66) can also be proven by first multiplying the integrand of the first integral in (3.66) by $e^{-\alpha|\omega|}$ ($\alpha>0$), secondly applying the convolution theorem, thirdly expressing

the convolution as a principal-value integral, and finally taking the limit of the integral as $\alpha \to 0$ by means of the theorem in Hobson [24, sec.225].)

Equations (3.64) and (3.67) enable us to calculate the z component of the Radon transform of the electric field from its x and y components.

The formulas derived in this section also hold for the magnetic field provided that $\bar{E}$ is replaced by $\bar{H}$ and $\bar{T}$ is replaced by $\bar{T}_H$, where $\bar{T}_H$ is the Radon transform of the magnetic field on the plane $z = 0$. The relation (2.16) between the spectrum $\bar{T}_\omega$ for the electric field and the spectrum $\bar{T}_{H\omega}$ for the magnetic field shows that

$$\bar{T}_{H\omega}(\omega\xi, \omega\eta) = \frac{1}{\mu}(\xi\hat{x} + \eta\hat{y} + \zeta\hat{z}) \times \bar{T}_\omega(\omega\xi, \omega\eta), \quad \omega > 0 \tag{3.68}$$

and the same result with ζ replaced by ζ^* for $\omega < 0$. Again, for $\xi^2 + \eta^2 < c^{-2}$, (3.68) shows that

$$\bar{T}_H(\xi, \eta, t) = \frac{1}{\mu}(\xi\hat{x} + \eta\hat{y} + \zeta\hat{z}) \times \bar{T}(\xi, \eta, t), \quad \xi^2 + \eta^2 < c^{-2} \tag{3.69}$$

and for $\xi^2 + \eta^2 > c^{-2}$

$$\bar{T}_H(\xi, \eta, t) = \frac{1}{\mu}(\xi\hat{x} + \eta\hat{y}) \times \bar{T}(\xi, \eta, t) + \frac{|\zeta|}{\mu}\hat{z} \times \mathcal{H}\bar{T}(\xi, \eta, t), \quad \xi^2 + \eta^2 > c^{-2}. \tag{3.70}$$

Thus the Radon transform of the magnetic field on the plane $z = 0$ is determined from the Radon transform of the electric field on that plane.

The far electric field formula analogous to (3.59) is

$$\bar{E}(\bar{r}, t) \sim \frac{\cos\theta}{cr}\frac{\partial}{\partial t}\bar{T}(c^{-1}\cos\phi\sin\theta, c^{-1}\sin\phi\sin\theta, t - r/c) + O\left(\frac{1}{r^2}\right), \quad z > 0 \tag{3.71}$$

and the far magnetic field can be expressed from (3.69) as

$$\bar{H}(\bar{r}, t) \sim \sqrt{\frac{\epsilon}{\mu}}\hat{r} \times \bar{E}(\bar{r}, t) \tag{3.72}$$

where $\bar{E}$ is the far electric field in (3.71).

The formulas derived in this section are time-domain analogs to the frequency-domain formulas of Section 2.1.1 and it is seen that the Radon transform in the time-domain formulas plays the role of the spatial Fourier transform in the frequency-domain formulas. Furthermore, the Radon transforms of the electric and magnetic fields on the plane $z = 0$ satisfy the relations (3.64)-(3.67) and (3.69)-(3.70) which are similar to, but more complicated than the relations (2.12) and (2.16) satisfied by the plane-wave spectra for the electric and magnetic fields. If the evanescent fields are negligible, then the second integrations in (3.56) and (3.62) are negligible and the time-domain Radon-transform relations take the simpler form of the analogous frequency-domain Fourier transform relations.

3.2.3 Formulas Obtained from the Analytic Fourier Transform

In this section it will be shown that by proceeding as in Section 3.2.2 with the *analytic* Fourier transform [19] instead of the standard Fourier transform one may obtain formulas that are in a simpler form than those in Section 3.2.2. However, the formulas of the present section are only valid for the so-called analytic field which is defined below and cannot be determined directly from measurements. The analytic field, which corresponds to the real measurable time-domain field Φ, is denoted by Φ^a and is given by the inverse analytic Fourier transform

$$\Phi^a(\bar{r},t) = 2\int_0^{+\infty} \Phi_\omega(\bar{r})e^{-i\omega t}d\omega, \quad \mathrm{Im}(t) \leq 0 \tag{3.73}$$

where Φ_ω is the usual Fourier transform of Φ given by

$$\Phi_\omega(\bar{r}) = \frac{1}{2\pi}\int_{-\infty}^{+\infty} \Phi(\bar{r},t)e^{i\omega t}dt. \tag{3.74}$$

The relation between the real field Φ and analytic field Φ^a is [40, pp.370-372], [19]

$$\Phi^a(\bar{r},t) = \Phi(\bar{r},t) - i\mathcal{H}\Phi(\bar{r},t), \quad t \text{ real} \tag{3.75}$$

where $\mathcal{H}\Phi(\bar{r},t)$ is the Hilbert transform of $\Phi(\bar{r},t)$

$$\mathcal{H}\Phi(\bar{r},t) = \int\!\!\!\!\!\!-_{-\infty}^{+\infty} \frac{\Phi(\bar{r},t')}{\pi(t-t')}dt'. \tag{3.76}$$

Again, the minus sign in (3.75) occurs because Φ^a is analytic in the "lower" half plane. The real field is thus recovered from the analytic field by the equation $\Phi(\bar{r},t) = \mathrm{Re}[\Phi^a(\bar{r},t)]$ for real t. From the definition (3.73) of the analytic field it follows that it is analytic in the lower half of the complex t plane, that is, in the region $\mathrm{Im}(t) \leq 0$.

One can now define the analytic field $T^a(\xi,\eta,t)$, which corresponds to $T(\xi,\eta,t)$ defined in (3.51), by

$$\begin{aligned} T^a(\xi,\eta,t) &= \frac{1}{\pi}\int_{-\infty}^{+\infty}\int_{-\infty}^{+\infty}\int_0^{+\infty} \Phi_\omega(x',y',0)e^{-i\omega(t+\xi x'+\eta y')}d\omega dx'dy' \\ &= \frac{1}{2\pi}\int_{-\infty}^{+\infty}\int_{-\infty}^{+\infty} \Phi^a(x',y',0,t+\xi x'+\eta y')dx'dy', \quad \mathrm{Im}(t) \leq 0 \end{aligned} \tag{3.77}$$

which is seen to equal the Radon transform of Φ^a on the plane $z = 0$.

Taking the inverse analytic Fourier transform of the frequency-domain formula (3.52) one finds that the analytic field in the half space $z > 0$ is given by

$$\Phi^a(\bar{r},t) = -\frac{1}{2\pi}\int_{-\infty}^{+\infty}\int_{-\infty}^{+\infty} \frac{\partial^2}{\partial t^2}T^a(\xi,\eta,t-\xi x-\eta y-\zeta z)d\xi d\eta, \quad z > 0, \quad \mathrm{Im}(t) \leq 0. \tag{3.78}$$

Note that (3.78) gives the analytic field in the half space $z > 0$ in terms of the Radon transform of the analytic field on the plane $z = 0$. Note also that this formula is much

simpler than the formula (3.56) obtained from the standard Fourier transform. It is easily seen that the time-domain far-field formula (3.59) also holds for the analytic field. That is

$$\Phi(\bar{r},t) \sim \mathrm{Re}\left(\frac{\cos\theta}{cr}\frac{\partial}{\partial t}T^a(c^{-1}\cos\phi\sin\theta, c^{-1}\sin\phi\sin\theta, t-r/c)\right) + O\left(\frac{1}{r^2}\right), \quad z>0 \quad (3.79)$$

which in turn is seen to be identical to the far-field formula (3.59).

To calculate the real field $\Phi = \mathrm{Re}(\Phi^a)$ for real times from (3.78) one has to know the Radon transform T^a for complex times because ζ becomes complex when $\xi^2+\eta^2 > c^{-2}$. Equation (3.77) shows that to get T^a for complex times, the analytic field Φ^a must be known on the plane $z=0$ for complex times. Consequently, to use (3.78) one has to compute the analytic field Φ^a for both complex and real times.

To derive the corresponding formulas for the electromagnetic field, start by defining

$$\bar{T}^a(\xi,\eta,t) = \frac{1}{2\pi}\int_{-\infty}^{+\infty}\int_{-\infty}^{+\infty}\bar{E}^a(x',y',0,t+\xi x'+\eta y')dx'dy', \quad \mathrm{Im}(t)\le 0 \quad (3.80)$$

which is the Radon transform of the analytic electric field

$$\bar{E}^a(\bar{r},t) = 2\int_0^{+\infty}\bar{E}_\omega(\bar{r})e^{-i\omega t}d\omega, \quad \mathrm{Im}(t)\le 0 \quad (3.81)$$

on the plane $z=0$ where

$$\bar{E}_\omega(\bar{r}) = \frac{1}{2\pi}\int_{-\infty}^{+\infty}\bar{E}(\bar{r},t)e^{i\omega t}dt. \quad (3.82)$$

From (3.78) it is then found that the time-domain electric field is given by the Radon transform

$$\bar{E}^a(\bar{r},t) = -\frac{1}{2\pi}\int_{-\infty}^{+\infty}\int_{-\infty}^{+\infty}\frac{\partial^2}{\partial t^2}\bar{T}^a(\xi,\eta,t-\xi x-\eta y-\zeta z)d\xi d\eta, \quad z>0, \quad \mathrm{Im}(t)\le 0. \quad (3.83)$$

The formula (3.63) along with the analytic Fourier transform (which only involves positive ω) shows that in agreement with (3.64) and (3.67)

$$\bar{T}^a(\xi,\eta,t)\cdot(\xi\hat{x}+\eta\hat{y}+\zeta\hat{z}) = 0 \quad (3.84)$$

that is, for all (ξ,η) the Radon transform of the electric field on the plane $z=0$ is perpendicular to the complex propagation direction $\xi\hat{x}+\eta\hat{y}+\zeta\hat{z}$ and thus is completely determined from two components of the electric field on the plane $z=0$. The formulas (3.80)-(3.84) hold also for the analytic magnetic field provided that $\bar{E}$ is replaced by $\bar{H}$. The relation (3.69) between the Radon transforms of the analytic electric and magnetic fields along with the analytic Fourier transform show that for all (ξ,η)

$$\bar{T}_H^a(\xi,\eta,t) = \frac{1}{\mu}(\xi\hat{x}+\eta\hat{y}+\zeta\hat{z})\times\bar{T}^a(\xi,\eta,t) \quad (3.85)$$

and thus, in agreement with (3.69) and (3.70), gives the Radon transform of the analytic magnetic field on the plane $z = 0$ in terms of the Radon transform of the analytic electric field on that plane. The far-field formulas (3.71) and (3.72) also hold for the analytic fields.

The Radon transform near-field formulas (3.78) and (3.83) are valid only for the analytic fields and cannot be used for the real fields. Consequently, to calculate the field at an arbitrary point of the half space $z > 0$, one has to first calculate the frequency-domain field on the plane $z = 0$ and then use (3.73) or (3.81) to determine the corresponding analytical field. After this is done these Radon transform formulas can be used to determine the field at the arbitrary point of the half space $z > 0$. Thus it seems as if the Green's function representations of Section 3.1 and the real Radon transform formulas of Section 3.2.2 would be more useful for numerical calculations since they involve only real fields that are obtainable directly from time-domain measurements. Moreover, the Radon transform formulas of Section 3.2.2 reduce in simplicity to that of the corresponding plane-wave spectrum formulas in the frequency domain when the evanescent fields [second integrals in (3.56) and (3.62)] are negligible. Also, the expressions for the far fields using any one of the three methods are identical.

3.3 Near Fields in Terms of Far Fields

In this section, we derive a formula that gives the field everywhere at all times in the half space $z > z_0$, in terms of the far field. The formula is similar to the frequency-domain formula obtained from Sections 2.2.4 and 2.1.1, giving the spectrum in terms of the frequency-domain far field. In Section 2.2.4 it was found that to calculate the spectrum from the far field for all (k_x, k_y), and thereby be able to use the far field to calculate the field everywhere in the half space $z > z_0$, one has to know the frequency-domain far field for complex angles of observation. Similarly in this section, one finds that to get the time-domain near field, at all times in the half space $z > z_0$, from the time-domain far field, one has to know the time-domain far field for complex angles of observation.

First, the formula for the acoustic field Φ is derived and then the corresponding formula for the electric field is obtained by using the result for the acoustic field.

According to (3.13), the time-domain far field can be written as

$$\Phi(\bar{r}, t) \sim \frac{\mathcal{F}(\theta, \phi, t - r/c)}{r}, \quad r \to \infty \tag{3.86}$$

where $\mathcal{F}$ is the time-domain far-field pattern. The far-field formula (3.86) can be obtained from the frequency-domain far field Φ_ω in (2.95) by means of the inverse Fourier transform:

$$\Phi(\bar{r}, t) = \int_{-\infty}^{+\infty} \frac{1}{r} \mathcal{F}_\omega(\theta, \phi) e^{-i\omega(t - r/c)} d\omega = \frac{1}{r} \mathcal{F}(\theta, \phi, t - r/c) \tag{3.87}$$

and it is seen that $\mathcal{F}_\omega(\theta, \phi)$ is simply the Fourier transform of $\mathcal{F}(\theta, \phi, t)$.

To derive the formula giving the field in the half space $z > 0$ in terms of the far field, begin by using (2.30) to show the following relation between the far-field function F_ω and

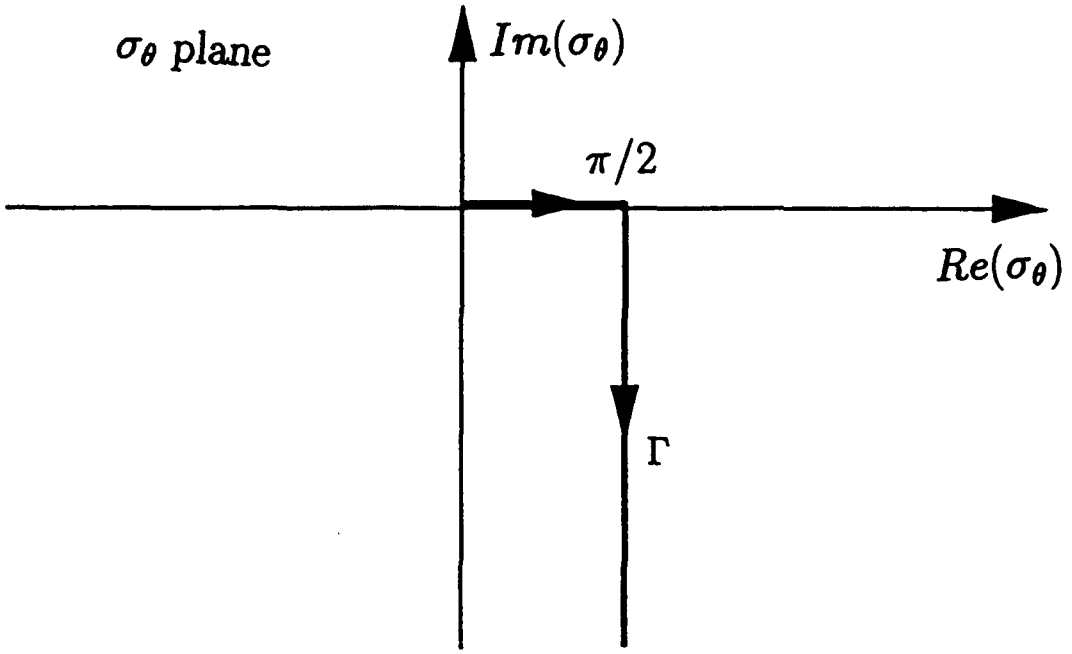

Figure 3.4: The contour Γ in the complex σ_θ plane.

the spectrum T_ω

$$T_\omega(\xi\omega, \eta\omega) = \frac{i}{\gamma(\omega)} F_\omega(\xi\omega, \eta\omega) \tag{3.88}$$

where $\gamma(\omega) = \omega\zeta$ for $\omega > 0$, $\gamma(\omega) = \omega\zeta^*$ for $\omega < 0$, and ζ is given by (3.53) [see the discussion below (3.53)]. Then insert (3.88) into (3.54) and use the definition (3.53) of ζ to get

$$\begin{aligned} \Phi_\omega(\bar{r}) &= \frac{1}{2\pi} \int\int_{\xi^2+\eta^2<c^{-2}} i\omega F_\omega(\omega\xi, \omega\eta) e^{i\omega(\xi x+\eta y+\zeta z)} \frac{1}{\zeta} d\xi d\eta \\ &+ \frac{1}{2\pi} \int\int_{\xi^2+\eta^2>c^{-2}} i\omega F_\omega(\omega\xi, \omega\eta) e^{i\omega(\xi x+\eta y)} \frac{\omega}{|\omega|} e^{-|\omega||\zeta|z} \frac{1}{\zeta} d\xi d\eta \end{aligned} \tag{3.89}$$

which is valid for all real ω.

Introduce the new integration variables $(\sigma_\theta, \sigma_\phi)$ given by

$$\xi = c^{-1} \cos\sigma_\phi \sin\sigma_\theta, \quad \eta = c^{-1} \sin\sigma_\phi \sin\sigma_\theta, \quad \zeta = c^{-1} \cos\sigma_\theta \tag{3.90}$$

with $0 \le \sigma_\phi \le 2\pi$, and with $\sigma_\theta \in \Gamma$, where Γ is the contour in the complex σ_θ plane consisting of the line segment from 0 to $\pi/2$ and the half line from $\pi/2$ to $\pi/2 - i\infty$, as shown in Figure 3.4.

Since $\sin(\pi/2 - i\alpha) = \cosh\alpha$ and $\cos(\pi/2 - i\alpha) = i\sinh\alpha$, it is seen from (3.90) that with $0 \le \sigma_\phi \le 2\pi$, $\sigma_\theta \in \Gamma$, the entire real (ξ, η) plane is covered through the transformation (3.90). Furthermore, with these new variables we have $\zeta^{-1} d\xi d\eta = c^{-1} \sin\sigma_\theta d\sigma_\theta d\sigma_\phi$. Inserting

this transformation into the spectral expression (3.89) for the frequency-domain field Φ_ω and using the relation (2.97) between the far-field pattern $\mathcal{F}$ and the far-field function F to show

$$\mathcal{F}_\omega(\sigma_\theta, \sigma_\phi) = F_\omega(\omega c^{-1} \cos\sigma_\phi \sin\sigma_\theta, \omega c^{-1} \sin\sigma_\phi \sin\sigma_\theta) \tag{3.91}$$

one finds that

$$\begin{aligned}\Phi_\omega(\bar{r}) &= \frac{1}{2\pi c}\int_0^{2\pi}\int_0^{\pi/2} i\omega \mathcal{F}_\omega(\sigma_\theta,\sigma_\phi) e^{i\omega c^{-1}(x\cos\sigma_\phi \sin\sigma_\theta + y\sin\sigma_\phi\sin\sigma_\theta + z\cos\sigma_\theta)} \sin\sigma_\theta d\sigma_\theta d\sigma_\phi \\ &+ \frac{1}{2\pi c}\int_0^{2\pi}\int_0^{+\infty} i\omega \mathcal{F}_\omega(\pi/2 - i\alpha, \sigma_\phi) e^{i\omega c^{-1}(x\cos\sigma_\phi\cosh\alpha + y\sin\sigma_\phi\cosh\alpha)} \\ &\qquad \cdot \frac{\omega}{|\omega|} e^{-(z/c)|\omega|\sinh\alpha}(-i)\cosh\alpha d\alpha d\sigma_\phi \end{aligned} \tag{3.92}$$

which is valid for all real ω. To obtain the last integral of (3.92) it has been assumed that $\mathcal{F}_\omega$ is known for complex angles of observation (see the discussion in Section 2.2.4). Taking the inverse Fourier transform of (3.92) and using the convolution rule (3.55) along with the identity

$$-i\int_{-\infty}^{+\infty} \frac{\omega}{|\omega|} e^{-(z/c)|\omega|\sinh\alpha} e^{-i\omega t} d\omega = -\frac{2t}{(zc^{-1}\sinh\alpha)^2 + t^2} \tag{3.93}$$

one finds that the time domain field is given by

$$\begin{aligned}\Phi(\bar{r},t) = &- \frac{1}{2\pi c}\int_0^{2\pi}\int_0^{\pi/2} \frac{\partial}{\partial t}\mathcal{F}(\sigma_\theta,\sigma_\phi, t - \bar{r}\cdot\hat{\sigma}_{\theta\phi}/c)\sin\sigma_\theta d\sigma_\theta d\sigma_\phi \\ &+ \frac{1}{2\pi^2 c}\int_0^{2\pi}\int_0^{+\infty}\int_{-\infty}^{+\infty} \frac{\partial}{\partial t}\mathcal{F}(\pi/2 - i\alpha, \sigma_\phi, t - t' - \bar{r}\cdot\hat{\sigma}_\phi c^{-1}\cosh\alpha) \\ &\qquad \cdot \frac{t'}{(zc^{-1}\sinh\alpha)^2 + t'^2} dt' \cosh\alpha d\alpha d\sigma_\phi \end{aligned} \tag{3.94}$$

where $\mathcal{F}(\theta,\phi,t)$ is the time-domain far-field pattern given in (3.86), and the unit vectors are given by $\hat{\sigma}_{\theta\phi} = \hat{x}\cos\sigma_\phi\sin\sigma_\theta + \hat{y}\sin\sigma_\phi\sin\sigma_\theta + \hat{z}\cos\sigma_\theta$ and $\hat{\sigma}_\phi = \hat{x}\cos\sigma_\phi + \hat{y}\sin\sigma_\phi$.

For sources in a finite region of the half space $z < 0$ the formula (3.94) gives the time-domain field everywhere in the half space $z > 0$ in terms of the time-domain far-field pattern $\mathcal{F}$. To calculate the last integral of (3.94), in general one has to know the time-domain far-field pattern $\mathcal{F}(\theta,\phi,t)$ for complex values of θ. If the far-field pattern is not known for complex angles of observation, (3.94) cannot in general be used to determine the near field. However, as will be shown below, one may derive a formula for the near field, first derived by Moses *et al.* [16], involving only the far-field pattern evaluated at real angles of observation, which is valid after all sources have been turned off so that $\Phi(\bar{r},t)$ satisfies the homogeneous wave equation (3.8) throughout *all* space.

To derive this formula, note that any acoustic field can be written as the Green's function superposition [10, p.225]

$$\Phi(\bar{r},t) = \int_V \int_{t'} f(\bar{r}',t') G(\bar{r},\bar{r}',t,t') dt' dV' \tag{3.95}$$

where

$$G(\bar{r},\bar{r}',t,t') = \frac{\delta(t-t'+R/c)}{4\pi R}, \quad R = |\bar{r}-\bar{r}'| \tag{3.96}$$

is the time-domain free-space Green's functions and $f(\bar{r}',t')$ is the source-distribution function. The volume integration in (3.95) is over the finite source region and the t' integration in (3.95) is over the time interval $t_0 < t' < t_1$ where t_0 and t_1 are the times at which the sources are turned on and off, respectively. Thus all fields are zero for $t < t_0$ and the sources are turned off at $t = t_1$ so that the field $\Phi(\bar{r},t)$ satisfies the homogeneous wave equation (3.8) throughout *all* space for $t > t_1$. Also the far-field pattern $\mathcal{F}(\theta,\phi,t)$ of the field $\Phi(\bar{r},t)$ can be written as a superposition

$$\mathcal{F}(\theta,\phi,t) = \int_V \int_{t'} f(\bar{r}',t')\mathcal{F}^G(\theta,\phi,t,t',\bar{r}')dt'dV' \tag{3.97}$$

where $\mathcal{F}^G(\theta,\phi,t,t',\bar{r}') = \frac{1}{4\pi}\delta(t-t'+\bar{r}'\cdot\hat{r}/c)$ is the far-field pattern (with respect to the origin) of the Green's function $G(\bar{r},\bar{r}',t,t')$ and the $(\bar{r}',t')$ region of integration is the same as in (3.95).

We will now derive a formula which expresses the near field of the Green's function $G(\bar{r},\bar{r}',t,t')$ for $t > t'$ in terms of its far-field pattern $\mathcal{F}^G(\theta,\phi,t,t',\bar{r}')$ evaluated at real angles of observation only. Since the source that produces this Green's function field is turned off (and on), at $t = t'$ this formula will enable us to express the general acoustic field (3.95) for $t > t_1$ in terms of its far-field pattern (3.97) evaluated at real angles of observation only.

The source that generates the field $G(\bar{r},\bar{r}',t,t')$ is located at $\bar{r}'$ and we start by letting the rectangular coordinate system (x,y,z) be located so that this source point is on the negative z axis, that is $\bar{r}' = z'\hat{z}$, $z' < 0$. The first integral of (3.94) is denoted by Φ^p because it represents the contribution to the acoustic field from the propagating modes and for the observation point $\bar{r}$ located on the positive z axis we find for the Green's function field that

$$\begin{aligned}
\Phi^p(z\hat{z},t) &= -\frac{1}{2\pi c}\int_0^{2\pi}\int_0^{\pi/2}\frac{\partial}{\partial t}\mathcal{F}^G(\sigma_\theta,\sigma_\phi,t-z\hat{z}\cdot\hat{\sigma}_{\theta\phi}/c,t',z'\hat{z})\sin\sigma_\theta d\sigma_\theta d\sigma_\phi \\
&= -\frac{1}{4\pi c}\int_0^{\pi/2}\delta'(t-t'-(z-z')c^{-1}\cos\sigma_\theta)\sin\sigma_\theta d\sigma_\theta \\
&= \frac{\delta(t-t'-(z-z')/c)-\delta(t-t')}{4\pi(z-z')}
\end{aligned} \tag{3.98}$$

where $z' < 0$, $z > 0$, and the substitution $u = t-t'-(z-z')c^{-1}\cos\sigma_\theta$ has been used to calculate the last integral. It is seen from (3.98) that $\Phi^p(z\hat{z},t) = G(z\hat{z},z'\hat{z},t,t')$ for $t > t'$, that is, at times after which the source has been turned off.

Since the z axis may be chosen arbitrarily, (3.98) enables us to calculate the field of the Green's function at any point in space from the far-field pattern evaluated at only real angles of observation. Geometrically (3.98) states that the Green's function field along the positive z axis can be calculated from the Green's function far-field pattern on the far-field hemisphere in the region $z \geq 0$ with center at $z = 0$ as shown in Figure 3.5.

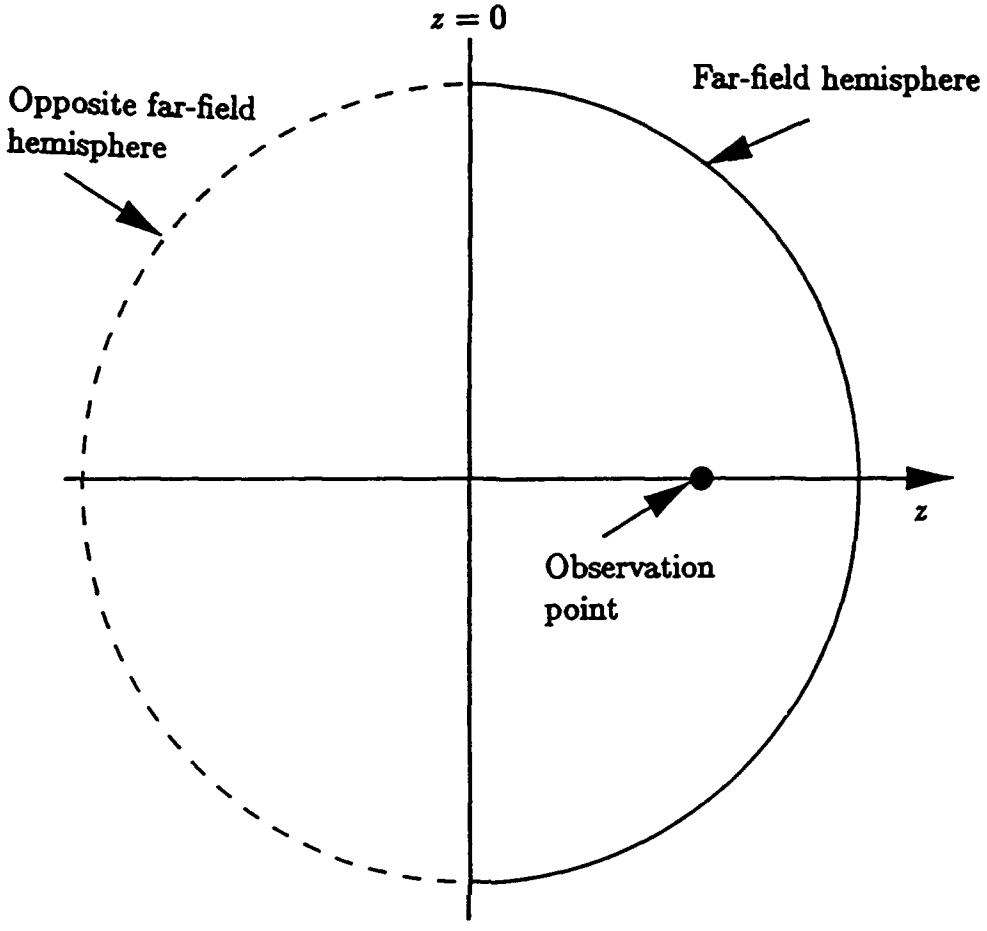

Figure 3.5: Far-field hemispheres.

To calculate the field at a point not on the z axis, one has to define a new z axis containing the new point of observation as well as the source point $\bar{r}'$ and then integrate over the corresponding new far-field hemisphere. Consequently, to use (3.98) one has to change the far-field hemisphere whenever one changes the angles of observation.

To obtain a near-field formula in which the region of integration does not depend on the angles of observation, note that if the upper limit of the σ_θ integration in (3.98) is changed from $\pi/2$ to π the result is

$$-\frac{1}{2\pi c}\int_0^{2\pi}\int_0^{\pi}\frac{\partial}{\partial t}\mathcal{F}^G(\sigma_\theta,\sigma_\phi,t-z\hat{z}\cdot\hat{\sigma}_{\theta\phi}/c,t',z'\hat{z})\sin\sigma_\theta d\sigma_\theta d\sigma_\phi$$

$$=\frac{\delta(t-t'-(z-z')/c)-\delta(t-t'+(z-z')/c)}{4\pi(z-z')} \tag{3.99}$$

which is also equal to $G(z\hat{z},z'\hat{z},t,t')$ for $t>t'$. Thus, after the source has been turned off there is no contribution to the field at the observation point in Figure 3.5 from an integration over the opposite far-field hemisphere also shown in Figure 3.5. Now let $z'=0$ in (3.99), that is, let the source be located at the origin of the (x,y,z) coordinate system. Then introduce the new coordinates (x_1,y_1,z_1) with the same origin as the original (x,y,z) coordinates. Let

the point of space that was represented by $z\hat{z}$ in the (x, y, z) coordinate system be represented by $\bar{r}_1$ in the new coordinate system (x_1, y_1, z_1). Because the region of integration in (3.99) is independent of the orientation of the coordinate system it is found that for the source located at the origin

$$\begin{aligned} G(\bar{r}_1, \bar{0}, t, t') &= -\frac{1}{2\pi c}\int_0^{2\pi}\int_0^{\pi}\frac{\partial}{\partial t}\mathcal{F}^G(\sigma_\theta, \sigma_\phi, t - \bar{r}_1 \cdot \hat{\sigma}_{\theta\phi}/c, t', \bar{0})\sin\sigma_\theta d\sigma_\theta d\sigma_\phi \\ &= \frac{\delta(t - t' - |\bar{r}_1|/c) - \delta(t - t' + |\bar{r}_1|/c)}{4\pi|\bar{r}_1|}, \quad t > t'. \end{aligned} \tag{3.100}$$

(This can also be proven directly by introducing new spherical coordinates $(\sigma'_\theta, \sigma'_\phi)$ with $\sigma'_\theta = 0$ corresponding to the direction $\hat{r}_1$.)

Thus, a formula is obtained expressing the Green's function field $G(\bar{r}_1, \bar{0}, t, t')$ for $t > t'$ at an arbitrary point of observation $\bar{r}_1$ as an integral of the Green's function far-field pattern over the full far-field sphere. Assume now that the source point is not located at the origin, but at $\bar{r}'_1 \neq \bar{0}$. Then clearly the formula (3.100) remains valid provided that we replace $\bar{r}_1$ with $\bar{r}_1 - \bar{r}'_1$ and refer the Green's function far-field pattern to the source point, that is let $\mathcal{F}^G = \frac{1}{4\pi}\delta(t - t')$. The formula obtained in this manner is equivalent to

$$G(\bar{r}_1, \bar{r}'_1, t, t') = -\frac{1}{2\pi c}\int_0^{2\pi}\int_0^{\pi}\frac{\partial}{\partial t}\mathcal{F}^G(\sigma_\theta, \sigma_\phi, t - \bar{r}_1 \cdot \hat{\sigma}_{\theta\phi}/c, t', \bar{r}'_1)\sin\sigma_\theta d\sigma_\theta d\sigma_\phi, \quad t > t_1 \tag{3.101}$$

with the Green's function far-field pattern referred to the origin (which does not coincide with the source point), that is, with $\mathcal{F}^G(\theta, \phi, t, t', \bar{r}'_1) = \frac{1}{4\pi}\delta(t - t' + \bar{r}'_1 \cdot \hat{r}/c)$. We have now obtained a formula that gives the general Green's function near field $G(\bar{r}_1, \bar{r}'_1, t, t')$ for $t > t'$, as an integration of the Green's function far-field pattern (referred to the origin) over the full far-field sphere. Inserting the expression (3.101) for the Green's function into the superposition (3.95) and employing the expression (3.97) for the far-field pattern, one obtains the following expression for the general acoustic near field in terms of its far-field pattern

$$\Phi(\bar{r}, t) = -\frac{1}{2\pi c}\int_0^{2\pi}\int_0^{\pi}\frac{\partial}{\partial t}\mathcal{F}(\sigma_\theta, \sigma_\phi, t - \bar{r} \cdot \hat{\sigma}_{\theta\phi}/c)\sin\sigma_\theta d\sigma_\theta d\sigma_\phi, \quad t > t_1 \tag{3.102}$$

where t_1 is the time after all sources have been turned off and $\hat{\sigma}_{\theta\phi} = \hat{x}\cos\sigma_\phi \sin\sigma_\theta + \hat{y}\sin\sigma_\phi \sin\sigma_\theta + \hat{z}\cos\sigma_\theta$. This is the final result giving the near field at times after all sources have been turned off in terms of the far-field pattern integrated over real angles of observation. This interesting result (3.102) was first derived, as far as we know, by Moses *et al.* [16]. The general result (3.94) appears to be new.

Consider now the electromagnetic field. One finds from (3.15) that the far electric field can be written as

$$\bar{E}(\bar{r}, t) \sim \bar{\mathcal{F}}(\theta, \phi, t - r/c)\frac{1}{r}, \quad r \to \infty \tag{3.103}$$

where $\bar{\mathcal{F}}$ is the time-domain far-field pattern satisfying $\hat{r} \cdot \bar{\mathcal{F}} = 0$. Performing a derivation similar to the one that led to the acoustic equation (3.94) one finds that the electric near

field for all times is given by

$$\begin{aligned}\bar{E}(\bar{r},t) = & -\frac{1}{2\pi c}\int_0^{2\pi}\int_0^{\pi/2}\frac{\partial}{\partial t}\bar{\mathcal{F}}(\sigma_\theta,\sigma_\phi,t-\bar{r}\cdot\hat{\sigma}_{\theta\phi}/c)\sin\sigma_\theta d\sigma_\theta d\sigma_\phi \\ & +\frac{1}{2\pi^2 c}\int_0^{2\pi}\int_0^{+\infty}\int_{-\infty}^{+\infty}\frac{\partial}{\partial t}\bar{\mathcal{F}}(\pi/2-i\alpha,\sigma_\phi,t-t'-\bar{r}\cdot\hat{\sigma}_\phi c^{-1}\cosh\alpha) \\ & \cdot\frac{t'}{(zc^{-1}\sinh\alpha)^2+t'^2}dt'\cosh\alpha d\alpha d\sigma_\phi \qquad (3.104)\end{aligned}$$

when the sources are located in the half space $z<0$ and the observation point is in the half space $z>0$. As for the acoustic field one finds that after the sources have been turned off ($\nabla\times\nabla\times\bar{E}-\frac{\partial^2}{\partial(ct)^2}\bar{E}=0$ and $\nabla\cdot\bar{E}=0$ throughout *all* space) the near field can expressed by the real integral [16]

$$\bar{E}(\bar{r},t) = -\frac{1}{2\pi c}\int_0^{2\pi}\int_0^{\pi}\frac{\partial}{\partial t}\bar{\mathcal{F}}(\sigma_\theta,\sigma_\phi,t-\bar{r}\cdot\hat{\sigma}_{\theta\phi}/c)\sin\sigma_\theta d\sigma_\theta d\sigma_\phi,\quad t>t_1 \qquad (3.105)$$

where t_1 is the time after which all sources have been turned off. (To prove this, replace the scalar Green's function (3.96) in the acoustic derivation with the corresponding dyadic Green's function, found by Fourier transforming the Green's function given in van Bladel [31, p.221], and noting that the far field again just involves a delta function.)

In summary, both acoustic and electromagnetic near fields, at all observation points and times, can be expressed as integrals of the far fields over both real and complex angles of observation. The near fields, at all points of observation and at times after all sources have been turned off, can be expressed in terms of integrals of the far fields over only real angles of observation. This rather surprising result was first derived by Moses *et al.* [16] for both acoustic and electromagnetic fields.

3.3.1 Electromagnetic Bullets

It may be tempting to insert an arbitrary desired far field into (3.104) or (3.105) to compute the near field that will generate this far field. However, care must be taken to choose a time-domain far field that is compatible with sources in a finite region of space. Specifically, the time-domain far field of sources confined to a finite region of space must be an analytic function of the far field angles θ and ϕ.

To prove this, express the time-domain far field in terms of the frequency-domain far field, that is, as the Fourier transform

$$\bar{\mathcal{F}}(\theta,\phi,t)=\int_{-\infty}^{+\infty}\bar{\mathcal{F}}_\omega(\theta,\phi)e^{-i\omega t}d\omega. \qquad (3.106)$$

We are assuming that the electromagnetic fields outside the source region can be written as a superposition of time-harmonic fields that satisfy Maxwell's equations. From Appendix A or Theorem 29 of Müller [44], or Section 4.3 of Nieto-Vesperinas [12], the frequency-domain far field $\bar{\mathcal{F}}_\omega(\theta,\phi)$ of sources in a finite region of space is an analytic function of θ and ϕ. The

analyticity of $\bar{\mathcal{F}}(\theta,\phi,t)$ with respect to θ and ϕ follows from the theorem in Section 5.32 of Whittaker and Watson [45] applied to (3.106), provided (i) the integral in (3.106) converges, (ii) the first derivatives of $\bar{\mathcal{F}}_\omega(\theta,\phi)$ with respect to θ and ϕ are continuous functions of ω, and (iii) the Fourier integrals over ω of the first derivatives converge uniformly in θ and ϕ. (Because θ and ϕ have finite domains, uniform convergence is assured if $\int_{-\infty}^{+\infty} |\frac{\partial}{\partial\theta}\bar{\mathcal{F}}_\omega(\theta,\phi)|d\omega$ and $\int_{-\infty}^{+\infty} |\frac{\partial}{\partial\phi}\bar{\mathcal{F}}_\omega(\theta,\phi)|d\omega$ are finite for all θ and ϕ.) These restrictions on $\bar{\mathcal{F}}_\omega(\theta,\phi)$ are extremely weak and are satisfied by physically generated fields that have continuous, effectively bandlimited (negligible for $|\omega| > \omega_0$) frequency spectra.

The analyticity of $\bar{\mathcal{F}}(\theta,\phi,t)$ implies, for example, that the far field of finite sources cannot have zero sidelobes (unless it is zero everywhere), because an analytic function that is zero on a line segment is identically zero everywhere. If, unknowingly, such a nonanalytic far field is inserted into (3.104) or (3.105), one obtains a near-field distribution that cannot be generated by sources in a finite region of space but requires a source of infinite extent. In particular, "electromagnetic bullets" (fields with zero far fields outside an angular cone) [16], [46] cannot be excited by physically realizable sources in a finite region of space, even though analytic far fields with very low sidelobes are permissible.

Of course, the impossibility of obtaining zero sidelobe far fields in the time domain (electromagnetic bullets) from sources in a finite region follows directly from (3.106). Specifically, taking the inverse Fourier transform of (3.106) in the angular region where $\bar{\mathcal{F}}(\theta,\phi,t)$ is chosen to be zero shows that $\bar{\mathcal{F}}_\omega(\theta,\phi)$ equals zero in the same angular region. Since analyticity of $\bar{\mathcal{F}}_\omega(\theta,\phi)$ from sources in a finite region implies $\bar{\mathcal{F}}_\omega(\theta,\phi)$ cannot equal zero throughout an angular region (unless it is zero everywhere), it follows that $\bar{\mathcal{F}}(\theta,\phi,t)$ cannot be chosen zero throughout an angular region, unless it is zero everywhere. However, it is emphasized that (3.104) and (3.105), like their frequency-domain counterparts, can still be useful for determining near fields and source distributions that produce low sidelobes.

3.3.2 Far Fields Integrated over Time

There are also restrictions on the time dependence that the far fields can have, as mentioned in Section 2.2.2. In particular, we shall show that the time-domain far electric and magnetic fields integrated over all time are zero, if the sources are located in a finite region of space and are turned on and off in a finite time period. One may be tempted to prove this result by integrating (3.15) and (3.32) over all time and interchanging the time and space integrals. Unfortunately, this interchange may not be a valid mathematical operation because the spatial limits of integration are infinite. As an illustration, such an interchange applied to the expression (3.13) for the acoustic far field produces the erroneous result that the acoustic far field integrated over all time must be zero for sources that are turned on and off in a finite time interval (see Section 4.4).

The behavior of the electromagnetic far fields integrated over all time can be found directly from the expressions for the far fields in terms of the current density $\bar{J}(\bar{r},t)$ located in a volume V of finite extent. Specifically, it is shown in Appendix B that the far magnetic

and electric fields are given by the expressions

$$\bar{H}(\bar{r},t) \sim -\frac{1}{4\pi cr}\hat{r} \times \int_V \frac{\partial}{\partial t}\bar{J}(\bar{r}', t - r/c + \hat{r}\cdot\bar{r}'/c)dV' + O\left(\frac{1}{r^2}\right) \tag{3.107}$$

$$\bar{E}(\bar{r},t) \sim \sqrt{\frac{\mu}{\epsilon}}\frac{1}{4\pi cr}\hat{r} \times \hat{r} \times \int_V \frac{\partial}{\partial t}\bar{J}(\bar{r}', t - r/c + \hat{r}\cdot\bar{r}'/c)dV' + O\left(\frac{1}{r^2}\right) \tag{3.108}$$

if the time derivative of the current is a continuous function of time that is bounded by a time-independent function that is integrable over the finite region V. Since the current is in a volume of finite extent, (3.107) and (3.108) can be integrated over all time, and the integrations over time and space can be interchanged to prove that the integrated far electric and magnetic fields must be zero if the current turns on and off in a finite time interval.

Only if the current remains nonzero as $t \to \infty$ can the far electric and magnetic fields integrated over all time be nonzero. For example, if the time-domain current is zero for $t < t_0$ and approaches a nonzero static value as $t \to \infty$

$$\lim_{t\to\infty} \bar{J}(\bar{r},t) = \bar{J}_0(\bar{r}) \tag{3.109}$$

the integrals of the far fields (3.107) and (3.108) over all time can be written as

$$\int_{-\infty}^{+\infty} \bar{H}(\bar{r},t)dt \sim -\frac{1}{4\pi cr}\hat{r} \times \int_V \bar{J}_0(\bar{r}')dV' + O\left(\frac{1}{r^2}\right) \tag{3.110}$$

$$\int_{-\infty}^{+\infty} \bar{E}(\bar{r},t)dt \sim \sqrt{\frac{\mu}{\epsilon}}\frac{1}{4\pi cr}\hat{r} \times \hat{r} \times \int_V \bar{J}_0(\bar{r}')dV' + O\left(\frac{1}{r^2}\right). \tag{3.111}$$

With $\bar{J}_0$ inserted from the vector identity, $\nabla\cdot(\bar{r}\bar{J}_0) = \bar{r}(\nabla\cdot\bar{J}_0) + \bar{J}_0$, the equations (3.110) and (3.111) become

$$\int_{-\infty}^{+\infty} \bar{H}(\bar{r},t)dt \sim \frac{1}{4\pi cr}\hat{r} \times \int_V \bar{r}'\frac{\partial}{\partial t}\rho_0(\bar{r}',\infty)dV' + O\left(\frac{1}{r^2}\right) \tag{3.112}$$

$$\int_{-\infty}^{+\infty} \bar{E}(\bar{r},t)dt \sim -\sqrt{\frac{\mu}{\epsilon}}\frac{1}{4\pi cr}\hat{r} \times \hat{r} \times \int_V \bar{r}'\frac{\partial}{\partial t}\rho_0(\bar{r}',\infty)dV' + O\left(\frac{1}{r^2}\right) \tag{3.113}$$

where use has been made of the divergence theorem and the continuity equation

$$-\frac{\partial}{\partial t}\rho_0(\bar{r},\infty) = -\lim_{t\to\infty}\frac{\partial}{\partial t}\rho_0(\bar{r},t) = \nabla\cdot\bar{J}_0(\bar{r}). \tag{3.114}$$

The divergence of $\bar{J}_0(\bar{r})$ is not a function of time in (3.114) so that the charge distribution increases linearly with time as $t \to \infty$, that is

$$\rho_0(\bar{r},t) \sim -\nabla\cdot\bar{J}_0(\bar{r})t, \quad t \to \infty. \tag{3.115}$$

Thus, the electromagnetic far fields integrated over all time can be nonzero when the current approaches a static value as $t \to \infty$, but only if the static charge distribution, or more precisely, the electric dipole moment of the charge distribution, grows linearly with time as $t \to \infty$. (Of course, the continuity equation valid for all times implies that the *total* charge remains zero because it is assumed zero for $t < t_0$.)

3.3.3 Electromagnetic Missiles

In 1985 Wu published a paper [17] in which he showed that the energy in an electromagnetic pulse of finite width and length could decay more slowly than $1/r^2$ as r approaches infinity. He proved these results mathematically from the classical Maxwell equations for sources in a finite region of space radiating a finite amount of energy. He called these unusual far-field pulses "electromagnetic missiles." In this section we shall give the necessary conditions in both the time and frequency domains for the far fields to decay more slowly than $1/r$, and for the far-field energy to decay more slowly than $1/r^2$, that is, for the existence of an "electromagnetic missile." (The necessary conditions for an electromagnetic missile are more restrictive than for the far fields to decay slower than $1/r$, because the time duration of the far-field pulse may approach zero as r becomes infinite.)

We shall derive these necessary conditions for two kinds of sources: first, sources composed of a finite number of moving point charges, and secondly, for a continuum of charge-current.

For a finite number of separate point charges, each point charge q that moves with velocity $\bar{u}$ and acceleration $\dot{\bar{u}}$ has far fields given by [39, p.475]

$$\bar{E}(\bar{r},t) \sim \frac{q\gamma_r^3}{4\pi\epsilon r c^2}\hat{r} \times \left[(\hat{r} - \bar{u}'/c) \times \dot{\bar{u}}'\right] = \frac{q\gamma_r^2}{4\pi\epsilon r c^2}|\dot{\bar{u}}'| \left[\gamma_r(\hat{r} - \bar{u}'/c)(\hat{r}\cdot\hat{\dot{u}}') - \hat{\dot{u}}'\right] \tag{3.116}$$

$$\bar{H}(\bar{r},t) \sim \sqrt{\frac{\epsilon}{\mu}}\hat{r} \times \bar{E}(\bar{r},t) \tag{3.117}$$

where $\gamma_r = 1/(1-\hat{r}\cdot\bar{u}'/c)$ and the primes on the velocity and acceleration indicate that they are evaluated at the retarded time $t' = t - |\bar{r} - \bar{r}_q(t')|/c$. The vector $\bar{r}_q(t')$ is the position of the charge at the retarded time t'. The origin of the coordinate system, and thus that of the asymptotically large vector $\bar{r}$, is chosen in the vicinity of the charge during the retarded times of interest.

Equations (3.116) and (3.117) reveal that the far electric and magnetic fields of the point charge decay as $1/r$ (or faster) unless the acceleration of the charge is infinite at some point (or points) in time. Thus, we conclude that *the far fields of a finite number of moving point charges decay more slowly than* $1/r$ *only if the acceleration of a least one of the point charges becomes infinite at some point in time.* (Of course, it is assumed that each point charge q is finite.) Also, the square brackets in (3.116) cannot be zero (for nonzero $\dot{\bar{u}}$) in all directions of observation $\hat{r}$. Thus, for a single point charge, the above necessary condition is sufficient as well.

For rectilinear motion, these points of infinite acceleration must be isolated points in time, and must integrate over time to a value less than c, because the speed of each point charge must be less than the speed of light.

The magnitude of the Fourier transform of the acceleration can be written as

$$|\dot{\bar{u}}(t)| = \left|\int_{-\infty}^{\infty} -i\omega\bar{u}_\omega e^{-i\omega t}d\omega\right| \leq \int_{-\infty}^{\infty} |\omega\bar{u}_\omega|d\omega \tag{3.118}$$

which is finite if $|\bar{u}_\omega|$ decays as $|\omega|^{-(2+\alpha)}, \alpha > 0$. Using the even and odd functional dependence on ω of the real and imaginary parts of the velocity spectrum $\bar{u}_\omega$, and assuming that $\dot{\bar{u}}(t)$ is zero before some initial time, it can also be shown that the condition $|\bar{u}_\omega| \sim 1/\omega^2$ as $|\omega| \to \infty$ produces a finite acceleration. Thus, we conclude that *the far fields of a moving point charge can decay more slowly than* $1/r$ *only if the frequency spectrum of the velocity of the point charge decays slower than* $1/\omega^2$ *as* $|\omega| \to \infty$. In addition, if $|\bar{u}_\omega| \sim |\omega|^{-(2-\alpha)}$ as $|\omega| \to \infty$, examples of $\bar{u}_\omega$ can be found that produce infinite acceleration at some point in time.

The energy radiated per unit area in a far-field pulse can be expressed from (3.116) and (3.117) as

$$\int_{pulse} (\bar{E} \times \bar{H}) \cdot \hat{r} dt \sim O\left(\frac{1}{r^2}\right) \int_{pulse} |\dot{\bar{u}}|^2 dt = 2\pi O\left(\frac{1}{r^2}\right) \int_{-\infty}^{\infty} \omega^2 |\bar{u}_\omega|^2 d\omega \,. \tag{3.119}$$

(Only $|\dot{\bar{u}}|^2$ is retained in the second integral of (3.119) because the expression in the square brackets of the last part of (3.116) is never infinite but is nonzero for most far-field directions. Because $dt = dt'/\gamma_r$ and $1/\gamma_r$ is never infinite or zero, it also has been omitted from the time integration of $|\dot{\bar{u}}|^2$ in (3.119).) Thus, *the necessary condition for the finite number of point charges to radiate an "electromagnetic missile" is that at least one point charge have infinite acceleration at some time, and in addition*

$$\int_{pulse} |\dot{\bar{u}}|^2 dt = 2\pi \int_{-\infty}^{\infty} \omega^2 |\bar{u}_\omega|^2 d\omega = \infty \tag{3.120}$$

which implies that the magnitude of the velocity spectrum $|\bar{u}_\omega|$ *decays as* $1/|\omega|^{3/2}$ *or slower as* $|\omega| \to \infty$. Furthermore, examples of velocities (such as $t^\alpha \exp(-t)$, $t \geq 0$, and zero for $t \leq 0$) are easily constructed that produce electromagnetic missiles ($0 < \alpha \leq 1/2$), or no electromagnetic missile, yet slower than $1/r$ far-field decay ($1/2 < \alpha < 1$).

For rectilinear motion, the condition (3.120) also implies from (3.116) and (3.117) that the point charge radiates an infinite amount of energy because the energy radiated per unit area decays slower than $1/r^2$ over most of the far-field sphere.

Now assume the source region consists of a continuum of current rather than a finite number of moving point charges. We prove in Appendix B that the electromagnetic far fields decay as $1/r$ (or faster) provided the first time derivative of the source current exists and is bounded by an integrable time-independent function in the finite source region V. Therefore, *only if the first time derivative of the current in a region of space (or secant slope if the time derivative does not exist)*[1] *is infinite at some point in time*[2] *can the far fields*

[1]If the first time derivative does not exist, bringing the curl operator under the integral sign in Appendix B to obtain (3.107) and (3.108) is no longer a valid interchange. In that case, the derivatives operating on the vector potential integral can be expressed in terms of their defining limits to show that the far fields decay as $1/r$ unless the secant slope, $\left[\bar{J}(\bar{r}, t + \Delta t) - \bar{J}(\bar{r}, t)\right]/\Delta t$, becomes infinite for some t and Δt [47], [24, sec.246, p.355]. Of course, if the limit of the secant slope exists as $\Delta t \to 0$, the limit equals the time derivative.

[2]Note that the first time derivative of the current $\frac{\partial}{\partial t}\bar{J}(\bar{r}, t)$ must become infinite as a function of time t

decay more slowly than $1/r$. Taking the Fourier transform of the first time derivative of the current, as we did for acceleration in (3.118), shows that the necessary condition in the frequency domain for slower than $1/r$ far-field decay is that *the magnitude of the frequency spectrum of the current decays more slowly than* $1/\omega^2$ *as* $|\omega| \to \infty$.

As in the case of the accelerating point charge, an additional condition on the current is required to excite an electromagnetic missile. Namely, the energy carried by the far-field pulse must decay slower than $1/r^2$. From equations (B.9) and (B.10) of Appendix B, [or (3.107) and (3.108)], one finds that the energy radiated per unit area in a far-field pulse behaves as

$$\int_{pulse} (\bar{E} \times \bar{H}) \cdot \hat{r} dt \sim O\left(\frac{1}{r^2}\right) \int_V \int_V \left[\int_{pulse} \frac{\partial}{\partial t} \bar{J}(\bar{r}', t') \cdot \frac{\partial}{\partial t} \bar{J}(\bar{r}'', t'') dt \right] dV' dV'' \qquad (3.121)$$

where $t' = t - r/c + \hat{r} \cdot \bar{r}'/c$ and $t'' = t - r/c + \hat{r} \cdot \bar{r}''/c$, provided the time derivative of the current exists and is finite. (For surface current the volume integrals in Appendix B and (3.121) are replaced by surface integrals.)

Equation (3.121) implies that the far-field energy in the pulse cannot decay more slowly than $1/r^2$ unless the time integral is infinite over some region of $(\bar{r}', \bar{r}'')$. Specifically

$$\int_{pulse} \frac{\partial}{\partial t} \bar{J}(\bar{r}', t') \cdot \frac{\partial}{\partial t} \bar{J}(\bar{r}'', t'') dt = \infty \qquad (3.122)$$

for some $\bar{r}'$ and $\bar{r}''$. If we let $\bar{r}$ be the value of $\bar{r}'$ or $\bar{r}''$ in (3.122) that has the largest time derivative of the current, (3.122) implies that there must be some $\bar{r}$ for which

$$\int_{pulse} \left| \frac{\partial}{\partial t} \bar{J}(\bar{r}, t) \right|^2 dt = \int_{-\infty}^{\infty} \omega^2 |\bar{J}_\omega(\bar{r})|^2 d\omega = \infty \, . \qquad (3.123)$$

Thus, in addition to the first time derivative of the current being infinite at some point in time, (3.123) is a necessary condition on the singularity of the current to produce an electromagnetic missile. Specifically, *the first time derivative of the current in a region of space must be infinite at some point in time, and the time integral of the magnitude squared of the first time derivative of the current must be infinite to produce an electromagnetic missile. In terms of the frequency spectrum of the current,* $|\bar{J}_\omega|$ *must decay as* $1/|\omega|^{3/2}$ *or slower as* $|\omega| \to \infty$. For linearly polarized current, the singularities (infinities) of the first time derivative of the current must be isolated and integrate over time to a finite value if the current itself is to remain a finite function of time, even though the square of the first time derivative of current must integrate to an infinite value to produce an electromagnetic missile.

The exact expressions for the time-domain fields radiated by a circular current disk [47] demonstrate that a spatial distribution of current can be found that will produce an

(not just position $\bar{r}$) to generate an "electromagnetic missile". For example, the current parallel to a perfectly conducting sharp edge is infinite right at the edge. Yet this singularity is a function of the spatial coordinates and will not generate an "electromagnetic missile" because the singularity is integrable with respect to the spatial coordinates.

electromagnetic missile for any given time or frequency dependence satisfying (3.123). Note that the condition (3.123) does not imply that the current source radiates an infinite amount of energy, because a continuum of current, unlike an accelerating point charge, can have infinite directivity. Therefore, the energy in the far-field pulse that decays slower than $1/r^2$ can be confined to a finite transverse area as $r \rightarrow \infty$. Also it is emphasized that (B.9)-(B.10) and (3.121) are no longer valid expressions for the far fields and for the far-field energy when $\partial \bar{J}/\partial t$ is infinite. To find the exact behavior of the far fields when $\partial \bar{J}/\partial t$ is infinite, one must return to the expressions (B.1) and (B.2), keeping the curl operators outside the vector potential integral in (B.3), as is done in [47] for the circular current disk.

In summary, classical sources of finite charge and current in a finite region of space can produce classical Maxwellian far-field pulses that decay slower than $1/r$ and carry energy that decays slower than $1/r^2$. [3] However, these anomalous pulses require either infinite acceleration of point charges or infinite first time derivatives in the current. Presumably, the infinite acceleration of a point charge and infinite time derivatives of current are not realizable in the classical laboratory, and thus "electromagnetic missiles" cannot be generated within the realm of classical physics (Maxwell's equations with sources that are finite and have finite first time derivatives in a finite region of space).

In reality, of course, electromagnetic missiles exist in the form of single photons, which travel indefinitely without decay, have a rapidly decreasing narrow frequency spectrum (certainly faster than $1/\omega^2$), and are generated by finite energy sources in a finite region of space. Thus, as a corollary to the theorems proven in this section, photons are not solutions to the classical Maxwell equations with classical finite sources in a finite region of space. Moreover, when the photons and their sources combine in great numbers to form a statistical continuum of sources and fields that obey Maxwell's equations, the far fields cannot decay slower than $1/r$ if the first time derivative of the current is finite, and electromagnetic missiles cannot be generated. Is a nonclassical physical mechanism possible for generating a source frequency spectrum that decays as $1/|\omega|^{3/2}$ or slower as $|\omega| \rightarrow \infty$, so that an infinite time derivative of current can be synthesized to produce a classical electromagnetic missile? As unlikely as this possibility may seem, as far as we know, this is an unanswered question.

[3] Although the far-field energy decays slower than $1/r^2$, it still must go to zero as $r \rightarrow \infty$ for finite sources with finite energy in a finite region of space. The reason the far-field energy must approach zero is simply that finite sources with finite energy must have an energy spectrum that approaches zero as $|\omega| \rightarrow \infty$, and for finite sources in a finite region of space, it is only the energy in the increasingly higher frequencies that contributes to the slower than $1/r^2$ far-field energy decay as $r \rightarrow \infty$ [17].

Chapter 4

A Time-Domain Sampling Theorem and Numerical Far-Field Calculations

In this chapter we derive sampling theorems and present two different computation schemes to numerically calculate the time-domain far-field pattern from sampled time-domain near-field data. The sampled time-domain near-field data are obtained by measuring the near field at discrete points on the scan plane at discrete times.

The first scheme is based on the frequency-domain formulation and is presented in Section 4.1. This frequency-domain scheme consists of the following three steps: (1) use the Fourier transform to calculate the frequency-domain near field from the time-domain near field, (2) calculate the frequency-domain far field from the frequency-domain near field, and (3) use the inverse Fourier transform to calculate the time-domain far field from the frequency-domain far field. This scheme makes use of well-known frequency-domain far-field formulas, sampling theorems, and the fast Fourier transform (FFT).

The second scheme is based on the time-domain formulation and is presented in Section 4.2. This time-domain scheme simply uses the formula that directly gives the time-domain far field in terms of the time-domain near field. A time-domain sampling theorem is derived to determine how small the sample spacing between points on the scan plane has to be in order to calculate the far field accurately.

Two numbers determine the amount of computer time required to perform a far-field calculation using each of the two computation schemes. The first is the number of spatial sample points on the scan plane, which is determined from the maximum effective frequency of the near field and the size of the scan plane. The second is the number of time samples taken at each near-field point on the scan plane. This number depends on the maximum effective frequency of the near field and on its effective time duration. Section 4.3 determines the number of time samples needed to perform accurate far-field calculations from the near fields of different types of radiators.

Finally, in Section 4.4 the two computation schemes are compared and used to calculate the far-field pattern of a simple acoustic point-source antenna from near-field data. For different types of antennas we compare the convenience and the computer time for the two

computation schemes. It is found that the direct time-domain computation scheme of Section 4.2 is much simpler to program and use than the frequency-domain computation scheme of Section 4.1. However, because the frequency-domain computation scheme uses the FFT it is much faster for large antennas than the time-domain computation scheme when the full far field is calculated for all times. When only part of the far field is calculated, the difference in computer time for the two computation schemes becomes smaller and the time-domain computation scheme therefore becomes more advantageous because of its simplicity.

Most of the results of this chapter are derived for acoustic fields. The corresponding results for the electromagnetic fields are immediately obtained by noting that the electromagnetic time-domain, near-field to far-field transformations have the same form as the acoustic transformations.

4.1 Frequency-Domain Computation Scheme

The frequency-domain computation scheme consists of first calculating the frequency-domain near field by taking the Fourier transform of the measured time-domain near field

$$\Phi_\omega(\bar{r}_0) = \frac{1}{2\pi}\int_{-\infty}^{+\infty} \Phi(\bar{r}_0, t)e^{i\omega t}dt, \quad \bar{r}_0 = x_0\hat{x} + y_0\hat{y} \tag{4.1}$$

and then using the frequency-domain far-field formula (2.47) to get the frequency-domain far-field pattern

$$\mathcal{F}_\omega(\theta,\phi) = -\frac{i\omega\cos\theta}{2\pi c}\int_{-\infty}^{+\infty}\int_{-\infty}^{+\infty} \Phi_\omega(\bar{r}_0)e^{-i\omega\hat{r}\cdot\bar{r}_0/c}dx_0dy_0. \tag{4.2}$$

The time-domain far-field pattern is then found by Fourier transforming the frequency-domain far-field pattern

$$\mathcal{F}(\theta,\phi,t) = \int_{-\infty}^{+\infty} \mathcal{F}_\omega(\theta,\phi)e^{-i\omega t}d\omega. \tag{4.3}$$

We will now show how the integrals (4.1)-(4.3) can be calculated using the fast Fourier transform (FFT).

If the time-domain near field is effectively bandlimited, so that Φ_ω can be set equal to zero for $|\omega| > \omega_{max}$, the sampling theorem [48, sec.5.4] can be applied to convert (4.1) to the summation

$$\Phi_\omega(\bar{r}_0) = \frac{1}{2\pi}\sum_{m=-\infty}^{+\infty} \Phi(\bar{r}_0, m\Delta t)e^{i\omega m\Delta t}\Delta t, \quad |\omega| < \omega_{max} \tag{4.4}$$

where $\Delta t = \pi/\omega_{max}$ is the time sample spacing determined from the sampling theorem. In practice, the time signal begins at some time t_0 (which may depend on the position in the scan plane) and ends approximately at some time which can be expressed as $t_0 + (N_\omega - 1)\Delta t$. Then (4.4) can be written as

$$\Phi_\omega(\bar{r}_0) = \frac{1}{2\pi}\sum_{m=0}^{N_\omega-1} \Phi(\bar{r}_0, t_0 + m\Delta t)e^{i\omega(t_0+m\Delta t)}\Delta t, \quad |\omega| < \omega_{max}. \tag{4.5}$$

According to Nussbaumer [49, p.88], if N_ω is chosen such that $N_\omega = 2^I$ where I is an integer, the FFT requires $M = \frac{1}{2}N_\omega \log_2(N_\omega)$ complex multiplications and $A = N_\omega \log_2(N_\omega)$ complex additions to calculate (4.5) for the following N_ω values of ω: $\omega = n\Delta\omega$, $n = 0, 1, 2, ..., N_\omega - 1$ with $\Delta\omega = 2\omega_{max}/N_\omega$. (There appears to be no significant reduction in the number of complex multiplications if Φ_ω is calculated only for $n = 0$ to $n = N_\omega/2$.) Since complex multiplications take considerably longer than complex additions, the required computer time is approximately proportional to $M = \frac{1}{2}N_\omega \log_2(N_\omega)$.

Having calculated the frequency-domain near field we can now use (4.2) and the two-dimensional FFT to calculate the frequency-domain far-field pattern. According to the frequency-domain sampling theory Yaghjian [1, Fig.10] one has to sample the near field (outside the reactive zone of the radiator) with a sample spacing of approximately $\Delta x_0 = \Delta y_0 = \lambda_{min}/2$ where $\lambda_{min} = 2\pi c/\omega_{max}$ is the minimum effective wavelength occurring in the time-domain field. The double integral in (4.2) is thereby replaced by an infinite double summation. For actual measurements the scan area is finite and the infinite double summation is given by

$$\mathcal{F}_\omega(\theta,\phi) = -\frac{i\omega\cos\theta}{2\pi c}\sum_{m=-N_x}^{N_x}\sum_{n=-N_y}^{N_y}\Phi_\omega(\bar{r}_{0mn})e^{-i\omega\hat{r}\cdot\bar{r}_{0mn}/c}\Delta x_0\Delta y_0 \tag{4.6}$$

where $\bar{r}_{0mn} = m\Delta x_0\hat{x} + n\Delta y_0\hat{y}$ is a sampling point on the scan plane. The integers N_x and N_y are determined by the size of the scan plane and are proportional to $k_{max}r_s$ where $k_{max} = 2\pi/\lambda_{min} = \omega_{max}/c$ and r_s is the radius of the circle circumscribing the scan plane.

From Nussbaumer [49, p.103] the number of complex multiplications it takes for the two-dimensional FFT to calculate the full far-field pattern (4.6) for a fixed ω at $4N_xN_y$ far-field points is $M = 2N_xN_y\log_2(4N_xN_y)$ which is proportional to $(k_{max}r_s)^2\log_2(k_{max}r_s)$. (Again it is assumed that N_x and N_y are chosen equal to 2 raised to an integer.) If we are interested only in a single principal-plane far-field cut ($\phi = 0$ or $90°$) the number of operations for large scan planes is dominated by the $4N_xN_y$ complex additions needed to collapse [50] the data in one of the rectangular coordinates before performing the FFT in the remaining rectangular coordinate. Thus the number of operations required to compute the far field in a principal plane is proportional to $(k_{max}r_s)^2$.

Now that the frequency-domain far-field pattern is calculated, (4.3) can be used to calculate the time-domain far-field pattern. The integral in (4.3) is converted to

$$\mathcal{F}(\theta,\phi,t) = \sum_{m=-N_\omega/2}^{N_\omega/2}\mathcal{F}_{m\Delta\omega}(\theta,\phi)e^{-im\Delta\omega t}\Delta\omega, \quad \Delta\omega = \frac{2\omega_{max}}{N_\omega} \tag{4.7}$$

by means of the sampling theorem if the far field $\mathcal{F}(\theta,\phi,t)$ has about the same duration as the near field $\Phi(\bar{r}_0,t)$. The values of $\mathcal{F}_\omega$ for negative ω are obtained from the equation $\mathcal{F}_\omega = \mathcal{F}^*_{-\omega}$ where * indicates complex conjugation. If the time duration of the far field is longer than that of the near field one has to decrease the frequency sample spacing $\Delta\omega$ (by increasing N_ω in the FFT's used to compute (4.5) and (4.7)) to avoid significant time-domain aliasing. Specifically, if the duration of the far field is T_f the frequency sample spacing $\Delta\omega$

should be chosen less than or equal to $2\pi/T_f$ according to the sampling theorem. (This is seen by shifting the far-field pattern to make it symmetric around $t = 0$ and then noting that the shifted far-field pattern is zero for $|t| > \frac{1}{2}T_f$. In Section 4.4 it will be shown that T_f, in general, depends not only on the near field but also on the size of the scan plane. This is because the artificial edges of the scan plane produce a diffracted field that will make the time duration of the far-field pattern calculated from (4.6) longer than that of the exact far-field pattern.) The FFT calculation of the summation (4.7) for N_ω different values of t requires $M = \frac{1}{2}N_\omega \log_2(N_\omega)$ complex multiplications.

Let us now calculate the total number of complex multiplications required for the computation of the full time-domain far-field pattern at $4N_xN_y$ different angles of observation and N_ω different times. To calculate the frequency-domain near field from the summation (4.5) for $4N_xN_y$ near-field points and for N_ω different frequencies requires $M_1 = 2N_xN_yN_\omega \log_2(N_\omega)$ complex multiplications. Furthermore, to calculate the frequency-domain far-field pattern from (4.6) for $4N_xN_y$ different angles of observation and N_ω different frequencies requires $M_2 = 2N_xN_yN_\omega \log_2(4N_xN_y)$ complex multiplications. Finally, to calculate the time-domain far-field pattern from (4.7) for $4N_xN_y$ different angles of observation and N_ω different times requires $M_3 = 2N_xN_yN_\omega \log_2(N_\omega)$ complex multiplications. Consequently, the total number of complex multiplications required for this FFT computation of the full far field is

$$\begin{aligned} M_f &= M_1 + M_2 + M_3 = N_xN_yN_\omega \left[4\log_2(N_\omega) + 2\log_2(4N_xN_y)\right] \\ &\sim (k_{max}r_s)^2 N_\omega \left[\log_2(N_\omega) + \log_2(k_{max}r_s)\right]. \end{aligned} \tag{4.8}$$

Similarly, the number of operations required to calculate a principal-plane far-field cut (for example the $\phi = 0$ cut) at N_ω different times is dominated by

$$M_c = M_1 = 2N_xN_yN_\omega \log_2(N_\omega) \sim (k_{max}r_s)^2 N_\omega \log_2(N_\omega) \tag{4.9}$$

complex multiplications required to calculate the frequency-domain near-field at $4N_xN_y$ near-field points and N_ω different frequencies.

Section 4.4 shows a numerical example illustrating the use of the frequency-domain computation scheme and discusses some of its advantages and disadvantages. Having explained the frequency-domain computation scheme in this section, we deal with the time-domain computation scheme in the next section.

4.2 Time-Domain Computation Scheme

The time-domain computation scheme consists simply of using the direct time-domain formula (3.13) for the far-field pattern

$$\mathcal{F}(\theta,\phi,t) = \frac{\cos\theta}{2\pi c}\int_{-\infty}^{+\infty}\int_{-\infty}^{+\infty}\frac{\partial}{\partial t}\Phi(\bar{r}_0, t + \hat{r}\cdot\bar{r}_0/c)dx_0dy_0, \quad \bar{r}_0 = x_0\hat{x} + y_0\hat{y} \tag{4.10}$$

which uses the time-domain near field directly. Assume for simplicity that we know the time derivative of the near field on the scan plane. (This is a realistic assumption because some probes actually measure the time derivative of the field [51].)

Equation (4.10) can be obtained by Fourier transforming the frequency-domain formula (4.2), which was converted to the double summation in (4.6) by means of the sampling theorem. Therefore, (4.10) can be converted to a summation by Fourier transforming (4.6) to get

$$\mathcal{F}(\theta,\phi,t) = \frac{\cos\theta}{2\pi c}\sum_{m=-N_x}^{N_x}\sum_{n=-N_y}^{N_y}\frac{\partial}{\partial t}\Phi(\bar{r}_{0mn}, t+\hat{r}\cdot\bar{r}_{0mn}/c)\Delta x_0\Delta y_0 \qquad (4.11)$$

where $\bar{r}_{0mn} = m\Delta x_0\hat{x} + n\Delta y_0\hat{y}$ is a sampling point on the scan plane and $\Delta x_0 = \Delta y_0 = \lambda_{min}/2$. This formula represents a time-domain sampling theorem that requires one to sample the time-domain near field at a spatial sample spacing of $\lambda_{min}/2$, the same spacing required by the frequency-domain computation scheme.

The direct time-domain formula (4.11) reveals a useful property of the time-domain computation scheme. If the source is turned on at $t = t_0$ one can calculate the far-field pattern for times $t < t_1$ by measuring the near field only for $t < t_2$. (This is not true for the frequency-domain computation scheme because the calculation of the frequency-domain near field requires the values of the near field over its entire duration.) To determine t_2 as a function of t_1 and the angle of observation θ we assume that the scan plane is large enough that the near field has not reached its edges at $t = t_2$. Because the source is turned on at $t = t_0$ the near field $\Phi(\bar{r}_0, t)$ is zero for $|\bar{r}_0| > c(t - t_0)$ when $\bar{r}_0$ is far from the source region, so that the minimum distance from the source region to $\bar{r}_0$ is approximately $|\bar{r}_0|$. From the time-domain formula (4.11) it is then seen that the latest time t_2 required to calculate the far-field pattern at the angle of observation θ and time t_1 is approximately given by $t_2 \simeq t_1 + |\bar{r}_{0max}|c^{-1}\sin\theta$ where $|\bar{r}_{0max}|$ is the radius of the circle in the scan plane circumscribing the nonzero near field at $t = t_2$. Consequently, $|\bar{r}_{0max}| = c(t_2 - t_0)$ and it is found that $t_2 \simeq \frac{t_1 - t_0}{1-\sin\theta} + t_0$. Therefore, to calculate the far-field pattern at an angle θ for $t_0 < t < t_1$ one only has to measure the near field for $t_0 < t < t_2$. In particular, if the far-field pattern is calculated on the z axis ($\theta = 0$) we have that $t_2 = t_1$ as can be seen immediately from the time-domain formula (4.11) since $\hat{r}\cdot\bar{r}_{0mn} \equiv 0$ on the z axis. Thus, in contrast to the frequency-domain computation scheme, the time-domain computation scheme can calculate the far-field pattern for early times from near-field data measured at early times.

To calculate the far field at the angles of observation (θ,ϕ) and time t from the formula (4.11) one has to know the near field at the point $\bar{r}_{0mn}$ on the scan plane at the time $\tau_{mn}(\theta,\phi) = t + m\Delta t\cos\phi\sin\theta + n\Delta t\sin\phi\sin\theta$ where $\Delta t = c^{-1}\Delta x_0 = c^{-1}\Delta y_0 = \pi/\omega_{max}$. Similarly, to calculate the far field at the angles of observation (θ',ϕ') and time t, one has to know the near field at the point $\bar{r}_{0mn}$ at the time $\tau_{mn}(\theta',\phi')$. The time difference $|\tau_{mn}(\theta,\phi) - \tau_{mn}(\theta',\phi')|$ for the two different angles of observation can be smaller than Δt, and therefore, in general, one needs the value of the near field at each $\bar{r}_{0mn}$ at times that lie between time samples with spacing Δt. However, since the near field is bandlimited, the standard sampling theorem shows that it is sufficient for reconstruction to sample the near field with time-sample spacing given by $\Delta t = \pi/\omega_{max} = \lambda_{min}/(2c)$. Assuming this has been done, the reconstruction theorem [48, p.83] shows that the near field can be calculated at an

arbitrary time t from the summation

$$\frac{\partial}{\partial t}\Phi(\bar{r}_{0mn},t)=\sum_{p=-\infty}^{+\infty}\frac{\sin(\pi(t/\Delta t-p))}{\pi(t/\Delta t-p)}\frac{\partial}{\partial t}\Phi(\bar{r}_{0mn},p\Delta t). \tag{4.12}$$

As in the previous section we assume that the time-domain near field is significant only in the time interval $t_0 < t < t_0+(N_\omega-1)\Delta t$, where t_0 may depend on the position $\bar{r}_{0mn}$. Then the summation (4.12) becomes

$$\frac{\partial}{\partial t}\Phi(\bar{r}_{0mn},t)=\sum_{p=0}^{N_\omega-1}\frac{\sin\left[\pi\left(\frac{t-t_0}{\Delta t}-p\right)\right]}{\pi\left(\frac{t-t_0}{\Delta t}-p\right)}\frac{\partial}{\partial t}\Phi(\bar{r}_{0mn},t_0+p\Delta t) \tag{4.13}$$

where N_ω is the integer occurring in the frequency-domain formula (4.5). This reconstruction formula requires the calculation of N_ω values of the sinc function, N_ω real multiplications, and N_ω real additions. The reconstruction calculation has to be performed for a number of time values depending on the far-field points, and at every near-field measurement point. Consequently, if N_ω is large, it may require a considerable amount of computer time.

However, for practical applications it may not be necessary to use the exact reconstruction formula (4.13). Instead one may be able to calculate the near field at a time t between the two time-sample points $p\Delta t$ and $(p+1)\Delta t$ by using the linear approximation formula

$$\frac{\partial}{\partial t}\Phi(\bar{r}_{0mn},t)=\frac{1}{\Delta t}\left\{[(p+1)\Delta t-t]\frac{\partial}{\partial t}\Phi(\bar{r}_{0mn},p\Delta t)+[t-p\Delta t]\frac{\partial}{\partial t}\Phi(\bar{r}_{0mn},(p+1)\Delta t)\right\}. \tag{4.14}$$

If this linear formula is inaccurate one can oversample, that is, let $\Delta t < \pi/\omega_{max}$, and then again use (4.14).

Assume that the linear approximation formula (4.14) can be used to accurately calculate the near field between time samples at times required by the far-field formula (4.11). Then it takes 5 real additions and 3 real multiplications to obtain the near field at each value of time between the time samples. On a typical computer (VAX 8650) the time it takes to perform one real multiplication is approximately 1.5 times larger than the time it takes to perform one real addition. Therefore the calculation of the near field at a time between two time samples requires approximately the time it takes to perform 10 real additions. Thus, the time it takes to calculate the full time-domain far-field pattern in (4.11) for $4N_xN_y$ far-field points and N_ω times is approximately equal to the time it takes to perform

$$A_f = 160N_\omega(N_xN_y)^2 \sim N_\omega(k_{max}r_s)^4 \tag{4.15}$$

real additions. Similarly, to calculate a principal-plane far-field cut (for example the $\phi = 0$ cut) requires the time it takes to perform

$$A_c = 80N_\omega N_xN_y^2 \sim N_\omega(k_{max}r_s)^3 \tag{4.16}$$

real additions. No complex multiplications are needed and it is seen that the number of additions required to calculate a principal-plane far-field cut is significantly smaller than the number required to calculate the full far field.

Note from the expression (4.11) for the far-field pattern that if all fields are zero for $t < t_0$, the finite scan plane does not introduce any error into the far-field pattern calculation at times before the near field has reached the edges of the scan plane. This follows from the fact that $\Phi(\bar{r}_0, t) \equiv 0$ for $s > c(t - t_0)$ where s is the shortest distance from the source region to the point $\bar{r}_0$. In Section 4.4 we show a numerical example that illustrates this important property of the time-domain computation scheme.

4.3 Number of Near-Field Time Samples Needed for Far-Field Calculation

This section computes the time-sample spacing Δt and the number of time samples N_ω required to calculate the far field accurately from near-field data for different types of acoustic and electromagnetic antennas.

Acoustic point-source antenna

We start by considering a simple acoustic point-source antenna located at $\bar{r}_1$. Its field is given by

$$\Phi(\bar{r}, t) = \frac{f(t - |\bar{r} - \bar{r}_1|/c)}{4\pi|\bar{r} - \bar{r}_1|} \tag{4.17}$$

where $f(t)$ is the time dependence. Since the time dependence of the far-field pattern of this antenna is the same as that of its near field, the required number of time samples is determined such that the reconstruction formula [48, p.83]

$$f(t) = \sum_{p=0}^{N_\omega - 1} \frac{\sin\left[\pi\left(\frac{t-t_0}{\Delta t} - p\right)\right]}{\pi\left(\frac{t-t_0}{\Delta t} - p\right)} f(t_0 + p\Delta t) \tag{4.18}$$

is accurate. Here the time sample spacing $\Delta t = \pi/\omega_{max}$ is determined from the sampling theorem, t_0 is the time at which the time signal begins, and N_ω is determined such that $t_0 + \Delta t(N_\omega - 1)$ is the time at which the time signal ends. The field of the acoustic point-source antenna will be analyzed for two different types of time functions $f(t)$.

We start with the Gaussian time function, which, along with its spectrum, are shown in Figure 4.1 and are given by

$$f(t) = e^{-4t^2/\tau^2}, \quad f_\omega = \frac{\tau}{4\sqrt{\pi}} e^{-\omega^2\tau^2/16} \tag{4.19}$$

where τ equals half the signal width. The signal width 2τ is defined such that $|f(t)| < 0.02|f(0)|$ for $|t| > \tau$. Strictly speaking, this Gaussian pulse is not bandlimited. However, as seen from Figure 4.1, the spectrum is approximately zero for $\omega > 12/\tau$ and therefore the Gaussian pulse (4.19) can be approximated by a pulse that is bandlimited with a bandlimit given by $\omega_{max} = 12/\tau$. With $\Delta t = \pi/\omega_{max} \simeq \tau/4$ being the sample spacing found from the standard sampling theorem, the curve obtained from the reconstruction formula (4.18)

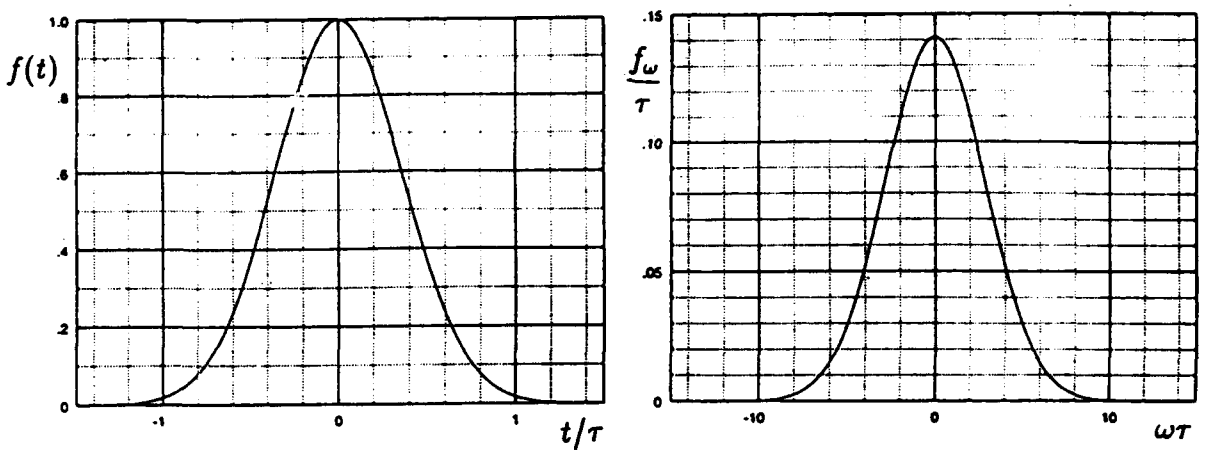

Figure 4.1: Gaussian time function $f(t)$ and its spectrum f_ω.

with $N_\omega = 10$ and $t_0 = -1.25\tau$ was impossible to distinguish from the exact curve in Figure 4.1. This means that any Gaussian signal, no matter how wide a bandwidth it has, can be reconstructed quite accurately from 10 time samples.

Having considered the Gaussian time function, which is nonzero for all times, consider now the more realistic time function

$$f(t) = \begin{cases} 0, & t \le 0 \\ e^{-\tau^2/(16t^2)} \frac{2-4t/\tau}{1+(4t/\tau-2)^4} \left[23e^{-4t^2/\tau^2} + 4t/\tau\right], & t > 0 \end{cases} \tag{4.20}$$

which is shown in Figure 4.2 and is constructed so that it is identically zero for $t \le 0$, it is of order t^{-2} at infinity, it is infinitely differentiable for all t, and it has a zero time integral, that is, its spectrum is zero for $\omega = 0$. The spectrum f_ω, which decays faster than ω^{-n} for all $n > 0$ as $|\omega| \to \infty$, is found by straightforward numerical integration and is also shown in Figure 4.2. This spectrum reveals that the realistic time function (4.20) is approximately bandlimited with bandlimit $\omega_{max} \simeq 32/\tau$ so that the sample spacing for the reconstruction formula (4.18) is $\Delta t = \pi/\omega_{max} \simeq 0.10\tau$. It was found that the reconstruction formula (4.18) with $N_\omega = 20$ and $t_0 = 0$ could not be distinguished from the exact curve in Figure 4.2 and thus 20 time samples are sufficient to accurately reconstruct the fairly complicated time function (4.20) no matter how broad its bandwidth.

The analysis of these two types of near fields has shown that only a small number of time samples is required to accurately reconstruct them even in the case of the fairly realistic pulse shown in Figure 4.2. The corresponding far fields can be calculated accurately from the same small number of near-field time samples as will be demonstrated in Section 4.4.

Open-ended waveguide antenna

Let us now consider the more complicated electromagnetic antenna consisting of an open-ended rectangular waveguide fed by a source that has a time dependence $f^i(t)$ and is located

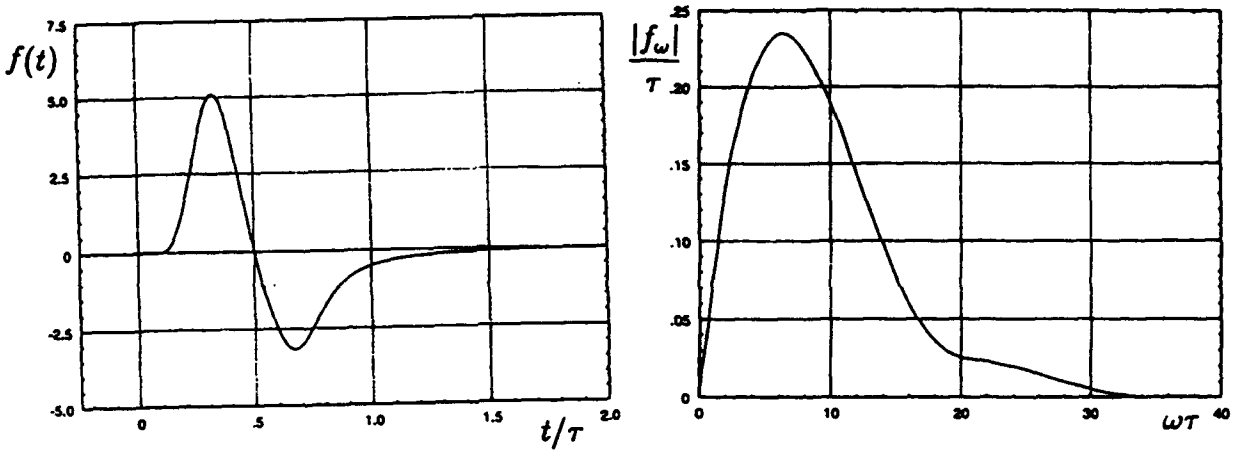

Figure 4.2: Realistic time function $f(t)$ and the amplitude of its spectrum $|f_\omega|$.

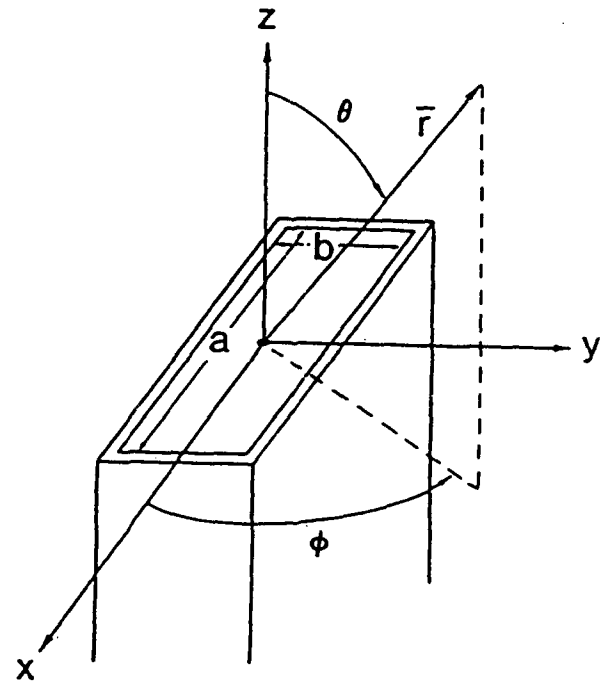

Figure 4.3: Open-ended waveguide antenna.

at the point $(x, y, z) = (0, 0, -d)$ in the waveguide shown in Figure 4.3. Assuming that the source is such that only the TE_{10} mode is excited, the part of the electric waveguide field that propagates in the direction of the positive z axis is given by

$$\bar{E}_{10}(\bar{r}) = \hat{y} f_\omega^i \cos\left(\frac{\pi x}{a}\right) e^{ik_z z} \tag{4.21}$$

where the longitudinal propagation constant is

$$k_z = \begin{cases} ik\sqrt{\left(\frac{\omega_c}{\omega}\right)^2 - 1}, & \omega < \omega_c \\ k\sqrt{1 - \left(\frac{\omega_c}{\omega}\right)^2}, & \omega > \omega_c \end{cases} . \tag{4.22}$$

Furthermore, $\omega_c = \pi c/a$ is the cutoff frequency for the TE_{10} mode and f_ω^i is the spectrum of the input signal. Note that the spectrum of the electric field is exponentially attenuated below cutoff and that its value at the center of the aperture is given by

$$E_{A\omega} = \begin{cases} e^{-kd\sqrt{\left(\frac{\omega_c}{\omega}\right)^2 - 1}} f_\omega^i, & 0 < \omega < \omega_c \\ e^{ikd\sqrt{1 - \left(\frac{\omega_c}{\omega}\right)^2}} f_\omega^i, & \omega > \omega_c \end{cases} . \tag{4.23}$$

The on-axis value of the far-field pattern $\bar{\mathcal{F}}_\omega(\theta = 0)$ is given approximately by [52, eqs.(1), (6)]

$$\bar{\mathcal{F}}_\omega(\theta = 0) = \mathcal{F}_\omega(\theta = 0)\hat{y} = C_0 \omega E_{A\omega} \left[1 + \Gamma + \frac{k_z}{k}(1 - \Gamma)\right] \hat{y} \tag{4.24}$$

where C_0 is a frequency independent constant and Γ is a reflection coefficient that is approximately frequency independent over the recommended usable bandwidth of the waveguide.

Let us now calculate the time dependence of the aperture electric field and the on-axis far field for the special case where the source is Gaussian and the waveguide is X-band. In this case the TE_{10} cutoff frequency is $\omega_c = \pi c/a = 4.1 \cdot 10^{10} \mathrm{s}^{-1}$, $\Gamma \simeq 0.27 e^{i1.4}$, $a = 2.86$ cm, and $b = 1.016$ cm. The Gaussian source is chosen so that its spectrum, at the midpoint of the interval from ω_c to the next cutoff frequency $2\omega_c = 2\pi c/a = 8.2 \cdot 10^{10} \mathrm{s}^{-1}$, equals half its value at $\omega = 0$, as shown in Figure 4.4. In this case the input pulse and its spectrum are given by (4.19) with $\tau = 5.4 \cdot 10^{-11}$s. For $d = 5$ cm the absolute value of the spectrum $E_{A\omega}$ and the time dependence $E_A(t)$ of the electric field at the center of the aperture are shown in Figure 4.5. It is seen from Figure 4.5 that the spectrum for the aperture electric field is significantly attenuated below cutoff and that its slope is very large around the cutoff frequency. This spectrum is thus very different from that in Figure 4.4 of the Gaussian input pulse because of the dispersion of the TE_{10} mode over the 5 cm of travel in the waveguide. The time dependence of the aperture electric field is also shown in Figure 4.5 and is seen to be completely different from the Gaussian input pulse (4.19). In particular the aperture electric field has a pulse width of approximately 80τ while the Gaussian input pulse has a pulse width of approximately 2τ. Since the bandwidth of the aperture field is the same

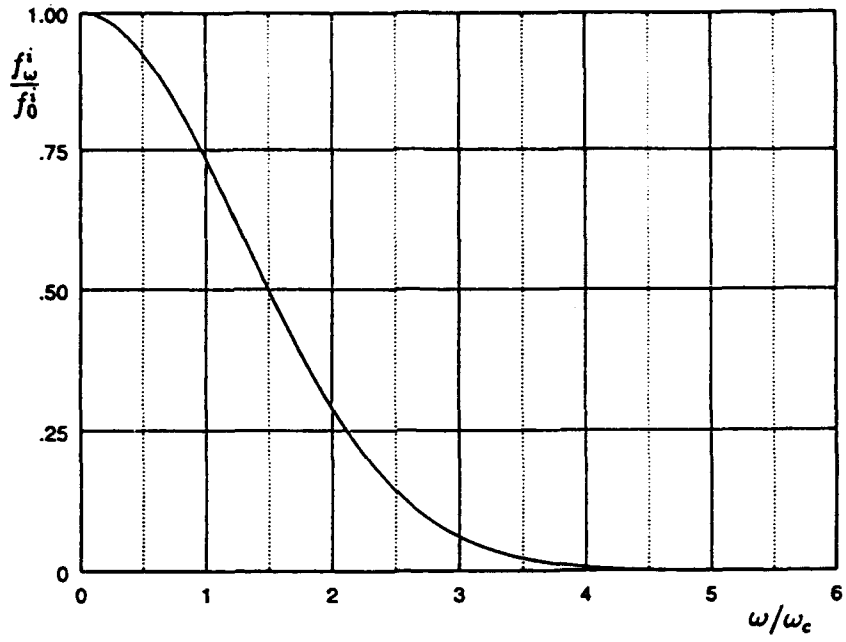

Figure 4.4: Spectrum of input pulse.

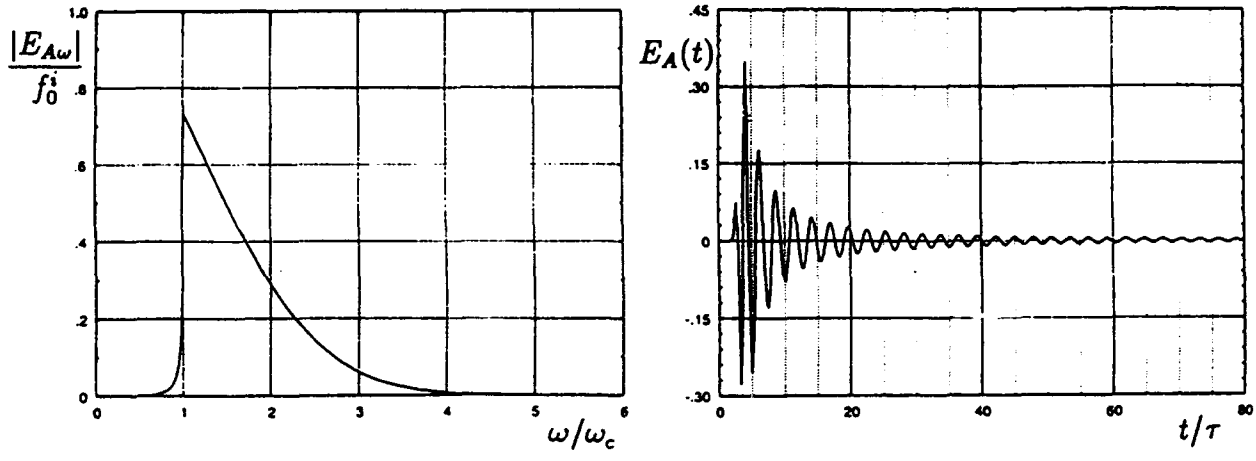

Figure 4.5: Amplitude of spectrum and time dependence of aperture electric field for open-ended wave-guide antenna.

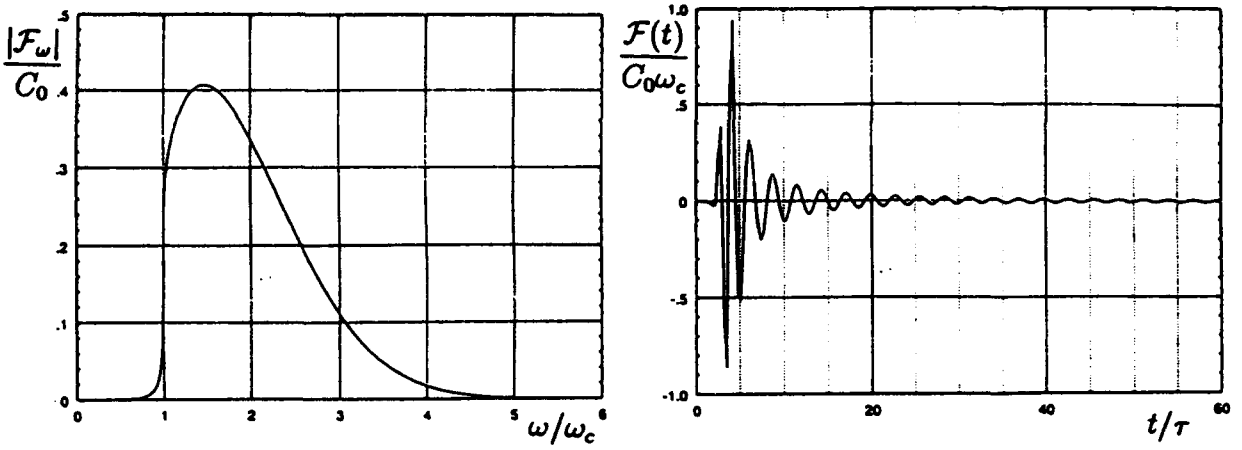

Figure 4.6: Amplitude of spectrum and time dependence of on-axis value of the far-field pattern for open-ended waveguide antenna.

as that of the input pulse, the time sampling spacing for the signals is the same. This means that the number of time samples required for the aperture electric field is 40 times the number of time samples required for the Gaussian input pulse. It was shown above that the Gaussian input pulse required approximately 10 time samples so the aperture electric field requires approximately 400 time samples. In other words, to reconstruct the aperture electric field by use of the reconstruction theorem [48, p.83] one has to sample this field at 400 different times. And therefore, when a near-field to far-field calculation is performed for this near field one has to use 400 time samples to make sure that the far field is calculated accurately.

Let us now consider the on-axis value of the far-field pattern (4.24) whose spectrum and time dependence are shown in Figure 4.6. It is seen that the spectrum of the on-axis far field is very similar to that of the aperture electric field and that it is very different from the spectrum of the Gaussian input pulse. Near the cutoff frequency the spectrum of the on-axis far field is much smoother than the spectrum of the aperture electric field. The time dependence of the on-axis far-field pattern, also shown in Figure 4.6, is very similar to the time dependence of the aperture electric field. However, because of the smoother spectrum, the far field dies off faster with time than the aperture electric field and the pulse width of the far field is approximately 40τ which is 20 times that of the input pulse.

In summary, for the open-ended waveguide antenna the time dependence of the aperture electric field and of the far field are very different from the time dependence of the input pulse because of the dispersive effects of the waveguide on the TE_{10} mode. In particular, for a Gaussian input pulse the time widths of the aperture electric field and the on-axis far field are approximately 40 and 20 times larger than the time width of the input pulse, respectively. Assuming that the near field behaves as the aperture field, this means that one has to measure the near field (at every near field point) at approximately 400 different times

when the waveguide is fed by a Gaussian pulse, which alone only requires 10 time samples.

Monopole antenna

In [53] the time-domain radiation from a monopole on a ground plane, fed by a Gaussian input pulse, is calculated using the Finite-Difference Time-Domain method. From [53, Figs.7, 11] it is also seen that for this type of antenna the number of time samples required for the radiated field is much larger than the number required for the input pulse. In particular, [53, Fig.7] shows that when the Gaussian input pulse is given by [53, eq.(6)] (which requires approximately 10 time samples and has a pulse width of approximately $5.7\tau_p$), the radiated field has a pulse width of approximately $5\tau_a \simeq 62\tau_p$. This is 11 times wider than the input pulse and therefore requires approximately 110 time samples. Consequently, as for the open-ended waveguide, the number of time samples required for the field radiated by the monopole is much larger than the number required for the input pulse.

4.4 Comparisons of the Two Computation Schemes

Having determined in the previous section the number of time samples required for different types of near fields, we shall now compare and discuss the advantages and disadvantages of the frequency-domain computation scheme of Section 4.1 and the time-domain computation scheme of Section 4.2. To compare the efficiency and convenience of the two schemes we start by using them to numerically calculate the far-field pattern of a simple acoustic antenna from near-field data taken on a square scan plane.

Acoustic point-source antenna

The simple acoustic antenna radiates the point-source field given in (4.17) with $f(t)$ being the Gaussian time function (4.19). As explained in Section 4.3 this antenna field is effectively bandlimited with bandlimit $\omega_{max} = 12/\tau$ which means that $\lambda_{min} = 2\pi c/\omega_{max} \simeq c\tau/2$ and thus the spatial sample spacing is $\Delta x_0 = \Delta y_0 = \lambda_{min}/2 \simeq c\tau/4$. The point source is located at $\bar{r}_1 = -d\hat{z}$ where $d = 2\lambda_{min} \simeq c\tau$ and the scan plane is taken to be a square of side length $10d$ located in the plane $z = 0$.

We start by showing results for the on-axis values of the far-field pattern $\mathcal{F}(\theta = 0, t)$ obtained from the time-domain formula (4.11) and the linear approximation formula (4.14). Figure 4.7 shows three plots of the time dependence of the on-axis values of the far-field pattern $\mathcal{F}(\theta = 0, t)$: (a) the exact value, (b) the value obtained from (4.11) and (4.14) with $\Delta t = \pi/\omega_{max}$ (as prescribed by the standard sampling theorem), and (c) the value obtained from (4.11) and (4.14) with $\Delta t = \pi/(3\omega_{max})$ (that is, a value obtained by oversampling in time).

The first curve (a), which is exact, has the Gaussian wave form and is only significantly nonzero on the interval $-0.1\tau < t < 2.1\tau$. The second curve (b), which is obtained by using the standard time sample spacing $\Delta t = \pi/\omega_{max}$ and the linear approximation formula (4.14), has some visible discontinuities in its slope and approximates the exact curve well on the interval $-\tau < t < 4\tau$. On the interval $4\tau < t < 8\tau$ it is negative and erroneous. The third

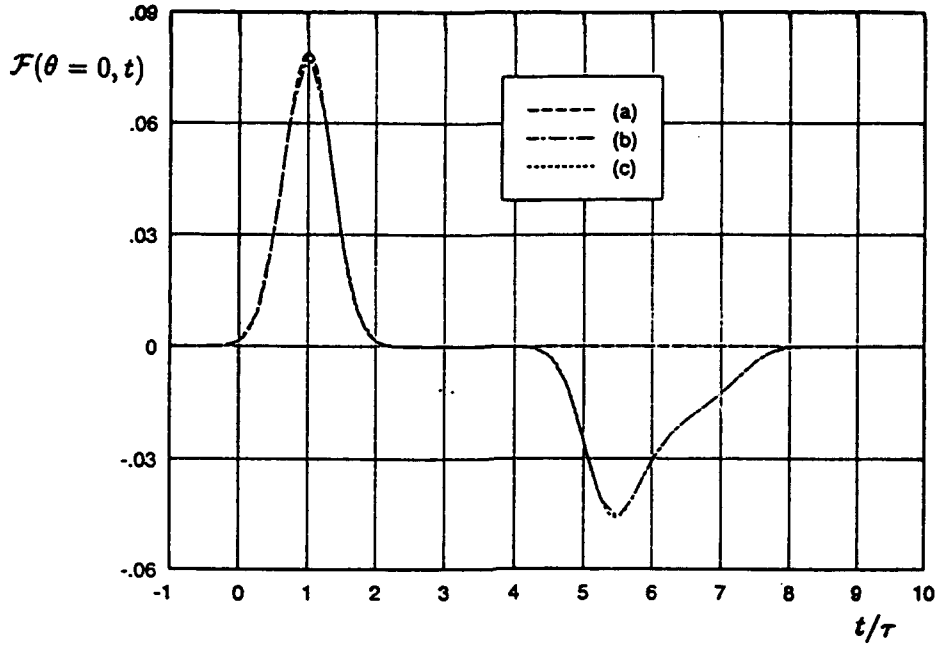

Figure 4.7: On-axis values of the far-field pattern for a Gaussian point source calculated with the time-domain computation scheme. (a) exact; (b) $\Delta t = \pi/\omega_{max}$; (c) $\Delta t = \pi/(3\omega_{max})$.

curve (c), which is obtained by oversampling with $\Delta t = \pi/(3\omega_{max})$ and using (4.14), cannot be distinguished from the exact curve on the interval $-\tau < t < 4\tau$ and is erroneous (like the second curve) on the interval $4\tau < t < 8\tau$. Before discussing the erroneous behavior of the two approximate curves (b) and (c) over this late-time interval, we note that by oversampling with $\Delta t = \pi/(3\omega_{max})$ one can use the simple linear approximation formula (4.14) to obtain an excellent approximation to the exact curve.

The erroneous behavior of the two approximate curves (b) and (c) on the interval $4\tau < t < 8\tau$ can be explained by first noting that the time integral of the expression (4.11) from $t = -\infty$ to $t = +\infty$ is zero for finite (truncated) scan planes because $\Phi(t = -\infty) = \Phi(t = +\infty) = 0$. This means that for the far-field patterns approximated by the summation in (4.11), $\int_{-\infty}^{+\infty} \mathcal{F}(\theta = 0, t)dt = 0$ which, of course, is not the case for the exact non-negative Gaussian far-field pattern. The integral representation (4.10) of the far-field pattern is exact and since the near field is sampled with spatial spacing of $\lambda_{min}/2$ (as required by the near-field sampling theorem [1]), we conclude that the erroneous behavior of the two approximate curves is due to the finite scan plane. This observation is confirmed by the fact that the time between the arrival of the direct signal ($t \simeq -0.1\tau$) and the arrival of the erroneous signal ($t \simeq 4.1\tau$) is equal to the time it takes the signal to travel the distance $l_1 - d$, where $l_1 = \sqrt{26}d$ is the distance from the source to the midpoint of the edges of the scan plane (recall that $\tau \simeq d/c$). Similarly, the time difference between the end of the direct signal ($t \simeq 2.1\tau$) and the end of the erroneous signal ($t \simeq 8\tau$) is the time it takes the signal to travel the distance $l_2 - d$, where $l_2 = \sqrt{51}d$ is the distance from the source to the corners of the scan plane.

Thus, the erroneous parts of the approximate far-fields are caused by the finite scan plane

and represent diffraction from the artificial edges of the truncated scan plane. Enlarging the scan plane makes the erroneous part of the approximate far field move to later times but it will never disappear when the scan plane is finite. Furthermore, from the exact integral (4.10) it is seen that for $t < 4\tau$ there is no contribution from the region outside the square scan plane with side length $10d$. Thus, for early times the truncated scan plane does not introduce any error into the calculation of the far-field pattern because the signal has not yet reached the edges of the scan plane. However, as time gets larger the signal reaches these edges and the finite scan plane introduces an error which is separated in time from the exact far-field pattern as demonstrated above.

This simple example shows that by oversampling in time, one may avoid using the time consuming reconstruction formula (4.13) and instead use the simple linear approximation (4.14). Furthermore, it shows that the errors due to the finite scan plane are separated in time from the exact far field and can therefore be eliminated when using the direct time-domain computation scheme.

Having shown and discussed results obtained from the time-domain computation scheme, we now turn to the frequency-domain computation scheme. As explained in Section 4.1, the frequency sample spacing $\Delta\omega = 2\omega_{max}/N_\omega$ for this scheme depends on the bandwidth ω_{max} of the near field and on the duration of the far field. Moreover, we have just shown that the duration of the far field is erroneously extended beyond that of the near field by the truncation of the scan plane. Thus, in practice, the required frequency sample spacing $\Delta\omega = 2\omega_{max}/N_\omega$ depends not only on the bandwidth ω_{max} (and the duration of the near field) but also on the size of the scan plane.

From Figure 4.7 showing the time dependence of the on-axis values of the far-field pattern calculated from the time-domain computation scheme, it is seen that with our chosen scan-plane size the duration of the calculated time-domain far-field pattern is $T_f = 8.2\tau$ and therefore to avoid significant time-domain aliasing one must chose $\Delta\omega = 2\pi/T_f = 0.77\tau^{-1}$. This means that the number of time samples needed to avoid significant time-domain aliasing is $N_\omega = 2\omega_{max}/\Delta\omega \simeq 32$.

Figure 4.8 shows the following three plots of the on-axis values of the time-domain far-field pattern $\mathcal{F}(\theta = 0, t)$ calculated with the frequency-domain calculation scheme: (a) the exact value, (b) the value obtained from the frequency-domain formulas (4.5)-(4.7) with $N_\omega = 16$ (which is sufficient for reconstructing the near-field pulse), and (c) the value obtained by using (4.5)-(4.7) with $N_\omega = 32$ (the number prescribed by the sampling theorem to compute the far field extended in time by the truncated scan plane). The exact Gaussian curve (a) is significantly nonzero only on the interval $-0.1\tau < t < 2.1\tau$. The second curve (b) is periodic with period $T = \pi N_\omega/\omega_{max} = 4.2\tau$ and is clearly erroneous due to time-domain aliasing. The third curve (c) is periodic with period $T = 8.4\tau$ and cannot be distinguished from the exact curve (a) on the interval $-0.5\tau < t < 4.1\tau$. No significant time-domain aliasing occurs for the curve (c) and from Figure 4.7 it is seen that curve (c) is simply a periodic repetition of the far-field pattern calculated from the time-domain computation scheme. Consequently, it has been demonstrated that the frequency-domain computation scheme produces the same field as the time-domain computation scheme when the frequency sample spacing $\Delta\omega$ is chosen

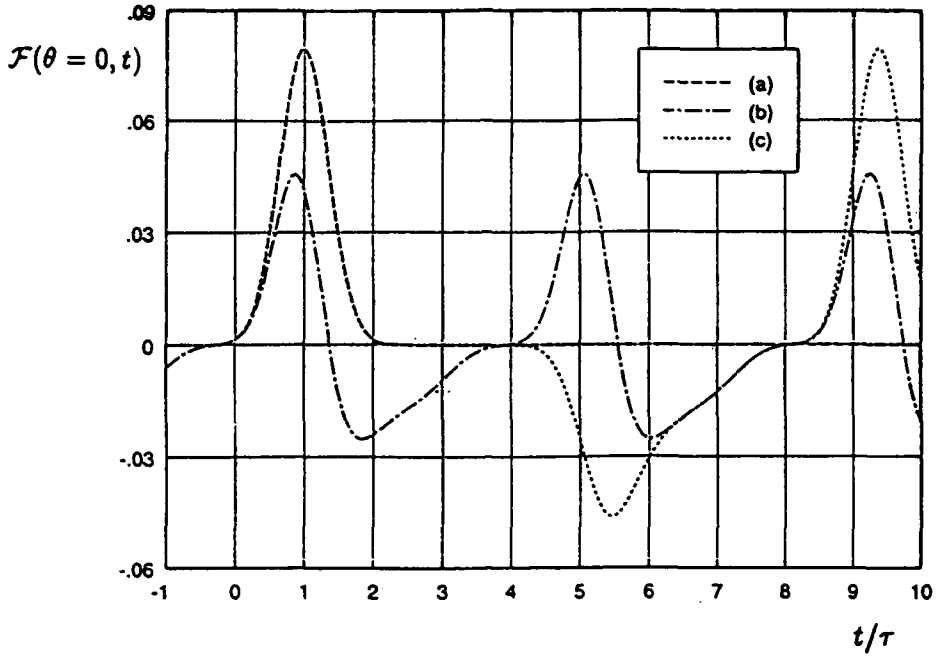

Figure 4.8: On-axis values of the far-field pattern for a Gaussian point source calculated with the frequency-domain computation scheme. (a) exact; (b) $N_\omega = 16$; (c) $N_\omega = 32$.

small enough to avoid time-domain aliasing caused by the field diffracted at the edges of the finite scan plane.

Open-ended waveguide antenna

Without actually calculating the far-field pattern for the open-ended waveguide antenna of Section 4.3, we will now discuss some of the consequences of using the two computation schemes to determine this far-field pattern. Assuming that the time dependence of the near field is similar to that of the aperture field shown in Figure 4.5, 400 near-field time samples are required to calculate the far-field pattern. (The open-ended waveguide antenna is directive so it is assumed that the diffraction due to the edges of the scan plane is negligible.) The on-axis values of the far-field pattern of the open-ended waveguide antenna, shown in Figure 4.6, consists of a main (early-time) part ($0 < t < 10\tau$) which contains most of the power and an oscillatory part ($t > 10\tau$). For applications one may only be interested in the main part of the far-field pattern. From Section 4.2 it is found that the time-domain computation scheme can determine this early-time part of the on-axis far field from measured near-field data taken in the time interval $0 < t < 10\tau$. Since the duration of the near field is approximately 80τ (see Figure 4.5) this means that only $\frac{1}{8} \cdot 400 = 50$ time samples are needed to calculate the main part of the far field using the time-domain computation scheme. Because the calculation of the frequency-domain near field requires the near field for its entire duration, the frequency-domain computation scheme needs all the 400 time samples of the near field to calculate the main part of the far field. This example shows that if one is only interested in the far-field pattern for early times, the number of time samples of the near field required by the time-domain computation scheme can be much smaller than the number required by

the frequency-domain computation scheme.

Computer time

Let us now compare the computer time required by the two computation schemes. For the far-field calculation performed in this section for the acoustic point-source antenna with Gaussian pulse excitation, the number of near-field sample points was $4N_xN_y = 1600$ because $N_x = N_y = 20$. To avoid time-domain aliasing caused by the edges of the scan plane, the number of time samples was $N_\omega = 32$ for the frequency-domain computation scheme (4.5)-(4.7) and therefore from (4.8) and (4.9) it is found that this scheme requires the calculation of $M_f = 5.3 \cdot 10^5$ and $M_c = 1.3 \cdot 10^5$ complex multiplications to compute the full far field and a principal-plane far-field cut, respectively. The on-axis result of this calculation is curve (c) of Figure 4.8, which cannot be distinguished from the exact far field on the time interval where the exact far field is nonzero.

To perform the same far-field calculation for the acoustic point-source antenna using the time-domain computation scheme (4.11) with the linear approximation formula (4.14), two different values of N_ω were used; namely $N_\omega = 10$ (giving curve (b) of Figure 4.7) and $N_\omega = 3 \cdot 10 = 30$ (giving curve (c) of Figure 4.7). The far-field obtained with $N_\omega = 10$ is a good approximation to the exact far field. The far-field obtained with $N_\omega = 30$ cannot be distinguished from the exact far field on the time interval where the exact far field is nonzero. From (4.15) it then follows that $A_f = 2.6 \cdot 10^8$ and $A_f = 7.7 \cdot 10^8$ real additions are needed to calculate the full far field with 10 and 30 time samples, respectively. Similarly, to calculate a principal-plane far-field cut $A_c = 6.4 \cdot 10^6$ and $A_c = 1.9 \cdot 10^7$ real additions are needed using 10 and 30 time samples, respectively.

Before comparing the results we note that on a typical computer (VAX 8650) the time it takes to perform one complex multiplication equals approximately 6 times the time it takes to perform one real addition. For the acoustic point-source antenna we see that when the full far field is calculated, the frequency-domain computation scheme is by far the fastest because it makes use of the FFT. When only a principal-plane far-field cut is calculated the computation time for the time-domain computation scheme reduces significantly whereas that of the frequency-domain computation scheme does not.

Next consider the open-ended X-band waveguide antenna of Section 4.3 fed by the Gaussian pulse with $\omega_{max} \simeq 4\omega_c = 1.6 \cdot 10^{11} \mathrm{s}^{-1}$ as shown in Figure 4.4. The scan plane is taken to be a square of side length 20 cm. Since $\lambda_{min} = 2\pi c/\omega_{max} = 1.1$ cm we find that $N_x = N_y = 18$ and that the total number of near-field scan points is $4N_xN_y = 1296$. From the discussion of Section 4.3 it follows that the number of near-field time samples is $N_\omega = 400$.

With these values of N_x, N_y, and N_ω one finds from (4.8) and (4.9) that the frequency-domain computation scheme requires $M_f = 7.1 \cdot 10^6$ and $M_c = 2.2 \cdot 10^6$ complex multiplications, respectively, to calculate the full far field and a principal-plane far-field cut. Similarly the formulas (4.15) and (4.16) show that the time-domain computation scheme requires $A_f = 6.7 \cdot 10^9$ and $A_c = 1.9 \cdot 10^8$ real additions, respectively, to calculate the full far field and a principal-plane far-field cut.

Again, when the full far field is calculated, the frequency-domain computation scheme

is by far the fastest while the difference in computer time for the calculation of a principal-plane far-field cut is small. Furthermore, as discussed above, if one is interested only in calculating the far field for early times the number of time samples required by the time-domain computation scheme reduces significantly whereas that of the frequency-domain computation scheme does not. Thus, when only the early part of the far field is needed the time-domain scheme becomes more attractive.

In summary, when far fields are calculated for all times and all angles of observation, the FFT makes the frequency-domain computation scheme much faster than the time-domain computation scheme. When only part of the far field is calculated, the difference in computer time for the two computation schemes becomes smaller and the time-domain computation scheme becomes more advantageous because of its simplicity. In general, the time-domain computation scheme is much more direct and simpler than the frequency-domain computation scheme and it does not have the problems of time-domain aliasing caused by the finite scan plane. The time-domain computation scheme is much easier to use than the frequency-domain computation scheme and it is consequently the more attractive scheme when one is not concerned with the amount of computer time it takes to perform the far-field calculations. Regardless of what computation scheme is used, planar time-domain near-field antenna measurements, unlike single-frequency near-field measurements, have the capability of eliminating finite scan errors. For some radiators, such as broadbeam antennas, this may be ample reason to consider time-domain measurements even when the final characterization of the radiator or scatterer is required in the frequency domain.

References

[1] Yaghjian, A.D. (1986) An overview of near-field antenna measurements, *IEEE Trans. Antenna Propagat.*, **AP-34**:30-45.

[2] Appel-Hansen, J., Dyson, J.D., Gillespie, E.S., and Hickman, T.G. (1982) Antenna measurements, Chapter 8 of *The Handbook of Antenna Design,* Rudge, A.W., Milne, K., Olver, A.D., and Knight, P., Eds., London: Peter Peregrinus.

[3] Kerns, D.M. (1982) *Plane-Wave Scattering-Matrix Theory of Antennas and Antenna-Antenna Interactions*, NBS Monograph 162.

[4] Newell, A.C. (1988) Error analysis techniques for planar near-field measurements, *IEEE Trans. Antenna Propagat.*, **36**:754-768.

[5] Leach, W.M. and Paris, D.T. (1973) Probe compensated near-field measurements on a cylinder, *IEEE Trans. Antenna Propagat.*, **AP-21**:435-445.

[6] Yaghjian, A.D. (1977) *Near-field antenna measurements on a cylindrical surface: a source scattering-matrix formulation*, NBS Tech. Note 696 (revised).

[7] Wacker, P.F. (1974) Near-field antenna measurements using a spherical scan: efficient data reduction with probe correction, *IEE Conf. Publ.* **113**:286-288.

[8] Hansen, J.E., Ed., Hald, J., Jensen, F., and Larsen, F.H. (1988) *Spherical Near-Field Antenna Measurements,* London: Peter Peregrinus.

[9] Yaghjian, A.D. and Wittmann, R.C. (1985) The receiving antenna as a linear differential operator: application to spherical near-field measurements, *IEEE Trans. Antenna Propagat.*, **33**:1175-1185.

[10] Jackson, J.D. (1975) *Classical Electrodynamics,* 2nd edition, New York: Wiley.

[11] Sherman, G.C., Stammes, J.J., and Lalor, E. (1976) Asymptotic approximations to angular-spectrum representations, *J. Math. Phys.*, **17**:760-776.

[12] Nieto-Vesperinas, M. (1991) *Scattering and Diffraction in Physical Optics*, New York: Wiley.

[13] Harmuth, H.F. (1986) Correction of Maxwell's equations for signals I and II, *IEEE Trans. Electromagnetic Compatibility*, **EMC-28**:250-266.

[14] Baum, C.E. (1987) *Focused aperture antennas*, Air Force Weapons Laboratory, Sensor and Simulation Notes, Note 306.

[15] Hill, D.A. (1986) *Far-Field Transient Response of an Antenna from Near-Field Data*, NBS Internal Report 86-3063.

[16] Moses, H.E., Nagem, R.J., and Sandri, G.V.H. (1992) The general solution of the three-dimensional acoustic equation and of Maxwell's equations in the infinite domain in terms of the asymptotic solution in the wave zone, *J. Math. Phys.*, **33**:86-101.

[17] Wu, T.T. (1985) Electromagnetic Missiles, *J. Appl. Phys.*, **57**:2370-2373.

[18] Courant, R. and Hilbert, D. (1962) *Methods of Mathematical Physics*, New York: Interscience.

[19] Steinberg, B.Z., Heyman, E., and Felsen, L.B. (1991) Phase-space beam summation for time-dependent radiation from large apertures: continuous parameterization, *J. Opt. Soc. Am. A*, **8**:943-958.

[20] Kerns, D.M. (1975) Scattering-matrix description and near field measurements of electroacoustic transducers, *J. Acoust. Soc. Am.*, **57**:497-507.

[21] Chandrasekharan, K. (1989) *Classical Fourier Transforms*, Berlin: Springer-Verlag.

[22] Bochner, S. and Chandrasekharan, K. (1949) *Fourier Transforms*, Princeton: Princeton University Press.

[23] Jones, D.S. (1986) *Acoustic and Electromagnetic Waves*, New York: Oxford University Press.

[24] Hobson, E.W. (1957) *The Theory of Functions of a Real Variable*, New York: Dover, Vol. II.

[25] Erdélyi, A., Magnus, W., Oberhettinger, F., and Francesco, G. (1954) *Tables of Integral Transforms*, New York: McGraw-Hill, Vol. II.

[26] Olmsted, J.M.H. (1959) *Real Variables*, New York: Appleton-Century-Crofts.

[27] Weyl, H. (1919) Ausbreitung elektromagnetischer Wellen über einem ebenen Leiter, *Ann. Physik*, **60**:481-500.

[28] Lalor, E. (1968) Conditions for the validity of the angular spectrum of plane waves, *J. Opt. Soc. Am.*, **58**:1235-1237.

[29] Yaghjian, A.D. (1992) Antenna coupling and near-field sampling in plane-polar coordinates, *IEEE Trans. Antenna Propagat.* **40**:304-312.

[30] Yaghjian, A.D. (1975) *Upper-bound errors in far-field antenna parameters determined from planar near-field measurements,* NBS Technical Note 667.

[31] van Bladel, J. (1964) *Electromagnetic Fields*, New York: McGraw-Hill.

[32] Tai, C.T. (1971) *Dyadic Green's Functions in Electromagnetic Theory*, New York: Intext Educational Publishers.

[33] Smythe, W.R. (1947) , The double current sheet in diffraction, *Phys. Rev.*, **72**:1066-1070.

[34] Bleistein, N. and Handelsman, R.A. (1986) *Asymptotic Expansions of Integrals*, New York: Dover.

[35] Yaghjian, A.D. (1982) Efficient computation of antenna coupling and fields within the near-field region, *IEEE Trans. Antenna Propagat.,* **AP-30**:113-128

[36] Devaney, A.J. and Wolf, E. (1974) Multipole expansions and plane wave representations of the electromagnetic field, *J. Math. Phys.,* **15**:234-244.

[37] Landau, L.D., Lifshitz, E.M., and Pitaevskii, L.P. (1984) *Electrodynamics of Continuous Media*, 2nd edition, New York: Pergamon Press.

[38] Post, E.J. (1962) *Formal Structures of Electromagnetics*, Amsterdam: North-Holland.

[39] Stratton, J.A. (1941) *Electromagnetic Theory*, New York: McGraw-Hill.

[40] Morse, P.M. and Feshbach, H. (1953) *Methods of Theoretical Physics*, New York: McGraw-Hill, Part I.

[41] Dettman, J.W. (1984) *Applied Complex Variables*, New York: Dover.

[42] Baum, C.E. (1968) *A simplified two-dimensional model for the fields above the distributed-source surface transmission line,* Air Force Weapons Laboratory, Sensor and Simulation Notes, Note 66.

[43] Muskhelishvili, N.I. (1953) *Singular Integral Equations*, Groningen-Holland: Noordhoff.

[44] Müller, C. (1969) *Foundations of the Mathematical Theory of Electromagnetic Waves*, New York: Springer-Verlag.

[45] Whittaker, E.T. and Watson, G.N. (1952) *A Course of Modern Analysis*, London: Cambridge University Press.

[46] Moses, H.E. and Prosser, R.T. (1990) Acoustic and electromagnetic bullets: derivation of new exact solutions of the acoustic and Maxwell's equations, *SIAM J. Appl. Math.*, **50**:1325-1340.

[47] Blejer, D.J., Wittmann, R.C., and Yaghjian, A.D. (1992) On-axis fields from a circular uniform surface current, in *Proceedings of International Conference on Ultra-Wideband, Short-Pulse Electromagnetics*, Polytechnic University, Brooklyn New York.

[48] Brigham, E.O. (1988) *The Fast Fourier Transform and Its Applications*, New Jersey: Prentice Hall.

[49] Nussbaumer, H.J. (1982) *Fast Fourier Transform and Convolution Algorithms*, New York: Springer-Verlag.

[50] Kaplan, L.J., Dowling, T., Hanfling, J.D., and Grimm, K. (1977) Rapid measurement and determination of antenna patterns using collapsed near-field data, *Digest Int. Symp. IEEE AP-S*, Stanford Univ.:370-373.

[51] Kanda, M. (1983) Time domain sensors for radiated impulsive measurements, *IEEE Trans. Antenna Propagat.* **AP-31**:438-444.

[52] Yaghjian, A.D. (1984) Approximate formulas for the far field and gain of open-ended rectangular waveguide, *IEEE Trans. Antenna Propagat.* **AP-32**:378-384.

[53] Maloney, J.G., Smith, G.S., and Scott, W.R., Jr. (1990) Accurate computation of the radiation from simple antennas using the finite-difference time-domain method, *IEEE Trans. Antenna Propagat.* **38**:1059-1068.

[54] Kottler, F. (1923) Elektromagnetische Theorie der Beugung an schwarzen Schirm, *Ann. Phys.* **71**:457-508.

[55] Franz, W. (1948) Zur Formulierung des Huygensschen Prinzips, *Z. Naturforschg.* **3a**:500-506 (also (1957) *Theorie der Beugung Elektromagnetischer Wellen.* Berlin: Springer-Verlag, sec.I.10.)

[56] Tai, C.T. (1972) Kirchoff theory: scalar, vector, or dyadic? *IEEE Trans. Antenna Propagat.* **AP-20**:114-115.

[57] Yaghjian, A.D. (1984) Equivalence of surface current and aperture field integrations for reflector antennas, *IEEE Trans. Antenna Propagat.* **AP-32**:1355-1358.

Appendix A

Differentiability and Analyticity of the Plane-Wave Spectrum and Far-Field Function

Since the derivation in this Appendix applied to the scalar acoustic spectrum is analogous and simpler than that of the electromagnetic spectrum, we will consider only the electromagnetic case.

The electromagnetic plane-wave spectrum can be expressed in terms of the source current density $\bar{J}(\bar{r})$ through the relationships [3, ch.3, eqs.(2.2-7a), (2.2-7b)]

$$\bar{T}(k_x, k_y) = \frac{i}{\gamma}\bar{F}(k_x, k_y) \tag{A.1}$$

where the far-field function $\bar{F}(k_x, k_y)$ is given by

$$\bar{F}(k_x, k_y) = -i\bar{k} \times \left[\bar{k} \times \bar{U}(k_x, k_y)\right] \tag{A.2}$$

with $\bar{U}$ defined as

$$\bar{U}(k_x, k_y) = \frac{1}{4\pi\epsilon\omega}\int_V \bar{J}(\bar{r})e^{-i\bar{k}\cdot\bar{r}}dV \tag{A.3}$$

for the *finite* source region V.

Assuming the magnitude of each component of the current is finite (or more generally, the absolute value of the current is integrable over the finite region V), the theorem in Hobson [24, sec.246, p.355] implies that the integral in (A.3), and thus $\bar{U}(k_x, k_y)$ is infinitely differentiable with respect to k_x and k_y if $e^{-i\bar{k}\cdot\bar{r}}$ is infinitely differentiable. Writing $\bar{k}\cdot\bar{r} = k_x x + k_y y + \gamma z$, where $\gamma = \sqrt{k^2 - k_x^2 - k_y^2}$ shows that $\bar{k}\cdot\bar{r}$ is an infinitely differentiable function of k_x and k_y for all (k_x, k_y) except at $\gamma = 0$. *Thus, $\bar{U}(k_x, k_y)$ and, from (A.2) and (A.1), $\bar{F}(k_x, k_y)$ are infinitely differentiable functions of k_x and k_y except possibly at $\gamma = 0$.*

Moreover, if $\bar{k}$ is expressed in polar coordinates so that $\bar{k}\cdot\bar{r} = k_\rho(x\cos k_\phi + y\sin k_\phi) + \gamma z$, where $k_\rho = \sqrt{k^2 - \gamma^2}$, $\bar{U}$ becomes a function of the independent variables (γ, k_ϕ). Then

$e^{-i\bar{k}\cdot\bar{r}}$ is infinitely differentiable with respect to γ and k_ϕ for all (γ, k_ϕ) except at $\gamma = k$ (since $dk_\rho/d\gamma = -\gamma/k_\rho = -\gamma/\sqrt{k^2-\gamma^2}$). *Therefore,* $\bar{U}(\sqrt{k^2-\gamma^2}\cos k_\phi, \sqrt{k^2-\gamma^2}\sin k_\phi)$ *and* $\bar{F}(\sqrt{k^2-\gamma^2}\cos k_\phi, \sqrt{k^2-\gamma^2}\sin k_\phi)$ *are infinitely differentiable functions of* γ *and* k_ϕ *for all* (γ, k_ϕ) *except possibly at* $\gamma = k$.

We can also express the propagation vector $\bar{k}$ in spherical coordinates so that $\bar{k}\cdot\bar{r} = k(x\sin k_\theta\cos k_\phi + y\sin k_\theta\sin k_\phi + z\cos k_\theta)$, and $\bar{U}$ becomes a function of the spherical angles (k_θ, k_ϕ). Then $e^{-i\bar{k}\cdot\bar{r}}$ is infinitely differentiable with respect to (k_θ, k_ϕ). Furthermore, $e^{-i\bar{k}\cdot\bar{r}}$ satisfies the Cauchy-Riemann conditions with respect to complex k_θ and k_ϕ for all (k_θ, k_ϕ). Thus, from the theorem in Hobson [24, sec.246, p.355], the rectangular components of $\bar{U}$ also satisfy the Cauchy-Riemann conditions for all complex (k_θ, k_ϕ), provided the magnitude of each component of the current in (A.3) is finite (or more generally, the current is absolutely integrable over the finite region V). *In other words,* $\bar{U}(k\sin k_\theta\cos k_\phi, k\sin k_\theta\sin k_\phi)$ *and* $\bar{F}(k\sin k_\theta\cos k_\phi, k\sin k_\theta\sin k_\phi)$ *are infinitely differentiable and analytic functions of* k_θ *and* k_ϕ *for all values* (k_θ, k_ϕ). Furthermore, for real values of (k_θ, k_ϕ) the relation $\bar{F}(k\sin k_\theta\cos k_\phi, k\sin k_\theta\sin k_\phi) = \bar{\mathcal{F}}(k_\theta, k_\phi)$ exists between the far-field function $\bar{F}$ and the far-field pattern $\bar{\mathcal{F}}$ defined in Section 2.2.4.

The above result on the differentiability and analyticity of the spectrum and far-field function required that the sources $\bar{J}(\bar{r})$ be located in a volume of finite extent, and that the magnitude of the current be an integrable function. We shall now show that these results can be proven without even requiring this condition of absolute integrability on the current.

Assume the sources are in a volume of finite extent and *outside* the source region produce continuous electric and magnetic fields that satisfy Maxwell's homogeneous curl equations

$$\nabla\times\bar{E} - i\omega\mu\bar{H} = 0, \quad \nabla\times\bar{H} + i\omega\epsilon\bar{E} = 0. \tag{A.4}$$

(If the divergence of $\bar{E}$ and $\bar{H}$ exist outside the source region, so that Maxwell's divergence equations also hold outside the source region, namely $\nabla\cdot\bar{E} = 0$, $\nabla\cdot\bar{H} = 0$, then $\bar{E}$ and $\bar{H}$ must be continuous functions of the spatial coordinates outside the source region.)

The fields outside the finite source region can be generated by equivalent electric and magnetic surface currents ($\bar{K}_e = \hat{n}\times\bar{H}$, $\bar{K}_m = -\hat{n}\times\bar{E}$) on a surface S (for example, a sphere) enclosing the sources [39, sec.8.14], [44, Theorem 35]. Taking the curl of these "Stratton-Chu" formulas, an operation allowed by the theorem of Hobson [24, sec.246, p.355], converts them to the Kottler-Franz formulas [54], [55], [56], [57]

$$\bar{E}(\bar{r}) = -\nabla\times\int_S \bar{K}_m(\bar{r}')G(\bar{r},\bar{r}')dS' - \frac{1}{i\omega\epsilon}\nabla\times\nabla\times\int_S \bar{K}_e(\bar{r}')G(\bar{r},\bar{r}')dS' \tag{A.5}$$

and

$$\bar{H}(\bar{r}) = \nabla\times\int_S \bar{K}_e(\bar{r}')G(\bar{r},\bar{r}')dS' - \frac{1}{i\omega\mu}\nabla\times\nabla\times\int_S \bar{K}_m(\bar{r}')G(\bar{r},\bar{r}')dS'. \tag{A.6}$$

The unit normal $\hat{n}$ is directed out of the surface S, that is, away from the source region.

In terms of these equivalent surface currents, the function $\bar{U}$ in (A.3) is given by

$$\bar{U}(k_x, k_y) = \frac{1}{4\pi\epsilon\omega}\int_S \left[\bar{K}_e(\bar{r}) - \frac{1}{k}\sqrt{\frac{\epsilon}{\mu}}\bar{k}\times\bar{K}_m(\bar{r})\right] e^{-i\bar{k}\cdot\bar{r}}dS. \tag{A.7}$$

(The relationship (A.1) with $\bar{F}$ and $\bar{U}$ substituted from (A.2) and (A.7) can be rigorously proven to be a valid expression for the electromagnetic plane-wave spectrum by inserting $\bar{E}$ from (A.5) into (2.11) and repeating the analysis applied to the acoustic plane-wave expressions in Section 2.1.2.)

Under the extremely weak condition that the electric and magnetic fields are continuous outside the finite source region, a condition that must hold if the fields obey Maxwell's curl and divergence equations outside the source region, $\bar{K}_e(\bar{r})$ and $\bar{K}_m(\bar{r})$ are continuous functions on S. Consequently, the above analysis applies to (A.7) to prove the same differentiability and analyticity of the spectrum and far-field function for sources in a volume of finite extent without requiring continuity or absolute integrability of the current $\bar{J}$ in (A.3).

In a similar manner, the theorem of Hobson [24, sec.246, p.355] can be applied to (A.5) and (A.6) to prove that the continuous electromagnetic fields everywhere in a source-less region are infinitely differentiable functions of their rectangular, cylindrical, and spherical spatial coordinates. Also, it follows that the rectangular components of $\bar{E}$ and $\bar{H}$ are part of analytic functions of complex spatial variables (in rectangular, cylindrical, or spherical coordinates) in a three-dimensional domain that contains the real spatial variables outside S. This analyticity of the electromagnetic fields everywhere outside the source region implies that the fields outside a finite source region must be zero everywhere if they are zero in any region with nonzero volume outside the source region.

Appendix B

Time-Domain Far Fields in Terms of Current Sources

The far-field equations derive rigorously from the vector-potential solution to Maxwell's equations in the time domain

$$\bar{H}(\bar{r},t) = \frac{1}{\mu}\nabla \times \bar{A}(\bar{r},t) \tag{B.1}$$

$$\bar{E}(\bar{r},t) = \frac{1}{\epsilon}\nabla \times \int^t \bar{H}(\bar{r},t')dt', \quad \bar{r} \notin V \tag{B.2}$$

where

$$\bar{A}(\bar{r},t) = \frac{\mu}{4\pi}\int_V \frac{\bar{J}(\bar{r}',t-R/c)}{R}dV' \tag{B.3}$$

and $R = |\bar{r} - \bar{r}'|$. The current in (B.3) is assumed integrable over its finite source volume V (at least for observation points $\bar{r}$ outside the source region).[1] Inserting $\bar{A}$ from (B.3) into (B.1), and bringing the curl operator under the integral sign produces the following expression for the magnetic field

$$\bar{H}(\bar{r},t) = -\frac{1}{4\pi}\int_V \left[\frac{\bar{R}\times\frac{\partial}{\partial t}\bar{J}(\bar{r}',t-R/c)}{cR^2} + \frac{\bar{R}}{R^3}\times\bar{J}(\bar{r}',t-R/c)\right]dV' \tag{B.4}$$

where we have introduced $\bar{R} = \bar{r} - \bar{r}'$ and used the identity [31, App.1, eq.(186)]

$$\nabla \times \frac{\bar{J}(\bar{r}',t-R/c)}{R} = -\frac{\bar{R}\times\frac{\partial}{\partial t}\bar{J}(\bar{r}',t-R/c)}{cR^2} - \frac{\bar{R}}{R^3}\times\bar{J}(\bar{r}',t-R/c). \tag{B.5}$$

[1] The interchange of the time integration with the curl operator on the right side of (B.2) can be proven valid by interchanging the space and time integrations in the integral form of Maxwell's second equation to get $\epsilon\int_S \bar{E}\cdot\overline{dS} = \oint_C\left(\int^t \bar{H}dt'\right)\cdot\overline{dl}$, where no point of the surface S or the curve C is in the source region V. Then Stokes' theorem is applied to obtain (B.2). This interchange of space and time integrations is permitted by standard theorems of integration [24, sec.237] under the very weak condition that $\bar{H}(\bar{r},t)$ is integrable over any finite space-time domain (C,t), where no point of the curve C is in the source region V. Alternatively, one could simply take the above integral equation as the fundamental form of Maxwell's second equation.

The interchange of differentiation and integration required to obtain (B.4) is valid outside the source region if the time derivative of the current exists and is finite, or more generally, $|\frac{\partial}{\partial t}\bar{J}(\bar{r}', t - R/c)| \leq \alpha(\bar{r}')$, where $\alpha(\bar{r}')$ is a function, independent of time, that is integrable over the finite region V [24, sec.246, p.355].

Multiplying (B.4) by r, then taking the absolute value and limit of (B.4) as $r \to \infty$ gives

$$\lim_{r\to\infty} \left|r\bar{H}(\bar{r}, t)\right| = \frac{1}{4\pi} \lim_{r\to\infty} \left| \int_V r \left[\frac{\bar{R} \times \frac{\partial}{\partial t}\bar{J}(\bar{r}', t - R/c)}{cR^2} + \frac{\bar{R}}{R^3} \times \bar{J}(\bar{r}', t - R/c) \right] dV' \right|$$

$$\leq \frac{1}{4\pi c} \int_V \alpha(\bar{r}') dV'. \tag{B.6}$$

Bringing the limit inside the last integral of (B.6) is allowed by standard theorems on limits of integrals [24, p.324]. To obtain the analogous results for the electric field, insert $\bar{H}$ from (B.4) into (B.2) to get

$$\bar{E}(\bar{r}, t) = -\frac{1}{4\pi}\sqrt{\frac{\mu}{\epsilon}} \int_V \left[\frac{1}{cR}\frac{\partial}{\partial t}\bar{J}(\bar{r}', t - R/c) - \frac{1}{cR^3}\left(\bar{R} \cdot \frac{\partial}{\partial t}\bar{J}(\bar{r}', t - R/c)\right)\bar{R} \right.$$

$$-\frac{3}{R^4}\bar{R} \cdot \bar{J}(\bar{r}', t - R/c)\bar{R} + \frac{\bar{J}(\bar{r}', t - R/c)}{R^2}$$

$$\left. -\frac{3c}{R^5}\bar{R} \cdot \left(\int^{t-R/c} \bar{J}(\bar{r}', t')dt' \right)\bar{R} + \frac{c}{R^3}\int^{t-R/c} \bar{J}(\bar{r}', t')dt' \right] dV'. \tag{B.7}$$

And as $r \to \infty$ one obtains the far-field result similar to (B.6), namely

$$\lim_{r\to\infty} \left|r\bar{E}(\bar{r}, t)\right| \leq \frac{1}{4\pi c}\sqrt{\frac{\mu}{\epsilon}} \int_V \alpha(\bar{r}') dV'. \tag{B.8}$$

The inequalities (B.6) and (B.7) prove that the far magnetic and electric fields decay as $1/r$ *(or faster) as* $r \to \infty$*, provided the first time derivative of the retarded current function is bounded by an integrable function in the finite source region* V*.*

If, in addition, the first time derivative of the current is a continuous function of time, the limit of (B.4) and (B.7) as $r \to \infty$ can be brought inside the integrals [24, p.324] to get the following explicit expression for the far magnetic and electric fields

$$\bar{H}(\bar{r}, t) \sim -\frac{1}{4\pi cr}\hat{r} \times \int_V \frac{\partial}{\partial t}\bar{J}(\bar{r}', t - r/c + \hat{r} \cdot \bar{r}'/c)dV' + O\left(\frac{1}{r^2}\right) \tag{B.9}$$

and

$$\bar{E}(\bar{r}, t) \sim \sqrt{\frac{\mu}{\epsilon}}\frac{1}{4\pi cr}\hat{r} \times \hat{r} \times \int_V \frac{\partial}{\partial t}\bar{J}(\bar{r}', t - r/c + \hat{r} \cdot \bar{r}'/c)dV' + O\left(\frac{1}{r^2}\right). \tag{B.10}$$

The far-field expressions in the time domain (B.9) and (B.10) check with the far-field expressions in the frequency domain (2.56) in that they are Fourier transforms of each other. However, in this appendix we have given conditions on the current that assure the validity of the time-domain far-field expressions; specifically, (B.9) and (B.10) are valid if the first time derivative of the retarded current function is bounded by an integrable function in the finite source region V, and is a continuous function of time.

MISSION

OF

ROME LABORATORY

Rome Laboratory plans and executes an interdisciplinary program in research, development, test, and technology transition in support of Air Force Command, Control, Communications and Intelligence (C3I) activities for all Air Force platforms. It also executes selected acquisition programs in several areas of expertise. Technical and engineering support within areas of competence is provided to ESC Program Offices (POs) and other ESC elements to perform effective acquisition of C3I systems. In addition, Rome Laboratory's technology supports other AFMC Product Divisions, the Air Force user community, and other DOD and non-DOD agencies. Rome Laboratory maintains technical competence and research programs in areas including, but not limited to, communications, command and control, battle management, intelligence information processing, computational sciences and software producibility, wide area surveillance/sensors, signal processing, solid state sciences, photonics, electromagnetic technology, superconductivity, and electronic reliability/maintainability and testability.